The probabilistic assessment of trench sedimentation in sand wave fields

Based on a case study at the Borssele Wind Farm Zone

B.W.J. van Heijningen

TUDelft   Boskalis

The probabilistic assessment of trench sedimentation in sand wave fields

Based on a case study at the Borssele Wind Farm Zone

Master Thesis Report

By

B.W.J. van Heijningen

In partial fulfilment of the requirements for the degree of

Master of Science

In Civil Engineering

at the Delft University of Technology,

Thesis committee:	Dr. Ir. Matthieu de Schipper,	TU Delft, Chairman
	Dr. Ir. Oswaldo Morales Napoles,	TU Delft
	Ir. Wiebe de Boer,	TU Delft, Deltares
	Dr. Ir. Bas Borsje,	Twente University
	Ir. Antoon Hendriks,	Boskalis, Daily supervisor
Version:	Final version	
Date:	06/07/2021	

TUDelft   **Boskalis**

Preface

With this report, I conclude my Master of Science in Hydraulic Engineering at the faculty of Civil Engineering and Geosciences at the Delft University of Technology. I was able to write my thesis as graduate intern at Boskalis. I am grateful for the warm welcome at the company and the opportunity they provided to graduate on this interesting topic, while getting to know Boskalis.

I would like to thank my graduation committee for their help during my thesis. Thanks to Matthieu de Schipper for being the chair of the committee and keeping in contact throughout the process, and giving me feedback on my work. Thanks to Bas Borsje, who was always willing to support me on the topic of sand waves and provided the model to work with. I am also grateful to Oswaldo Morales Napoles for his critical view on the probabilistic assessment part of my thesis. Moreover, I would like to thank Wiebe de Boer, for providing his comprehensive feedback throughout the process.

Special thanks goes out to Antoon Hendriks, my daily supervisor, for initiating this topic, but most importantly for the continuous support during my time at Boskalis. The help you gave me, especially during times I felt stuck, was very much appreciated.

Finally, I would like to thank my family and friends who always supported me, not only during my master thesis, but also during the previous years of my study.

Boudewijn van Heijningen
July 2021, Delft

Summary

The transition from fossil to renewable energy sources is an important but challenging task in the Netherlands. The Dutch government agreed to increase the contribution of renewable sources to 40% of the total energy production in the year 2030. Offshore windfarms have a crucial role in this strategy, with a planned share of 8.5% to the total energy production. This requires a more than tenfold increase of the current capacity. The North Sea is a suitable location for offshore windfarms due to the limited water depths and the favourable wind conditions.

For the transportation of offshore produced energy to the onshore grid, export cables have to be installed in the sea bed. These cables must be buried deep enough to ensure safe fishery and navigation. However, overheating may occur if the burial depth is too large. Usually, at first trenches are dredged, in which approximately one month later the cables are installed. During this period the trench should remain sufficiently open to install the cables, fulfilling the depth requirements. In order to minimize downtime resulting from adverse weather conditions, dredging operations are usually not executed during winter. This thesis focusses on the expected sedimentation during the month April.

Since large parts of the North Sea are covered by sand wave fields, the effect of this bedforms on trench sedimentation has to be known. This is researched based on a case study at the Borssele Wind Farm Zone, for which two models are used: the 1D-SedPit model (Van Rijn, 2013) and a more complex 2DV-sand wave model (Borsje *et al.*, 2013, 2014). A probabilistic assessment is made by means of a Monte Carlo analysis for SedPit, while Latin Hypercube Sampling was used for the 2DV-model due to the increased computation time. The goal is to investigate to what extent a reduced complexity model is able to assess trench siltation for trenches located in sand wave fields, or that more complex sand wave models arrive at significantly more reliable results.

Trench sedimentation can be caused by various mechanisms: shifting of shoals or banks, reduction of sediment transport capacity due to reduced flow velocities, and sliding of particles on the side slopes under the influence of gravitational effects. Shifting of shoals and banks can be neglected during the considered period of one month. The same holds for the sand waves, which do not migrate significantly during this time.

It was however found that sand waves still influence the trench sedimentation. Roughly three configurations can be distinguished: trenches located at sand wave crests, sand wave troughs and halfway. The largest sedimentation rates occur for trenches located at the sand wave crest, the smallest sedimentation rates are found for trenches located near sand wave troughs. This is mainly caused by the difference in bed load sediment transport. Due to the more gradual changes in bathymetry, the bed load transport is limited for trenches located at the trough, while the abrupt changes in the case of sand wave crests, enhance sedimentation. Since the sand wave height and sand wave length are positively related, larger sand wave perturbations are distributed over a larger area, reducing its effect on the sedimentation.

Besides the influence of sand waves, the reduction in sediment transport is the most important mechanism to consider, due to the mainly perpendicular directed flow with respect to the trench axis at the Borssele Wind Farm Zone. In this sedimentation process, the current speed is a sensitive parameter, which can be explained by the non-linear relation between sedimentation and flow velocity. If the angle between the trench axis and the flow direction is small, the sedimentation rate is small. Parallel flows can even enhance erosion of the trench due to the locally higher flow velocities.

Lastly, the water depth is an important parameter, which can be explained by the fact that in shallow water the shear stress increases and the influence of wave action is more significant. Changing the grain size diameter is of influence, but around an order of magnitude less than the water depth.

During the probabilistic assessment of the trench sedimentation in flat bathymetries, it was found that the uncertainty obtained by LHS with the 2DV-model is reduced compared to the MC-analysis in SedPit: the median is for both cases 0.06m, the 5-95 percentiles are 0.03m-0.09m and 0.04m-0.13m respectively. Including (idealized) sand wave perturbations in the 2DV-model increases the range of the P05-P95 values for in trench sedimentation to 0.01 and 0.13m.

Furthermore, data from sedimentation surveys and dredging operations along the cable trajectory, were not accurate enough for a detailed comparison with the model results. As expected, it was however found that decreasing water depths led to an increase in trench sedimentation. Due to the insufficient quality of the measurements, it can only be concluded that the sedimentation rate obtained during the model study is of the same order of magnitude as the data from the sediment survey and dredging campaigns. The data is not detailed enough to distinguish differences in sedimentation along the sand wave perturbations.

Based on the results, it is concluded that SedPit can be used as first assessment tool for the trench sedimentation, since it covers the range obtained with the more complex 2DV-model. The main advantage is the limited computation time of around 1.5 hours, compared to around 48 hours with the sand wave model. On the other hand, the 2DV-model is able to produce more accurate results.

The siltation rate in trenches located at sand wave crests, is underestimated by SedPit compared to the results obtained from the 2DV-model. The opposite holds for trenches located at sand wave troughs, in which more sedimentation is predicted by SedPit. Adjusting the calibration parameter of sand transport in SedPit within the ranges provided in Van Rijn (2013) (0.5 for a sand wave trough and 1.0 for a sand wave crest), can at most decrease the difference between the models. For trenches located near a sand wave crest or trough, it is therefore advised to use at least the 2DV-model to assess trench sedimentation.

Furthermore, the 2DV-model can only be used in the case of perpendicular flow with respect to the trench-axis. Although SedPit is theoretically able to include the effect of more parallel orientated flows, Van Rijn (2013) showed that the sedimentation rates are overestimated, underlining the importance of 2DH modelling for trench sedimentation in this case. Inclusion of the sand wave processes, which act in the 2DV-direction, therefore requires 3D modelling for non-perpendicular flows.

Moreover, due to the that for the probabilistic assessment of the 2DV-model is done by means of Latin Hypercube Sampling, extreme conditions cannot be taken into account. In this case, SedPit in combination with a Monte Carlo analysis is more suitable. With an additional computation with the 2DV-model, these results can be verified, increasing the quality of the prediction.

Content

1 Introduction

1.1 Background

In the foreseeable future the energy transition from fossil to renewable sources is one of the most challenging tasks in the Netherlands. In an agreement, the so-called 'Energieakkoord voor duurzame groei' signed in 2013, the Dutch government and more than 40 different organizations agreed to increase the contribution of renewable energy (Sociaal-economische raad, 2013). One of the most important resources is offshore wind energy. The North Sea is a suitable location for offshore windfarms due to the limited water depths and favourable wind conditions.

At present, the annual production of energy by offshore windfarms is around 1 Gigawatt (GW). According to the agreement, in the year 2030 this amount should be raised to 11 GW, contributing for 8.5% to the total energy consumption of the Netherlands. In total 40% of the energy should be generated by renewable resources in this year (Rijksoverheid, 2018).

To be able to construct windfarms, a proper understanding of the morphology in the area of interest is required. This concerns the location of the windfarm itself to ensure the stability of the monopiles, but also the areas where the export cables, which transfer the generated energy from the windfarm to the onshore grid, are located. For these cables, the burial depth is of importance: the cables must be buried deep enough to ensure safe fishery and navigation (Noordzeeloket, 2019). On the contrary, if the burial depth is too large, overheating of cables might occur.

The installation of the cables can often not be simultaneously executed with dredging of the trenches. A typical period between these operations is a month (Boskalis, 2017). During this period the trench should remain sufficiently open to install the cable, fulfilling the depth requirements. Therefore, it is important to know how quickly sedimentation of these trenches occurs.

The sedimentation rate is influenced by various factors such as current velocity, wave heights, grain size (distributions) and bed roughness. However, when using models to assess this siltation, model settings can significantly influence the results (Kroon *et al.*, 2019). Moreover sedimentation can be caused by external morphological processes, such as sand waves, which can be found in the North sea (Figure 1.1). Nemeth et al. (2003) stated that sand waves can expose cables, which may lead to vibrations damaging the cables. This underlines the importance of an assessment of cable trench siltation for locations in the North Sea.

Often contractors are responsible for the installation and the maintenance of the different cables afterwards (Hendriks, 2019). Due to potential (financial) risks, a proper assessment of sedimentation and the accompanied uncertainties is required. Therefore this thesis focusses on providing a guideline on how to probabilistically assess trench sedimentation for trenches located in sand wave fields.
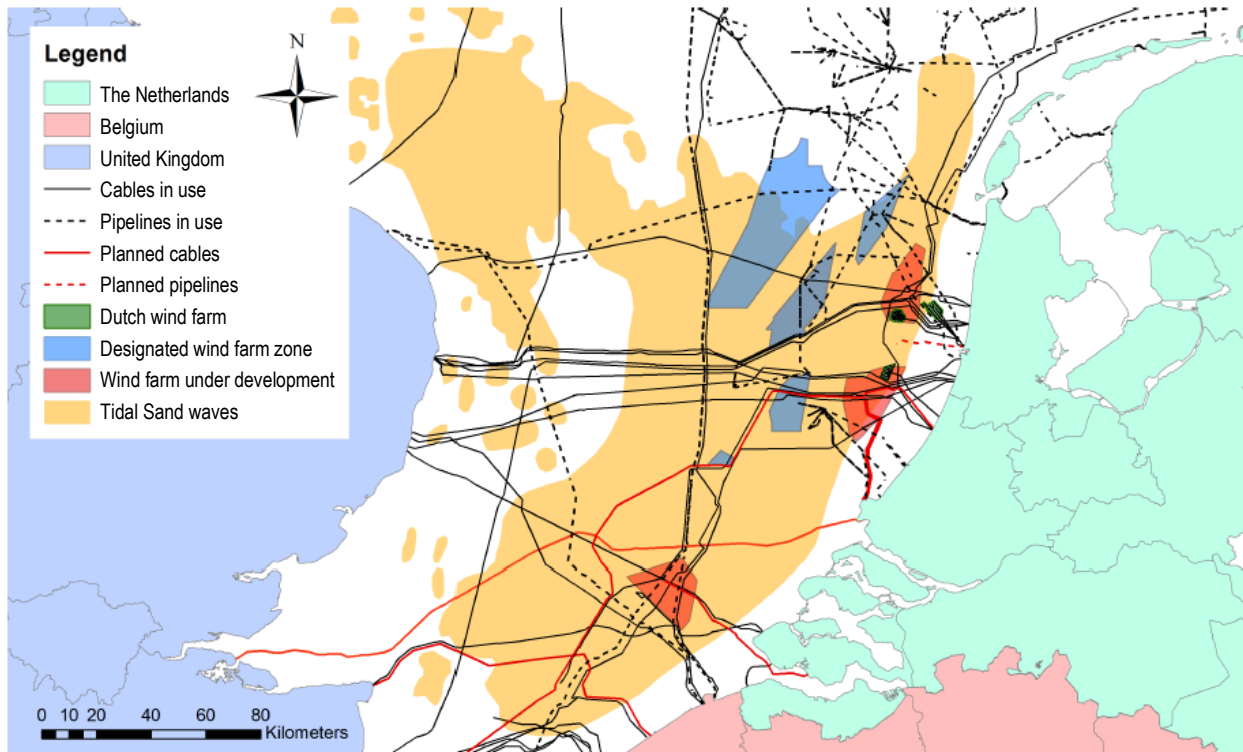
Figure 1.1: Sand wave fields on the North Sea, effecting present and future offshore windfarms (Krabbendam, 2018).

1.2 Problem description

In order to determine trench sedimentation, often process-based models (such as Delft3D) are used. Each model has its own characteristics, leading to different situations in which they can be applied. Generally however, more complex models are prone to longer computation times, limiting the possibilities for a probabilistic assessment of the results. On the other hand, the increased complexity usually leads to a better understanding of (morphodynamic) processes, resulting in more reliable model output. For all models, both complex and more simple, different types of uncertainties have to be taken into account, since an underestimation of these uncertainties may lead to a false sense of accuracy of the results (Kroon *et al.*, 2019).

A method widely used for uncertainty assessment is the Monte Carlo simulation, in which a model is ran many times, each time with randomly drawn values from the probabilistic distributions of the input variables (Li *et al.*, 2013; Yan *et al.*, 2017). However, since computation times of more complex morphological models are usually long and the period for tendering is often limited, Monte Carlo simulations are not feasible (Hendriks, 2019). This means other methods have to be used for the uncertainty assessment.

These methods can be divided into two categories. The first one focusses on reducing the computation times by simplification of the model. This can e.g. be done by simplifying it to a one or two dimensional model or lowering the resolution. Another solution is to reduce the amount of simulations necessary for uncertainty assessments by using sampling techniques (Berends *et al.*, 2019).

Latin Hypercube Sampling (LHS) is an example of a sampling technique. The performance of LHS was already analysed in various studies. Hossain et al. (2006) used it for the probabilistic assessment of satellite rainfall observations in flood prediction. It was found that with LHS the

same degree of reliability compared to a Monte Carlo analysis could be achieved, however with almost two orders of magnitude fewer simulations. In the field of coastal engineering, Dagalaki (2018) showed that LHS could potentially be a suitable method for coastline change uncertainty quantification, although it is difficult to predict how many simulations are needed to arrive at accurate results (Olsson *et al.*, 2003).

All in all a trade-off exist between model complexity and the possibilities to assess uncertainties: although the quality of the predictions of a complex model aims to be better, only a limited amount of runs can be made to assess uncertainties. On the other hand: in reduced complexity models, a more elaborate probabilistic assessment is possible. The question is to what extent a reduced complexity model is able to assess trench siltation for trenches located in sand wave fields, or that (more complex) sand wave models arrive at significantly more reliable results. In both cases uncertainties in model input have to be taken into account.

1.3 Objective

The aim of this study is to provide an overview in what situations a reduced complexity model with an extensive uncertainty analysis provides accurate results, or when a more computationally more demanding model in combination with a limited probabilistic assessment is required. This research is based on a case study at the Borssele Wind Farm Zone (BWFZ), on which more information is provided in Chapter 1.4. Therefore, the goal of this study is to answer the following research question:

> **How to probabilistically assess trench sedimentation for trenches located in sand wave fields, such as at the Borssele Wind Farm Zone?**

This research question is answered by means of 5 sub questions:

1. What are the morphological processes leading to trench siltation?
    Before being able to model trench sedimentation, a proper understanding of the different morphological processes leading to sedimentation in the trenches is required.

2. What is the influence of sand wave bottom perturbations on the trench infill?
    The influence of the sand waves on trench infill has to be investigated based on changes in hydrodynamic processes caused by the sand waves, as well as the morphological developments (sand wave growth and migration). This includes the effect of variations in sand wave dimensions and the location with respect to the trench.

3. What are the most important parameters when assessing trench sedimentation and how are they related?
    With this question, the most important parameters are identified. Furthermore, it is important to know what the distributions and relations between the various parameters are, since a similar occurrence of certain parameter values can strengthen or weaken sedimentation processes.

4. What is the difference in probabilistic sedimentation rate in the trenches computed by the different models?
    The probabilistic sedimentation rates of the different models are compared to get an insight in whether a more complex model reduces the uncertainty in trench sedimentation compared to a simple model with a more elaborate probabilistic assessment.

5. What is the quality of the predictions from the various models compared to measurements of back fill?
   Measurements from Boskalis on the back fill in the trenches (near the Borssele wind farms) are used to compare the model outcomes with. In this way a first assessment can be made whether the different models are likely to provide realistic sedimentation rates.

1.4 Case study

As mentioned, this thesis is based on a case study of the Borssele Wind Farm Zone, located more than 22 kilometers offshore from the Dutch coast (Zeeland). For the installation of this new windfarm, export cables need to be installed between the site and the onshore grid. These cables are routed via the Western Scheldt estuary, and come ashore at the high-voltage substation at Borssele, as is shown in Figure 1.2. The length of both export cables is around 67 kilometres.

Between the onshore connection to the grid and the Borssele Wind Farm Zone itself, the trajectory crosses different environments: an estuary, later on a site governed by nearshore conditions, and relatively deep water near the BWFZ. The focus of this thesis is on the BWFZ, since for in highly dynamic environments such as the Western Scheldt, the use of complex models is always required, limiting the possibilities to compare different models. Around the BWFZ, more models are available, and the sand wave field is well-developed. In Figure 1.2, the area considered in this study is indicated by the blue box.

Figure 1.2: Route of the export cables (green) between windfarms Borssele I + II and the main land (modified, based on Provinciale Zeeuwse Courant (2019)). The case study area is indicated by the blue box.

Due to the focus on the siltation of trenches in which export cables of offshore windfarms are installed, the typical sedimentation period of one month is considered, as mentioned in the background information of this chapter. To minimize the risk of downtime or other hindrance due to adverse weather conditions, dredging operations are often not executed during winter. Therefore, this study focusses on sedimentation during the month April. Furthermore, the focus of this study is on the most probable outcomes, and the extremes are not taken into account. Although these extremes are interesting to investigate, it usually not feasible for contractors as Boskalis to take such events into account. Therefore, this analysis is discarded from this study.

1.5 Research method

This research focusses on the probabilistic assessment of trench sedimentation in sand wave field. Therefore a literature study is conducted on trench sedimentation processes, sand wave dynamics and the uncertainties related to modelling. Furthermore, since this study is based on a case study at the Borssele Wind Farm zone, data is collected around this area including bathymetry measurements, wind and wave data and tide and current information. Based on these data, distributions and relations between different variables are derived.

The trench sedimentation is assessed by using two models:

- 1D-SedPit (Van Rijn, 2013)
- 2DV-sand wave model (Borsje *et al.*, 2013, 2014).

In Figure 1.3, the models are shown in a diagram based on model complexity and possibility for a probabilistic assessment. SedPit is the most reduced complexity model and is frequently used to determine trench sedimentation due to its limited computation times. Therefore, it can also be used as a tool for a quick probabilistic assessment. Due to the simplicity, it can however not take into account complicated flow patterns or the influence of bottom perturbations. For these processes, more sophisticated models are needed. Since this research focusses on the infill rates in cable trenches located in sand wave fields, as base an existing sand wave model is used as base.
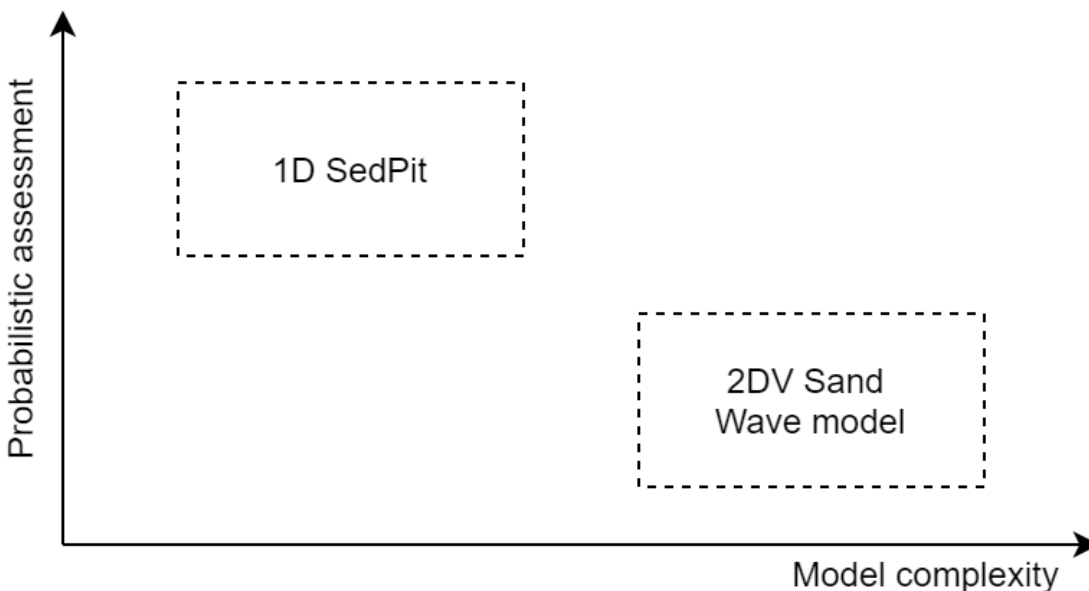

Figure 1.3: Model complexity versus uncertainty assessment possibilities for both SedPit and the 2DV-sand wave model.

The different models used in this study and the objectives are discussed separately.

Step 1: 1D – SedPit

The goal of using SedPit is twofold: besides determining the trench sedimentation with an extensive probabilistic assessment, it is also researched how simplifications in forcing may lead to comparable sedimentation rates, which can be used as starting point for the more complex 2DV-model.

To assess (the bandwidth in) trench sedimentation, the input variables are divided into intrinsic parameters in time and epistemic uncertainties. In this way, the uncertainties resulting from the forcing and the model itself are separated. Furthermore, by means of a sensitivity analysis, the most influential (epistemic) parameters are identified. Due to the non-constant forcing from waves and currents, these intrinsic parameters are not taken into account during the sensitivity analysis.

Based on the distributions of the different epistemic parameters and a representative forcing, on which more information is provided in Chapter 4, the probabilistic infill is assessed by means of a Monte Carlo analysis. At the end, it is furthermore researched how simplifications in forcing lead to similar results.

Step 2: 2DV-model

This step consists of two parts. At first, it is investigated whether with the sand wave model, the same processes are taken into account as with SedPit. This is done by performing a probabilistic assessment for a flat sea bottom, throughout the domain, in which a trench is located. Due to the increase in computation time, a Monte Carlo analysis is no longer suitable for a probabilistic assessment of the trench sedimentation. Therefore, LHS is used to get a better view of the uncertainties related to this model.

Secondly, the effect of sand wave perturbations is investigated. To do so, different base cases are used to research the conceptual impact of sand waves on trench sedimentation. Hereafter, variations in sand wave dimensions and the location of the trench with respect to the sand wave are made. Deltares (2015b, 2016), in which the sand wave dimensions are determined at the Borssele Wind Farm Zone, is used as base. By combining the most important epistemic uncertainties of the 2DV-model with this in LHS, a probabilistic assessment of the trench sedimentation under influence of sand waves is obtained.

Step 3: Measurements and conclusion

Before concluding the research, the model output is compared to sedimentation surveys of Boskalis and measurements obtained during dredging operations. In this way, the model performance can be verified.

At the end of this research, the probabilistic distribution of the sedimentation rate from the different models are compared. Based on the computation time, probabilistic assessment and the comparison with the measurements, it is concluded how trench sedimentation can be assessed best in sand wave fields. A schematization of the methodology can be found in Figure 1.4.
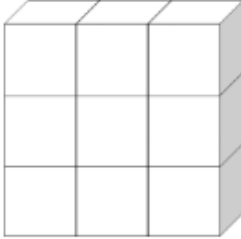
		Dimensions	Without sand waves	With sand waves
C1		Introduction		
C2		Literature review		
C3		Site analysis		
Model runs		Dimensions	Without sand waves	With sand waves
C4: 1D - SedPit		1D	Sensitivity analysis Monte Carlo-analysis Representative forcing	Not considered
Results		- Effect of yearly variations in wave climate - representative tidal currents and wave climate		
C5: 2DV - Sand wave		2DV	Process verification Latin Hypercube Sampling	Sand wave modelling Latin Hypercube Sampling
Results		- Importance of sand wave modeling		
C6: measurements		- Compare the model results with measurements of Boskalis - Sedimentation survey - Dredging data		
Results		-Computation time -Accuracy of the predictions -Range of applicability		
C7-9		Discussion, conclusion and recommendations		

Figure 1.4: Schematization of the methodology combined with the thesis outline.

1.6 Thesis outline

This report starts with the theoretical framework of the thesis, which consists of the trench siltation mechanisms, sand wave dynamics and uncertainties in modelling (Chapter 2). In Chapter 3, the system analysis is discussed. Chapter 4 provides the probabilistic assessment of the sedimentation rate for the reduced complexity model SedPit. In Chapter 5 the sedimentation is assessed by means of the 2DV-model. The measurements of the sedimentation surveys and dredging operations are discussed in Chapter 6. A discussion of the results can be found in Chapter 7. This research ends with the conclusions drawn in Chapter 8 and finally recommendations made in Chapter 9.

2 Theoretical Framework

This chapter discusses the theoretical framework of this thesis, which can be divided into three categories. Firstly, trench siltation mechanisms are explained in Chapter 2.1. Secondly, a review of literature on sand wave mechanics can be found in Chapter 2.2. To conclude with, Chapter 2.3 provides an overview of models and uncertainties.

2.1 Trench siltation mechanics

Trench sedimentation is dependent on various factors. In general, three main mechanisms can cause sedimentation and erosion in trenches (Van Rijn, 2013):

- Reduction of lateral sediment transport capacity in the trench due to smaller flow velocities, which results in sedimentation.

- Gravitational effects inducing a downward force on bed-load particles on the side slopes of the channel.

- Shifting of shoals and banks.

Which of the mechanism occurs, is dependent on the local conditions. In the next paragraphs they are discussed. A distinction is made between forcing due to currents (Chapter 2.1.1) and waves (Chapter 2.1.2). The influence of the trench dimensions is discussed Chapter 2.1.3.

2.1.1 Currents

The effect of the currents on trench sedimentation is dependent on the orientation with respect to the trench alignment. Jensen, *et al.*, (1999a) and Van Rijn (2013) summarised this based on three cases: perpendicular, parallel and oblique flow.

- Flow **perpendicular** to the trench axis induces erosion on the downstream slopes mainly under influence of bed load transport, upstream slopes on the other hand experience sedimentation. In the case of tidal flow, erosion at both slopes occurs due to the variations in flow direction. Furthermore, due to an increased water depth in the trench, current velocities decrease. This results in a reduced sediment transport capacity of the flow and hence sedimentation of suspended load in the trench. Lastly, special attention needs to be paid to steep side slopes. In this case, flow separation might occur, and reversal currents can result in complicated flow patterns.

- In the case of flow **parallel** to the trench, flattening of the side slopes occurs due to sediment transport from the slopes into the trench. This form of bed load transport is caused by gravitational slope effects inducing a downward force on the sediment particles. This does however not mean that sedimentation in the trench is expected: due to the increased depth, bottom friction is reduced, resulting in higher flow velocities. Consequently, the transport capacity increases and erosion of the bed might occur.

- For flows **oblique** to the trench axis, a combination of the described processes takes place: the flow component parallel to the channel axis increases due to the reduction in bed friction. The flow component perpendicular to the channel axis however, will decrease due to the increase in water depth. The result is a refraction pattern in the channel, which is the largest near the bottom. In general, if the flows are orientated less than 25° with

respect to the main axis of the trench, flow velocities increase, inducing erosion. Otherwise, sedimentation can be expected.

2.1.2 Waves

Besides the influence of currents on sedimentation, also the effect of waves needs to be considered. Orbital motions, caused by the waves, stir up sediment particles from the seabed. This process is especially dominant when water depths are limited. According to linear wave theory, the current velocity amplitude can be calculated with (Holthuijsen, 2017):

$$U_w = \frac{\pi H_s}{T_p \sinh(k h_0)}$$

In which:

- H_s: significant wave height
- T_p: peak period
- k: wave number
- h_0:   water depth

Following this relation, it can be seen that current velocities increases for larger wave heights and periods and decreasing water depths. Moreover, when considering trench sedimentation in the near shore zone refraction, diffraction, shoaling and energy dissipation by wave breaking and bottom fraction. These processes are however not dominant in offshore located areas. Lastly, due the limited width of trenches, the effects of the trench on the wave behaviour is not considered.

2.1.3 Trench dimensions

Lastly, the dimensions of the trench itself also influence the sedimentation rate. One would expect that the mechanisms described in Chapter 2.1.1 will be more pronounced in the case of deeper trenches. Deeper trenches attract more flow, leading to more erosion in the case of parallel flow and on the contrary, in the case of perpendicular flow more siltation can be expected due to a further decrease in flow velocity.

Moreover, the width of the trench is of importance. In the case of perpendicular flow, initially the flow pattern is disturbed. In the case of wider trenches, the flow might reach an equilibrium state again and the sedimentation effects disappear. Furthermore, oblique flows may be defected more in the channel direction, inducing less sedimentation or even erosion of the bed (Jensen, Madsen and Fredsoe, 1999b). It is however not expected that the trenches considered for export cables are large enough for this process to occur. The effect of the trench orientation is, as stated in the previous sections, the most important characteristic since this determines which of the earlier described mechanisms occurs.

2.2 Sand waves

Besides the sedimentation caused by the alignment of the trench, also morphological changes on the larger scale can induce trench infill: namely the movement of sand waves. To do so, first the sand wave characteristics needs to be placed in perspective to other seabed perturbations, discussed in Chapter 2.2.1. Chapter 2.2.2 provides more information on the role of different sediment transport modes. Lastly in Chapter 2.2.3, the formation and migration of sand waves is shown.

2.2.1 Bedform classification

In the North Sea, different bedform patterns can be identified (De Koning, 2007; Menninga, 2012). This study distinguishes four different bedforms based on wavelength, height, migration speed and evolution time. These perturbations are ripples, mega ripples sand waves and sand banks. Ripples are the smallest perturbations and sand banks the largest bedforms. The results are summarized in Table 2.1.

Table 2.1: Different bedform classifications occurring at the Dutch coast (Menninga, 2012).

Bedform	Length [m]	Height [m]	Migration speed [m/year]	Timescale
Ripples	0.1 – 1	0.01 – 0.1	100 – 1000	Hours
Mega Ripples	1 – 10	0.1 – 1	100 – 1000	Hours/days
Sand waves	100 – 1000	1 – 10	1 – 10	Decades
Sand banks	5000 – 10000	1 – 5		Centuries

Generally, a trade-off between the sand wave dimensions (length and height) and the migration speed can be observed: the larger the perturbations, the lower the migration speed, and vice versa. Sand banks are more or less stable with an evolution time in the order of centuries, compared to hours or days for ripples.

In reality, the bathymetry of the North Sea is characterized by the superposition of the different bedforms. This study focusses on the effect on sand waves since this is the largest, dynamic bottom perturbations for the considered time scale in the order of months. Although (mega) ripples may also affect the infill due to its highly dynamic character, it is chosen to exclude these from the research because of the smaller amplitude of the perturbation.

Besides the differences in dimensions and migration velocities, the bedforms can also be classified based on orientation (Hulscher, 1996b). Where the main axis of sand banks are oblique orientated with respect to the tide, sand waves migration and the crest orientation are perpendicular to the tidal currents. The differences in orientation can be explained by the forcing mechanisms of the bedforms. The Coriolis force and bottom friction lead to the wavy bottom pattern under an angle known as sand banks. Sand waves on the other hand are not influenced by Coriolis and the crest is perpendicular orientated with respect to the tidal currents (Figure 2.1). A more elaborate explanation of the forcing of sand waves is discussed in the next section.
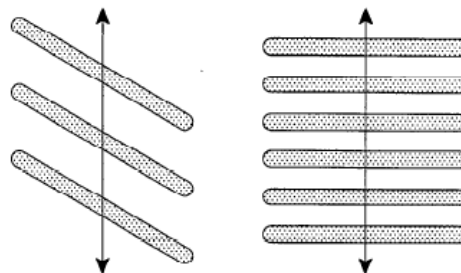

Figure 2.1: Orientation of the sand banks (left) and sand waves (right) with respect to the tidal flow directions (arrow) (Hulscher, 1996b).

2.2.2 Sediment transport modes

Different forms of sediment transport determine the development of the sand waves. Borsje et al. (2011, 2014) distinguished three dominant processes: bed load transport, suspended load transport and slope-induced transport. Bedload transport is dominant if the influence of turbulence (which is stirring up the sediment) is small. On the other hand, if the turbulence has a large influence, suspended load transport occurs. A measure to indicate the different sediment transport modes is the Rouse number, which is defined as the ratio between the particle settling velocity and the shear velocity (turbulence).

$$Rouse\ number: \frac{w_s}{k_c * u_*}$$

In which:

- w_s: particle settling velocity
- k_c: Von Karman's constant (0.4)
- u_*:   shear velocity

Bedload transport occurs for Rouse numbers > 2.5 and suspended load transport occurs for Rouse numbers between 0.8 – 2.5 (Whipple, 2004). Slope-induced sediment transport causes sediment particles to slide down due to, as indicated by the name, the gravitational effects on the grains.
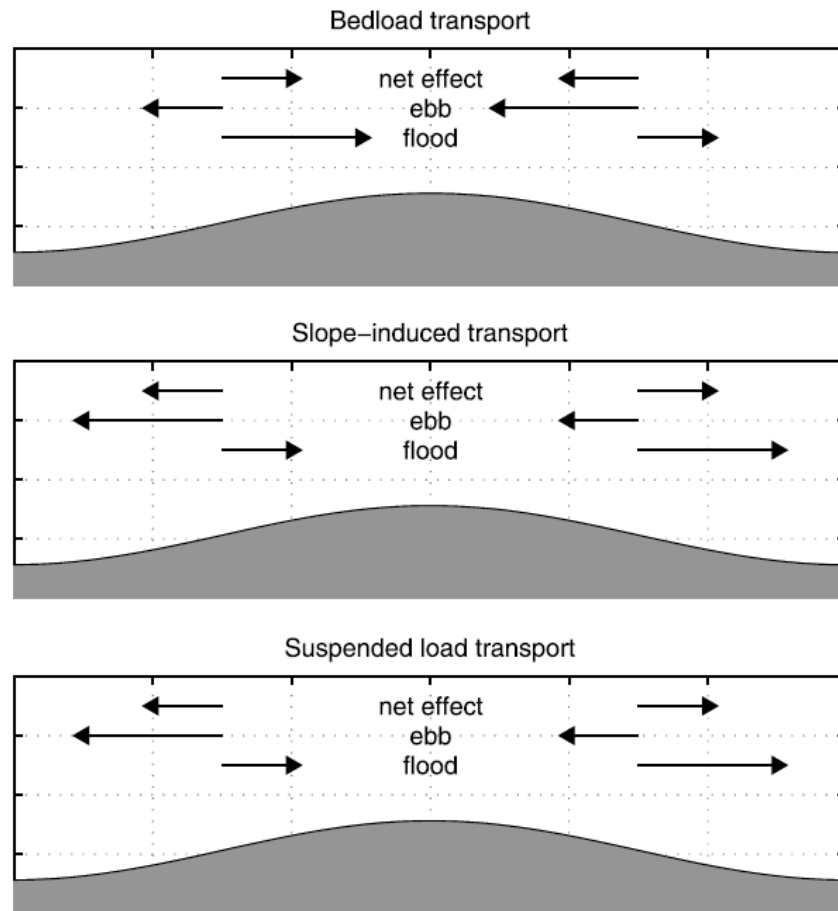

Figure 2.2: The effect of bedload, slope-induced and suspended load transport on sand wave growth during ebb and flood. The net effect of bed load transport leads to the growth of sand waves, while the suspended load transport and the slope-induced transport leads to a decay in sand wave amplitude.

Borsje et al. (2011) demonstrated that sand waves grow due to bed load transport. Suspended load transport has a damping effect: sediment is transported from the crests to the throughs instead of the other way around. The effect of the different transport modes on sand wave formation is shown in Figure 2.2. These findings were confirmed by Borsje *et al.* (2014) in which it was found that at locations where bedload transport is dominant (Rouse number > 2.5), sand wave fields can be observed, in contrast to regions with mainly suspended load transport.

Lastly, the wave motion also effects the height of the sand wave. McCave (1971) showed that wave action is in particular of influence on the wave crests, since it erodes the crest, causing reduction of the sand wave height. Moreover, due to the increased turbulence, the suspended sediment transport increases as well, leading to a decay of sand waves. The effect of waves is higher in shallow water due to the more direct exposure of the bed to the waves. In the next section a closer look is taken to the formation and migration of sand waves due to tidal currents.

2.2.3 Formation and migration

Hulscher (1996) stated that the interaction between bed perturbations and tidal currents can lead to the growth of sand waves. Averaged over a tidal cycle, a small vertical net circulation occurs, which is indicated in Figure 2.3. In this schematization the only considered tidal constituent is M2.

Near the bed, the flow is directed from the throughs to the crests, higher in the water column the flow is directed in the opposite way. The residual component of the vertical flow is small compared to the horizontal flow and upward directed at the crests and downward directed at the throughs. This leads to the growth of the bed perturbations. During both ebb and flood the tidal flow upslope is larger than the downward flow (see Figure 2.2 as well). When averaging over a tidal period this leads to the growth of the sand wave.
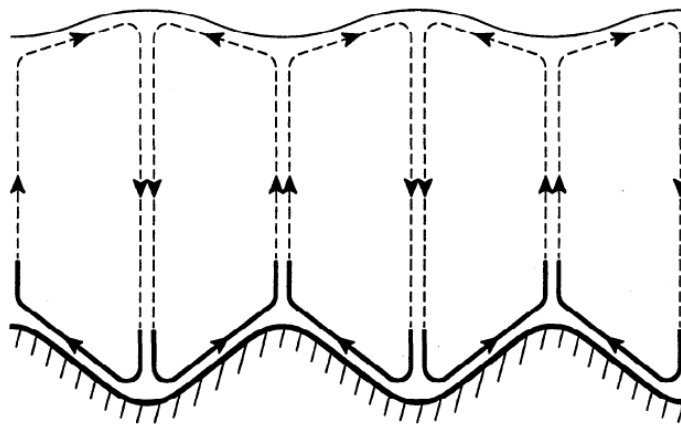

Figure 2.3: The tide-averaged water circulations resulting from the sand wave perturbations of the sea bed (Hulscher, 1996b).

Although the amplitude of sand waves can increase due to a M2 tide, it cannot explain the migration of the sand waves (Németh et al., 2002). This can be explained by the fact that in an oscillatory tidal current caused by one tidal constituent only, the recirculating cells are symmetric and therefore perturbations do not migrate. For migration of sand waves, distortion of the recirculating cells is required, which can be caused by two reasons: the presence of a residual current (Németh et al., 2002), or other tidal constituents (Besio *et al.*, 2003).

In the case of a residual current, sand waves migrate in the direction of the current. However, field data suggests that sand waves can also migrate in opposite direction (Besio *et al.*, 2003). The reason for this was found in the interaction between the M2 tide and higher tidal constituents. In Figure 2.4 this is illustrated with a M2 and M4 tide. However, not all interactions between the

M2 and M4 tidal constituents lead to an upstream migration of the sand waves. Besio *et al.* (2003) indicate that this only occurs for phase shifts between 30 and 180 degrees, as shown in Figure 2.4b. The growth rate itself is not affected by the phase shift between the M2 and M4 tide (see Figure 2.4a).
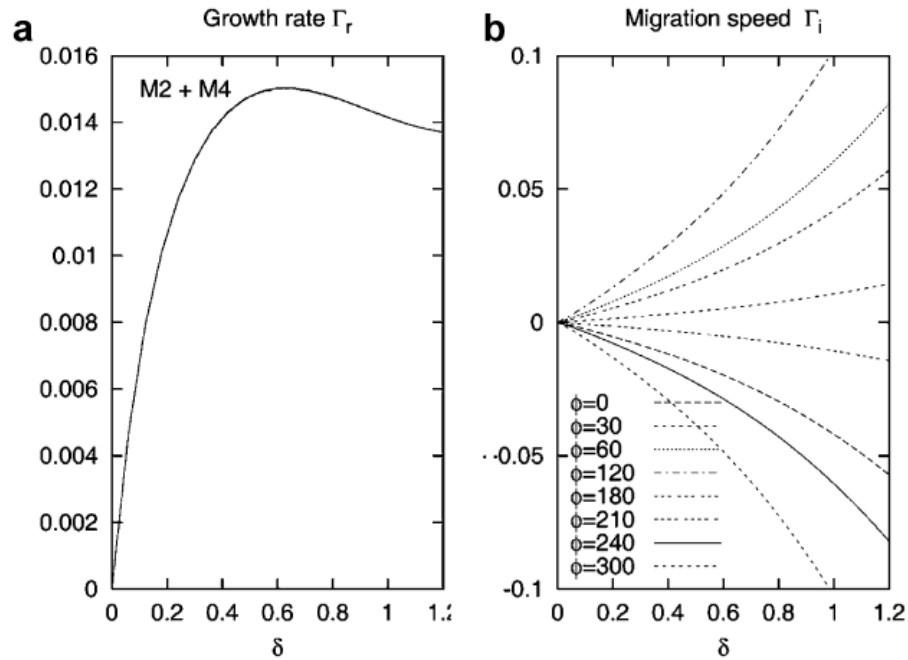

Figure 2.4: The influence of the phase shift of the phase shift of tidal constituents on the growth rate (left) and migration speed of sand waves (right) (Besio *et al.*, 2003). An upstream migration of sand waves (negative values) is obtained by a phase shift between 30 and 180 degrees.

2.3 Models and uncertainties

In order to assess morphological developments, of which sand wave dynamics and trench infill are examples, morphological models are used. This section discusses the various types of models and how uncertainties in modelling can be dealt with.
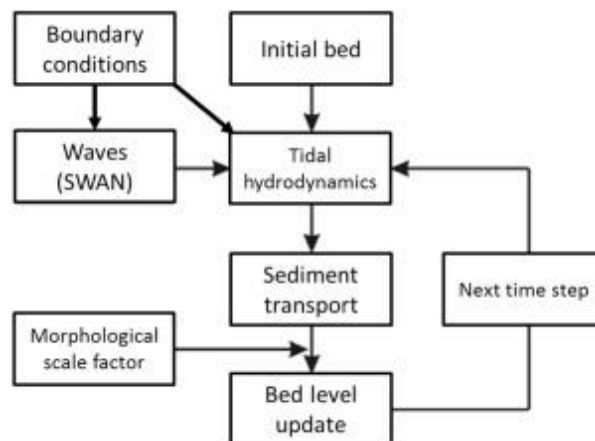

Figure 2.5: Morphodynamic feedback loop in Delft3D (Luijendijk *et al.*, 2017).

A distinction between two types of models can be made: empirical models and process-based models. Empirical models can provide insight in the initial understanding of relationships between variables, often based on measurements. In process-based models, physical processes are the base for the prediction of morphological changes. A widely used process-based model in morphology is Delft3D. In Delft3D, hydrodynamics, waves, sediment transport and morphology are computed under influence of tidal, wind, and wave-driven currents. Luijendijk et al. (2017) described the model structure as indicated in Figure 2.5.

2.3.1 Uncertainty classification

In every step of the schematization presented in Figure 2.5 different types of uncertainties are introduced, all effecting the quality of the model predictions. Therefore, identification of these uncertainties is important. To do so, Kroon et al. (2019), distinguished different types of uncertainties, as indicated in Figure 2.6.
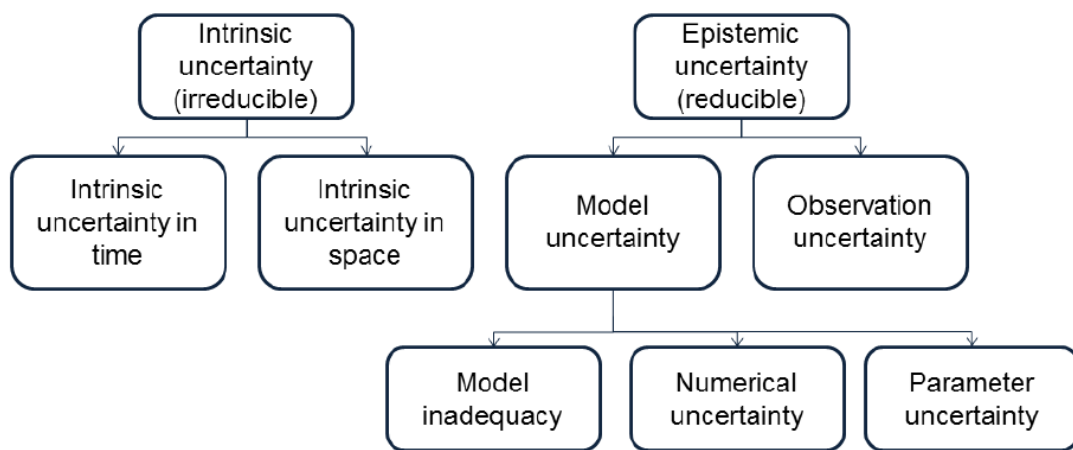
Figure 2.6: Uncertainty classification of the different parameters (Kroon *et al.*, 2019). The intrinsic uncertainty is irreducible, the epistemic uncertainty can be reduced by more complex models.

In general uncertainties can be identified as intrinsic (irreducible) or epistemic (reducible) uncertainties. Intrinsic uncertainties in time and space will always be present in modelling, no matter the investment in more sophisticated models or measurements. An example of this is the yearly variability in wave climate. On the other hand, epistemic uncertainties can be divided into model uncertainties and observation uncertainties. Observation uncertainty is caused by the instruments used during measurements or human errors introduced by performing observations.

Furthermore, three types of model uncertainties can be distinguished: model inadequacy, numerical uncertainty and parameter uncertainty. Model inadequacy are caused by simplifications made in the model (e.g., 1D or 2D modelling instead of 3D). Numerical uncertainties are related to the time steps and grid sizes used in the model. Morphological settings, such as the schematization and morphological acceleration factor, can also introduce these kind of errors. Parameter uncertainties are the last type of model uncertainty.

2.3.2 Deterministic and stochastic modelling

To take the uncertainties during modelling into account, deterministic and stochastic models can be used. In stochastic modelling, uncertainties are implemented in every step of the procedure to introduce a kind of randomness in the models. In this way the outcomes are not solely determined by the model input (Uusitalo *et al.*, 2015). In real life, most processes are stochastic and stochastic modelling is therefore more realistic. However, present morphological models are not able to

accommodate probabilistic modelling in this way, and therefore deterministic models are used in which the model output is often evaluated by means of an uncertainty analysis.

Rip (2015) described the differences in modelling based on a trade-off triangle (Figure 2.7) between simulation uncertainty, parametric uncertainty and model uncertainty. The simulation uncertainty is the uncertainty related to the number of replications performed in the simulation, the parametric uncertainty is the uncertainty in the input parameters of the (stochastic) model and the model uncertainty is related to the model complexity.
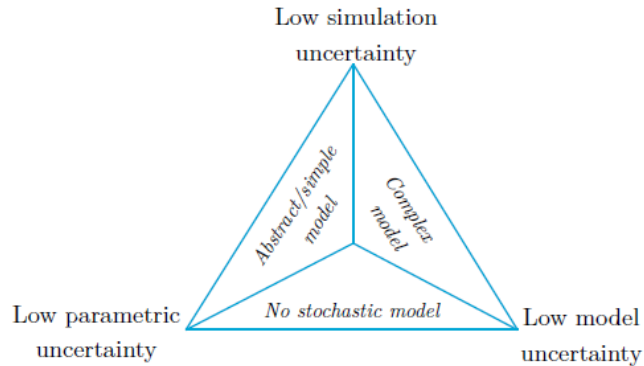

Figure 2.7: Trade-off triangle of simulation, parametric and model uncertainties involved in simulations (Rip, 2015).

If two uncertainties are relatively low, the third one generally increases. This means the uncertainties are balancing each other. In this balance, three different kind of models can be distinguished: an abstract model, a complex model and no stochastic model. A schematization of these different uncertainties and the corresponding models can be found in Figure 2.7.

- No stochastic model: this is directly based on observed data, and no stochastic model is used to produce synthetic data. This implies that there is no parametric uncertainty involved.
- Abstract model: due to the simplification in this model, some factors are not included in this model, hence the parametric uncertainty is low. The model uncertainty however is relatively high due to the fact that not all factors are included.
- Complex model: this describes a process as detailed as possible, resulting in a low model uncertainty. The consequence is however that the parametric uncertainty is higher because more parameters are described, which can be wrongly estimated.

2.3.3 Uncertainty assessment methods

There are numerous methods available for uncertainty assessment in numerical models. This section aims to provide an overview of the different methods which can be used and discusses the most important characteristics.

Standard Monte Carlo simulation

The Standard (Crude) Monte Carlo analysis (MC-analysis) is a widely used method. This analysis randomly draws numbers between 0 and 1 from a cumulative distribution function of a parameter. The corresponding value of this parameter is used as input for the model, as is shown in Figure 2.8. This process is repeated numerous times without taking into account the previous number. In this way a set of completely random scenarios is generated as input for a model.
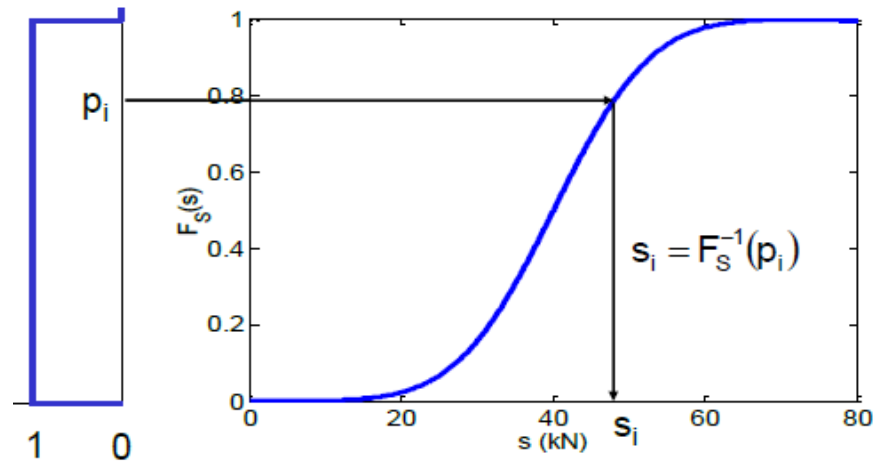
Morgan et. al (1992) defined a coefficient of variation $V_{p_f} \sim \frac{1}{\sqrt{N_r}}$, in which N_r is the number of simulations performed during the Monte Carlo analysis. Since this coefficient is an indication for the size of the introduced error, smaller values for V_{p_f} correspond to more accurate results. Therefore, it can be shown that the more simulations performed, the higher the accuracy of the method is.

The main advantage of the MC-analysis is the simplicity to apply. Furthermore, it is also applicable for non-linear models with different uncertainty distributions. This makes the MC-analysis a robust method for uncertainty assessment in various models. On the other hand, generally a large amount of simulations is required to reach the desired level of accuracy. Especially for complex models, which if often the case for morphodynamic Delft3D models, this results in unpractical long computation times (Van Maren and Cronin, 2016). Lowering the number of performed simulations, decreases the accuracy of the assessment and is therefore often not favourable.

To reduce the amount of simulation needed, however without losing the accuracy of the analysis, alternative techniques have been developed. These methods aim to reduce the variance (statistical errors in the MC-analysis) in the outcome and are therefore called *variance reduction techniques*. In this study importance sampling, a Bayesian network, stratified sampling and Latin Hypercube Sampling are discussed.

Importance sampling

Importance sampling is a variance reduction technique which aims to generate more sampling points of interest in the area of interest (as indicated by the name). This method is particularly interesting if the area of interest is in the tail of a distribution. During a MC-analysis, not many points in the area of interest are generated, which means an unpractical large amount of simulations needs to be performed to arrive at accurate results. In this case, by means of Importance Sampling, emphasis is placed on the area of interest by generating more samples in this region.

An example of application of Importance Sampling is shown in Figure 2.9, for the reliability assessment of a structure (Jonkman *et al.*, 2017). Since the probability of failure (i.e., limit state function: $Z < 0$) is typically small, the probability density functions are adjusted such that important

values are emphasized. In this way otherwise infeasible problems are amenable to Monte Carlo simulations (Owen and Basu, 2018).
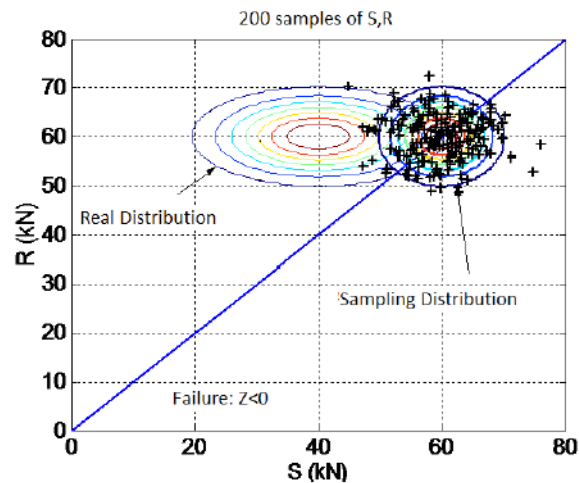

Figure 2.9: Importance sampling (Jonkman *et al.*, 2017). The limit state function is illustrated by the blue line, failure occurs for Z<0 (underneath the blue line, the limit state function)

Bayesian network

A Bayesian network can be displayed as a series of nodes and links between the different nodes. Each node is visualizing a variable (continuous or discrete). The link between the different nodes indicates that they influence each other. If no direct link between two variables exists, it does not mean that they are independent, since they may be connected via another way. This also underlines the difference between a Bayesian network and an Neural Network in which not all nodes are related (Kroon *et al.*, 2017).

Discrete variables are most easy to include in the Bayesian network, since the relations are relatively easy to calculate by means of probabilistic rules. It is however more difficult to make a Bayesian network for continuous distributions, of which the Gaussian (normal) distribution is often applied. A continuous function can be supported in a Bayesian network by means of a Conditional Linear Gaussian distributions (CLG). Figure 2.10 shows an example of a Bayesian network, with both continuous and discrete variables. For morphological modelling, a Bayesian Network is not suitable since not all variables are directly related and other relations are not possible to map due to the model complexity.
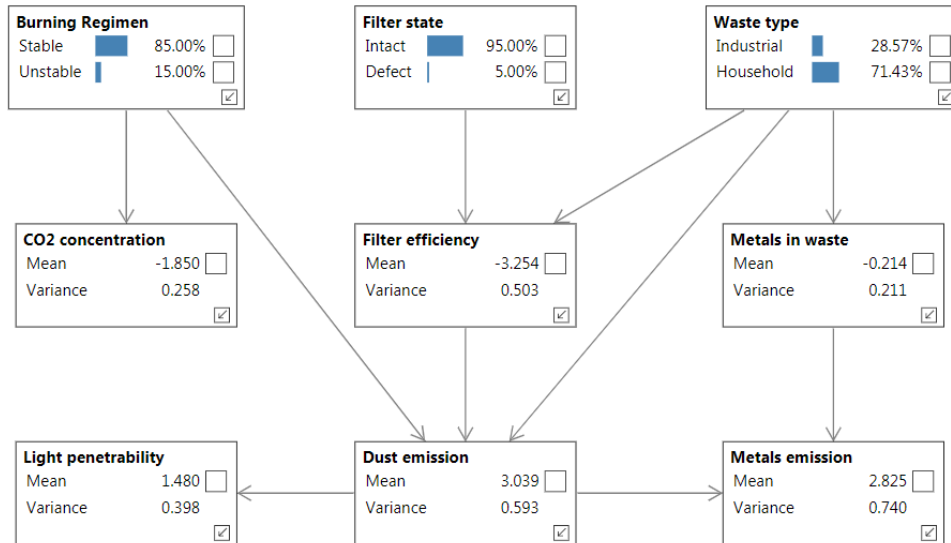
Figure 2.10: An example of a Bayesian Network, with both continuous and discrete variables (Bayes server, 2019).

Stratified sampling

During stratified sampling, the sample space is divided into *M* subsets of equal probability. For each parameter, one value is randomly selected in each subset. In stratified sampling, the different parameter values are combined, leading to a total of N^M simulations. It is clear that the more (and hence smaller) subsets are used, the more accurate the results are, although it is computationally more demanding. For illustrative purposes, in Figure 2.11 (left) the stratified sampling method is shown for 2 parameters (Hurtado and Barbat, 1998).

This also emphasizes the difference between a MC-analysis and stratified sampling: an MC-analysis is a memoryless approach in which the next simulation is not dependent on the input of previous simulations. Stratified sampling however does consider previous simulations, since the combinations of subsets of different parameters can only be used once.

Latin Hypercube Sampling

Latin Hypercube Sampling (LHS) can be seen as a form of stratified sampling. When dividing the sample space again into M subsets of equal probability when considering N parameters, one value is randomly selected for all subsets. However, this time the number of simulations is even further reduced. During one simulation, for each parameter one of the values is selected. Only now if a subset is used for a parameter, it is discarded for the other simulations. In this way the number of simulations during LHS is restricted to *M*. A schematization of this approach can be found in Figure 2.11 (right) (Hurtado and Barbat, 1998). A special case of LHS is Midpoint LHS, in which each variable takes the value of the median of each equal probability interval.
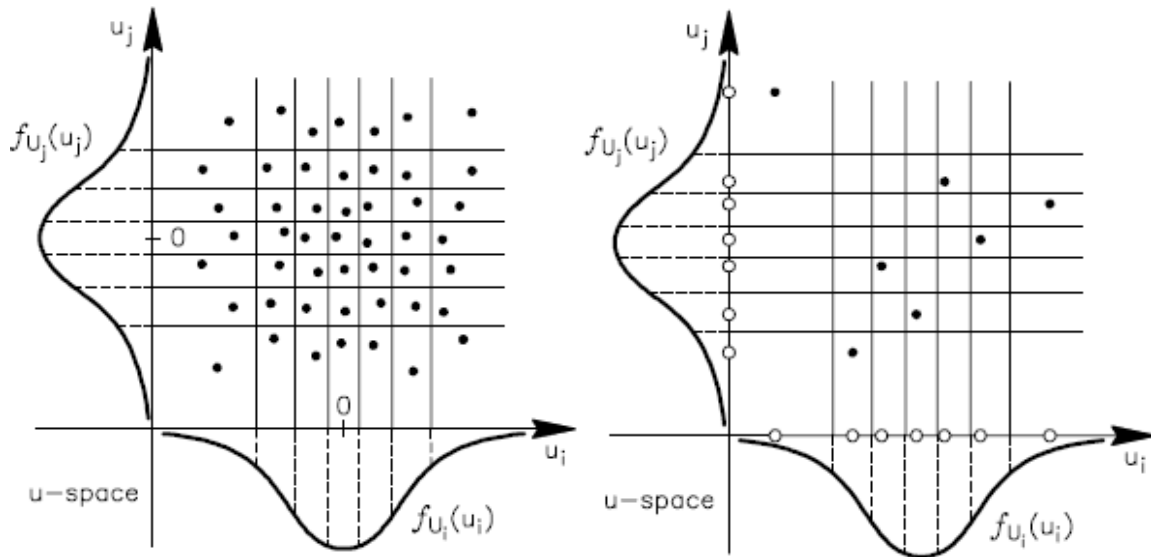
Although LHS is applicable for independent variables, Packham and Schmidt (2008) proposed a method to include dependencies in the LHS method. Furthermore, Iman and Conover (1982) described a way to include correlations, by choosing the hyperplanes such, that this correlation coefficient is the same as the correlation coefficient of the original sampled size.

A drawback of Latin Hypercube Sampling is that it is not possible to predict upfront how many subsets are needed to reach convergence in this method. Moreover, in LHS new subsets cannot simply be added since stratification is not maintained. However, Sallaberry et al. (2008) developed a method to extend the amount of samples while correlations are taken into account. In this method, the original LHS-sample of size *s* is extended to *2s* in which the rank coefficient of the extended sample, is close to the original rank correlation matrix C. Enschedé (2019) describes the procedure as follows:

- Generate a Latin Hypercube Sample with size *s*
- Select a second set of Latin squares (see Figure 2.12)
- Divide all squares in 4 sub-squares
- In the previous selected squares, a sub square is present with no sample in its row and column. From each of these sub squares, one sample is selected.

A schematization of this method can be found in Figure 2.12. Important to reminder is that it cannot be applied with Midpoint LHS.
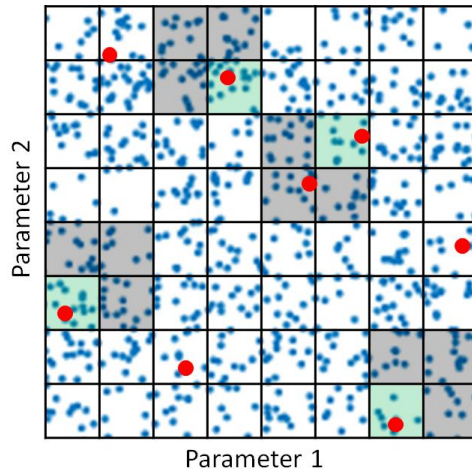
Figure 2.12: Extension of LHS (from 4 subsets to 8 subsets), while maintaining the properties (Enschedé, 2019). The red dots specify the specific cases for the different sub squares (gray and green areas)

2.3.4 Conclusion

Not all methods discussed are suitable for the probabilistic assessment in this study. A summarization of the methods and their applicability to assess trench sedimentation can be found in this part.

The MC-analysis is considered to be the most accurate method, since the other methods are variance reduction methods from the MC-analysis. However, due to the amount of simulations needed, the MC-analysis is only applicable to SedPit, the 2DV-model is too computationally demanding

Importance sampling is not suitable since the focus of this study is not on the tails of the distribution, which is the working range for this method. Furthermore, a Bayesian network is too complicated for complex models, meaning that this method cannot be applied in combination with the 2DV-model. Lastly, in stratified sampling the number of required simulations increases exponentially for extra variables and is therefore not suitable in this study.

LHS on the other hand could be an effective way for reducing the required iterations, although it is not possible on predict on forehand the amount needed. Furthermore, a method to implement relations between different variables by means of correlation coefficient seems to be promising. Therefore, LHS is applied on the 2DV models. A summary of the different uncertainty methods on the three models, is shown in Table 2.2.

Table 2.2: Summary of the applicability of the different probabilistic assessment methods on the two models used in this study. A '+' indicates a good applicability, while'-' means the method is not suitable.

Method	1D-SedPit	2DV-model
Monte Carlo analysis	+	-
Importance sampling	-	-
Bayesian network	-	-
Stratified sampling	+	-
Latin Hypercube Sampling	+	+

3 System analysis

In this chapter, an analysis of the relevant conditions at the site is discussed. This involves wind and wave statistics, the bathymetry and data on water levels and grain sizes. At first however, more information on the data collection is provided. Before zooming in on the wave, current and wind characteristics of the month April, this chapter provides an overview of the yearly conditions, since this also helps in the discussion of the results afterwards.

3.1 Data collection

For wind and wave data, the measurements at the Euro Platform, located 35 kilometres North East of the Borssele Wind Farm Zone (BWFZ), are used. Data from stations closer to the BWFZ was not available for suitable time ranges and therefore not used. For the Euro Platform, wind and wave data was available for the period 1997-2016. Furthermore, at this station the amplitude and phases of different tidal constituents are known. Bathymetry information is available from EMODnet. Soil characteristics are determined by Fugro (2015a, 2015b) for various locations in the BWFZ. Current information was collected with a buoy deployment in the BWFZ during a period of June 2015 and March 2017. An overview of the area considered, in which the locations of various measurement stations are shown, can be found in Figure 3.1. A summary of all available data, is provided in Appendix A.1.
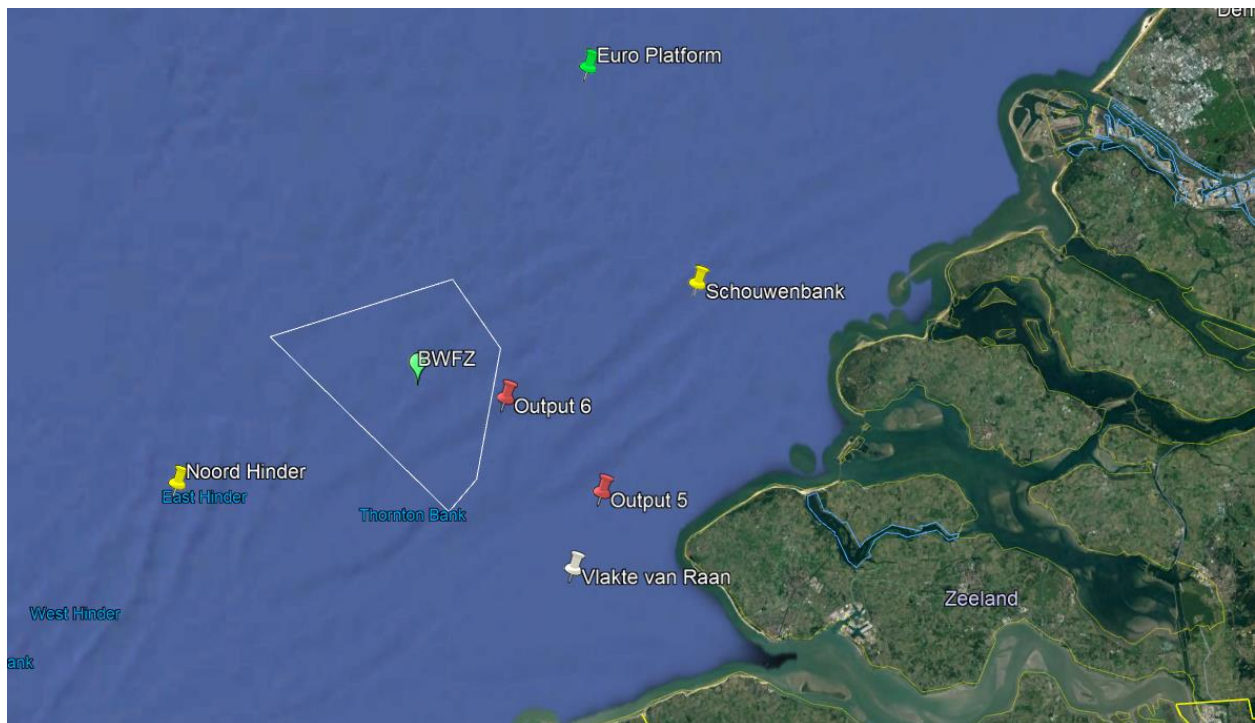

Figure 3.1: An overview of the Borssele Wind Farm Zone. Wave and wind data are available from the Euro Platform (green pointer). The red markers show the output locations which are modelled in the study of Svasek Hydraulics (2016). Wind data (white pointer) and tidal data (three constituents, yellow pointers) are also available at other locations closer to the BWFZ.

3.2 Bathymetry

At the BWFZ the water depth is around 30m. As can be seen in Figure 3.2, the water depth differs significantly throughout the domain. The largest water depths can be found at site IV, varying from 30-40 meters in general. More to the South East (Site II), water depths decrease to 17-35m. The trench is located between site I and II/III (see Figure 1.2), with water depths between 17 and 40m. It can also be clearly seen that the bathymetry is characterised by sand banks, sand waves and (mega) ripples. The sand banks are orientated oblique to the current direction, with large amplitude. Furthermore, sand waves can be identified as a perpendicular directed bedform, with a smaller amplitude, all in correspondence to literature (see Chapter 2.2). The smallest perturbations visible are the mega ripples.
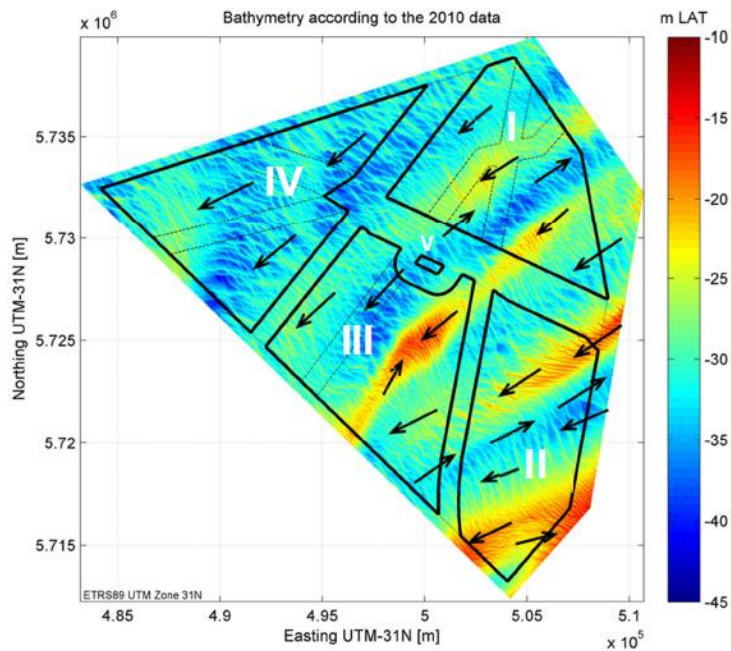
Figure 3.2: Bathymetry of the BWFZ (Deltares, 2015a). The migration direction of the sand waves are indicated by the black arrows.

The morphological changes of interest around the BWFZ, are governed by the sand wave dynamics: the sand wave growth and the sand wave migration. The black arrows in Figure 3.2 show the migration direction of the sand waves, which is mainly perpendicular to the trench orientation (see Figure 1.2). The median migration rate is around 0.3 m/year. The 10-90% non-exceedance rate is +/- 1.5 m/year (in North East of South West direction).

Throughout the domain of interest, the sand wave dimensions differ, although the wavelength is around 250-300m long, with an medium sand wave height of 4m, as indicated in Figure 3.3. Furthermore, it can be observed that with an increasing amplitude, the sand wave length tends to increase as well, which reduces the differences in the slopes. This analysis must be taken into account when investigating the influence of sand waves on trench infill later on. More detailed information on the (distribution of) the sand wave height and length is provided in Appendix A.3.

Figure 3.3: Sand wave length [m] (left) and sand wave height [m] (right) throughout the domain. (Deltares, 2015b)

3.3 Soil characteristics

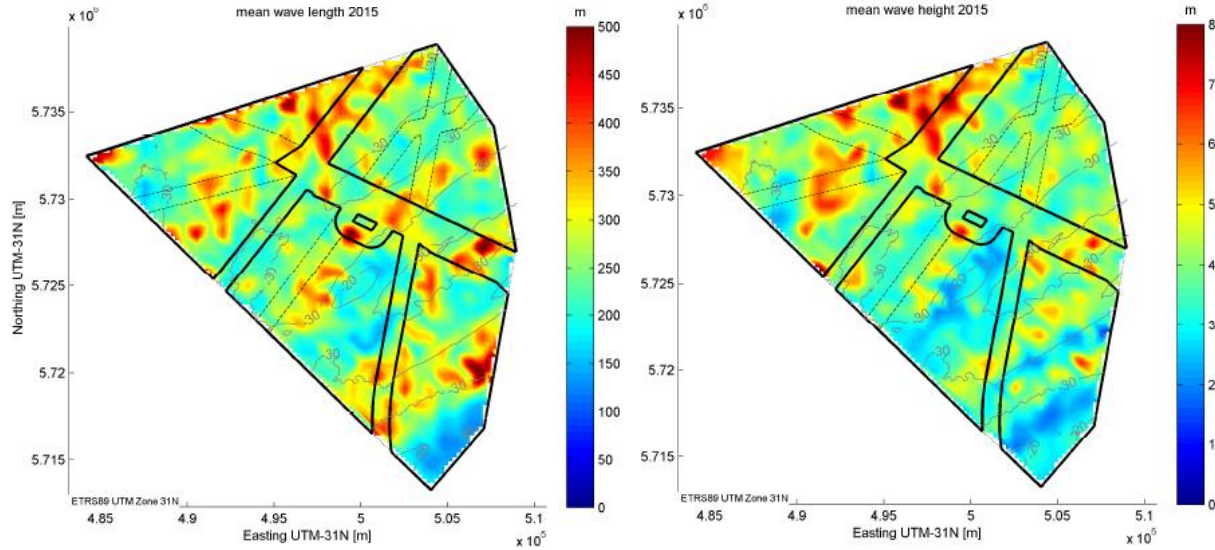During the geotechnical investigation in the BWFZ several boreholes were drilled to determine the local soil characteristics. The results are summarized in Fugro (2015a, 2015b). In this study, the soil type and the corresponding grain size distributions are of interest. During sieve tests, the grain size distributions were determined at various depths (1 to 60m) for each borehole. Generally, it was found that the deepest layer consists of fine material (silt and fine sand) covered by coarser material (medium sand) closer to the seabed. However, several boreholes also indicated the existence of limited percentages of gravel at large depths. Near the seabed the soil was more uniformly graded.

Since in this study the affected region during trench sedimentation is limited to the upper part of the seabed, only the measurements of the 5m closest to the seabed are taken into account. Sieve analysis shows that the d_{50} is typically between 0.25 and 0.3mm, with a minimum and maximum d_{50} of 0.1mm and 0.4mm respectively. Furthermore 95% or more of the soil can be classified as poorly graded sand.

3.4 Wave analysis

For the wave analysis, a distinction is made between the averaged wave climate and extreme events. Over 20 years, the hourly averaged significant wave height is 1.25m, which results in an average wave height of 0.8m, using the relation $\bar{H} = 0.63H_s$ (Bosboom and Stive, 2015). Furthermore, an averaged wave period T_2 of 4.4s could be found. With the lack of more information, the peak period is assumed to be $T_p = 1/0.7T_2 = 6.2\ s$ (Bosboom and Stive, 2015).

Besides this, the directional spreading of the waves has to be considered. In Figure 3.4 the wave rose near the Euro Platform is shown. In general, waves are arriving from the South-West and North, North-West. Main swell waves originate from North, North-West directions.
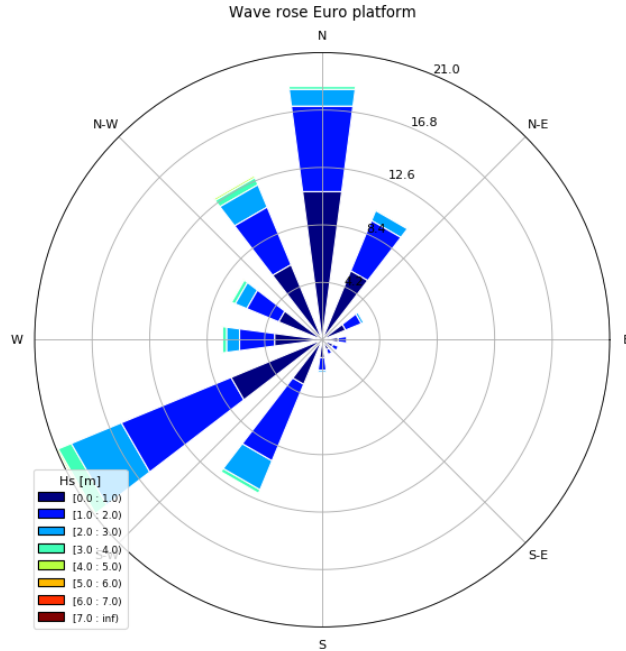
Figure 3.4: Wave rose at the Euro Platform.

A joint occurrence table of the wave direction and significant wave height can be found in Table 3.1.

Table 3.1: Joint occurrence table of the wave height and wave direction.

Wave direction [deg N]

	345-15	15-45	45-75	75-105	105-135	135-165	165-195	195-225	225-255	255-285	285-315	315-345	
6.0-6.5	0.00	0.00	0.00	0.00	0.00	0.00	0.00	0.00	0.00	0.00	0.00	0.00	0.00
5.5-6.0	0.00	0.00	0.00	0.00	0.00	0.00	0.00	0.00	0.00	0.00	0.00	0.00	0.01
5.0-5.5	0.00	0.00	0.00	0.00	0.00	0.00	0.00	0.00	0.01	0.01	0.01	0.01	0.04
4.5-5.0	0.01	0.00	0.00	0.00	0.00	0.00	0.00	0.01	0.04	0.02	0.02	0.05	0.14
4.0-4.5	0.03	0.00	0.00	0.00	0.00	0.00	0.00	0.02	0.09	0.03	0.05	0.12	0.35
3.5-4.0	0.06	0.01	0.00	0.00	0.00	0.00	0.00	0.06	0.30	0.11	0.11	0.20	0.86
3.0-3.5	0.16	0.06	0.00	0.00	0.00	0.00	0.01	0.23	0.78	0.22	0.19	0.38	2.04
2.5-3.0	0.38	0.18	0.04	0.00	0.00	0.00	0.02	0.65	1.58	0.36	0.34	0.66	4.22
2.0-2.5	0.88	0.62	0.16	0.02	0.02	0.03	0.11	1.66	2.53	0.62	0.62	1.08	8.35
1.5-2.0	1.91	1.32	0.42	0.15	0.08	0.07	0.24	2.78	3.74	0.93	1.00	1.82	14.47
1.0-1.5	4.48	2.71	0.81	0.45	0.29	0.26	0.62	3.32	5.16	1.55	1.48	2.74	23.85
0.5-1.0	7.52	3.83	1.28	0.80	0.57	0.47	0.90	2.88	5.51	1.99	1.82	3.64	31.20
0.0-0.5	3.72	1.72	0.55	0.32	0.22	0.22	0.25	0.59	1.78	1.36	1.41	2.34	14.47
	19.17	10.46	3.25	1.74	1.19	1.04	2.14	12.19	21.52	7.20	7.06	13.04	100.00

Significant wave height [m] (vertical axis label)

For short term wave analysis, the significant wave height is usually Weibull distributed (Bosboom and Stive, 2015), of which the cumulative distribution is given by:

$$P_{CDF,Hs} = 1 - \exp\left(-\left(\frac{H_s}{\lambda}\right)^k\right)$$

The best fit resulted in $\lambda = 1.41$ (scale parameter) and $k = 1.70$ (shape parameter). The cumulative distibution function of the estimated Weibull distribution and the measurements of the

significant wave height are shown in Figure 3.5 (left). The calculated peak periods are assumed to be normally distributed with a best fit of $\mu = 6.08$ and $\sigma = 1.04$. The cumulative distribution function of the peak period can be found in Figure 3.5 (right).
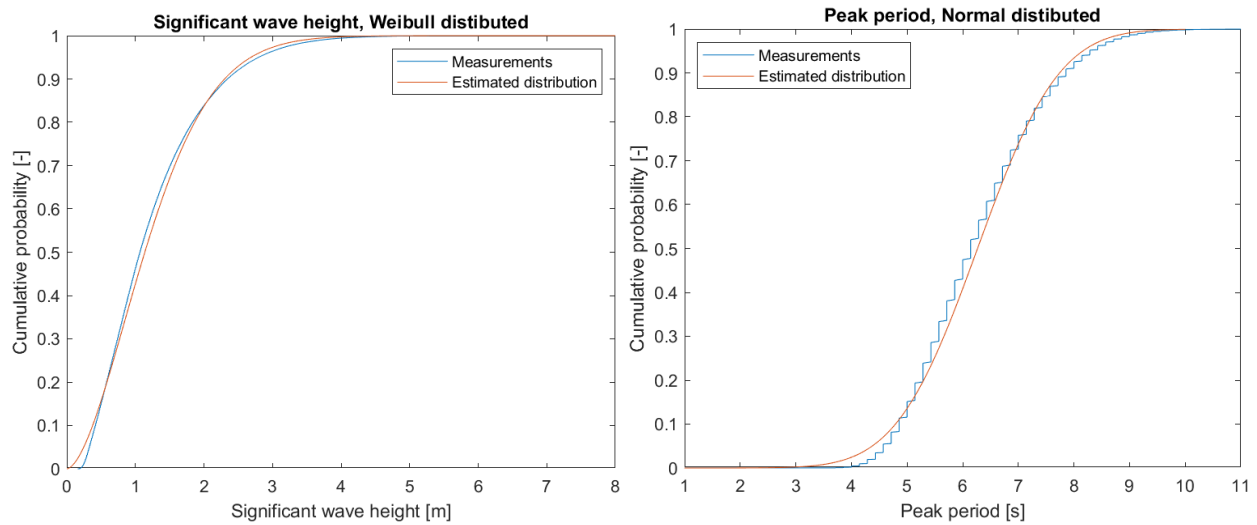
Figure 3.5: Fitted and measured cumulative distribution function of the significant wave height (left) and the peak period (right).

Relation between peak period and significant wave height

It is expected that the wave periods and wave heights are related. To investigate the relation, both parameters are plotted in Figure 3.6. As can be seen, there is a clear relation between the significant wave height and peak period. The calculated correlation coefficient is 0.77.
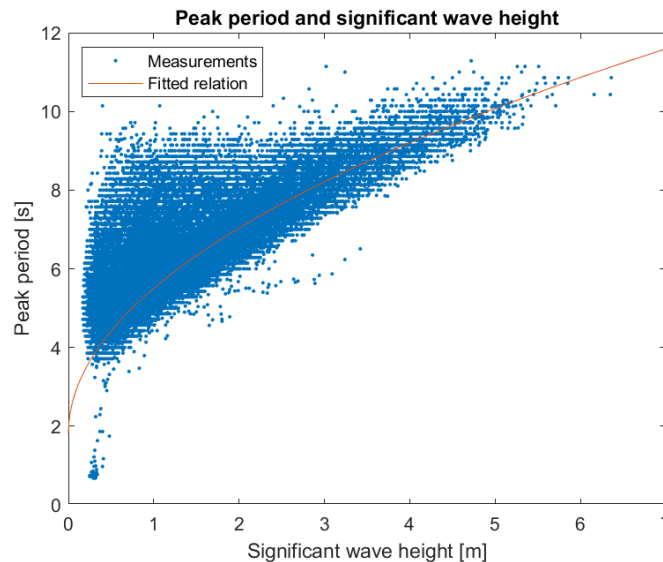
Figure 3.6: Significant wave height [m] and corresponding peak periods [s].

3.5 Wind

Besides the wave measurements, also wind measurements are available from the Europlatform for a period of 20 years. A mean hourly averaged wind speed of 7.8m/s was found. Winds mostly originate from (South-) West directions, see Figure 3.7.

Figure 3.7: Wind rose at the Euro Platform [m/s] over a period of 20 years.

The joint occurrence table for wind speed and wind direction at the Euro Platform can be found in Table 3.2.

Table 3.2: Joint occurrence table wind speed and wind direction based on 20 years.

Wind direction [deg N]

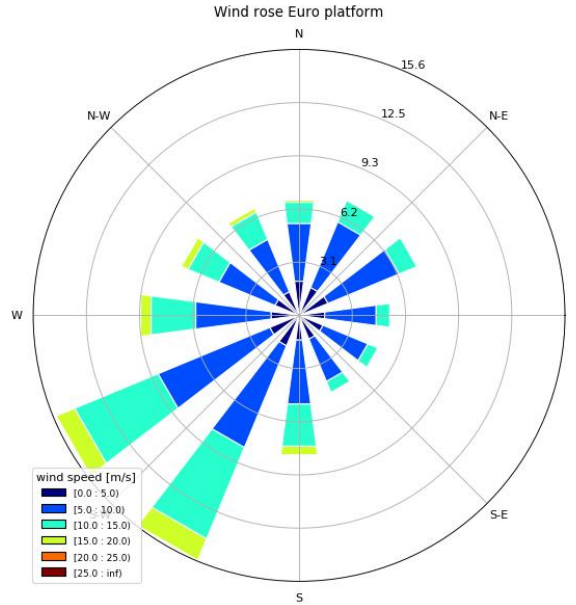| Wind speed [m/s]	345-15	15-45	45-75	75-105	105-135	135-165	165-195	195-225	225-255	255-285	285-315	315-345	
27.5-30.0	0.00	0.00	0.00	0.00	0.00	0.00	0.00	0.00	0.00	0.00	0.00	0.00	0.00
25.0-27.5	0.00	0.00	0.00	0.00	0.00	0.00	0.00	0.00	0.00	0.00	0.00	0.00	0.00
22.5-25.0	0.00	0.00	0.00	0.00	0.00	0.00	0.00	0.00	0.01	0.00	0.00	0.00	0.02
20.0-22.5	0.00	0.00	0.00	0.00	0.00	0.00	0.03	0.06	0.06	0.04	0.02	0.01	0.21
17.5-20.0	0.00	0.00	0.00	0.00	0.00	0.00	0.06	0.20	0.14	0.08	0.07	0.04	0.60
15.0-17.5	0.03	0.05	0.01	0.04	0.03	0.06	0.47	1.19	1.06	0.55	0.36	0.23	4.07
12.5-15.0	0.06	0.20	0.19	0.19	0.11	0.15	0.74	1.88	1.54	0.81	0.50	0.46	6.82
10.0-12.5	0.33	1.18	1.03	0.65	0.59	0.60	1.86	4.18	3.89	1.89	1.52	1.33	19.04
7.5-10.0	0.50	1.61	1.72	1.04	0.93	1.00	1.67	2.97	3.31	1.87	1.48	1.31	19.42
5.0-7.5	0.83	2.78	3.07	2.21	2.03	1.83	2.31	3.79	4.01	2.74	2.20	2.11	29.89
2.5-5.0	0.40	1.30	1.34	1.12	1.10	1.08	1.05	1.46	1.39	1.19	1.09	1.08	13.60
0-2.5	0.53	0.53	0.59	0.49	0.49	0.50	0.50	0.58	0.57	0.53	0.51	0.49	6.32
	2.68	7.65	7.95	5.73	5.28	5.23	8.68	16.31	15.99	9.71	7.75	7.04	100.00

Wind Speed, Weibull distibuted
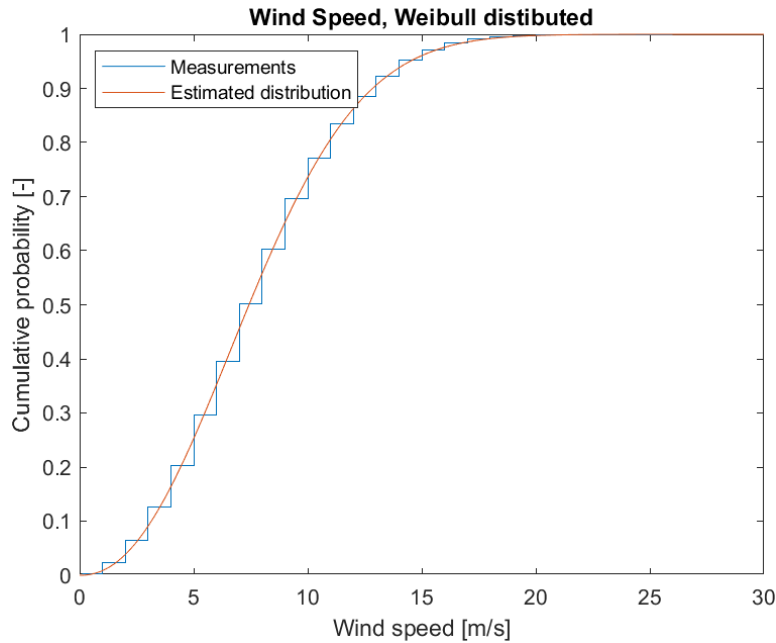
Figure 3.8: Cumulative distribution of the wind speed at the BWFZ.

The wind speed is, similar to the significant wave height, assumed to be Weibull distributed. The characteristic scale parameter $\lambda = 8.78$ and shape parameter $k = 2.19$. Furthermore, wind speed and wave height are obviously related. A correlation coefficient of 0.77 was found between those variables.

3.6 Tides

Near the Euro Platform, the tide is dominated by semi-diurnal constituents. This can be calculated by means of the form factor F, which is the ratio between the sum of the two main diurnal constituents and the sum of the two main semi-diurnal constituents (Bosboom and Stive, 2015):

$$F = \frac{K1 + O1}{M2 + S2}$$

For the Euro Platform the following amplitudes of the tidal constituents are known:

$$F = \frac{0.08 + 0.11}{0.74 + 0.18} = 0.21$$

Since the influence of the diurnal constituents K1 and O1 is quite significant, a relatively large daily inequality can be observed, although the tide can be characterised as semi-diurnal. An overview of the tidal constituents with an amplitude larger than 0.05m is shown in Table 3.3.

Furthermore, tidal asymmetry is caused by the interaction between the M2 and M4 tide. Since the phase difference between these two tidal constituents is $\phi_{M4} - 2\phi_{M2} = 128 - 2 * 54 = 20°$, the tidal signal can be characterised as positively skewed. This means the difference between the MSL and high water is larger than the difference between low water and MSL (Bosboom and Stive, 2015).

Tidal constituent	Description	Angular velocity [deg/hr]	Amplitude [m]	Phase [deg N]
M2	Principal lunar semidiurnal constituent	28.984	0.74	54
S2	Principal solar semidiurnal constituent	30.000	0.18	110
N2	Larger lunar elliptic semidiurnal constituent	28.440	0.12	26
O1	Principal lunar diurnal constituent	13.943	0.11	184
M4	Shallow water overtide of principal lunar constituent	57.968	0.10	128
SA	Solar annual constituent	0.041	0.09	213
K1	Lunar-solar declinational constituent	15.041	0.08	358
MS4	Shallow water quarter diurnal constituent	58.984	0.07	182
MU2	Variational constituent	27.968	0.06	179
2MN2	Shallow water interaction between M2 and N2 constituents	29.528	0.06	259
K2	Lunisolar semidiurnal constituent	30.082	0.05	112

By analysing the 11 main tidal constituents, the following tide levels were found at the BWFZ in Deltares (2015).

Table 3.4: Averaged tide levels derived from the BWFZ water levels relative to MSL and LAT. The levels are rounded to the nearest 0.05m (Deltares, 2015)

Tide level	Relative to MSL [m]	Relative to LAT [m]
Highest Astronomical tide (HAT)	1.90	3.40
Mean High Water Spring (MHWS)	1.45	2.95
Mean High Water Neap (MHWN)	0.85	2.35
Mean Water Level (MSL)	0.00	1.50
Mean Low Water Neap (MLWN)	-0.85	0.65
Mean Low Water Spring (MLWS)	-1.15	0.35
Lowest Astronomical Level (LAT)	-1.50	0.00

3.7 Currents

Current information is obtained by the deployment of a buoy in the BWFZ over a period between June 2015 and March 2017. From half September till half November 2015 and half December 2015 till February 2016 no measurements are available due to broken equipment. The depth averaged current speed during this period, is visible in Figure 3.9.
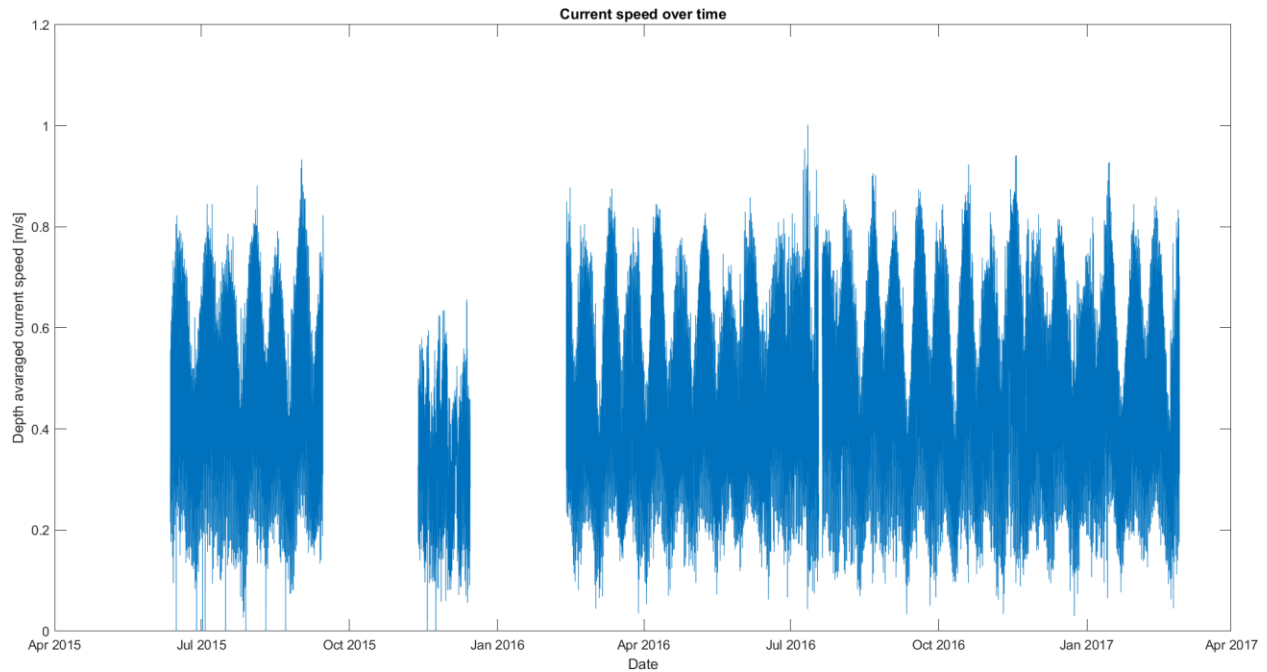
Figure 3.9: Depth averaged current speeds [m/s] from April 2015 to April 2017. The absence of measurements are indicated by the gaps.

Current in the BWFZ are mainly South East (eb) and North West (flood) directed, with typical current velocities between 0.5 and 0.8 m/s. The amplitude of the current velocity differs over time due to a spring-neap cycle. Figure 3.10 shows the current rose made based on all available data.

Figure 3.10: Current rose at the BWFZ [m/s].

4 SedPit

This chapter discusses the expected trench sedimentation when using the most reduced complexity model SedPit. The non-deterministic model input, categorized by type, can be found in Chapter 4.2. This section also discusses of the model set-up. Hereafter, a sensitivity analysis is performed to determine the most influential parameters (Chapter 4.3). After discussing the trench sedimentation computed by SedPit in Chapter 4.4, Chapter 4.5 pays special attention on a representative modelling of current and wave conditions. In Chapter 4.6, conclusions are drawn.

4.1 Introduction

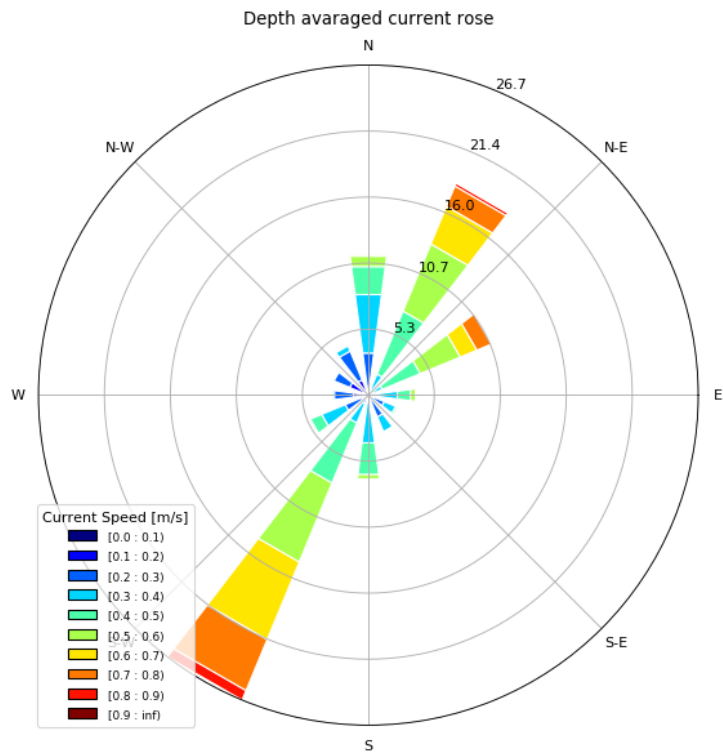SedPit is the most reduced complexity model considered in this case study. SedPit is a tool developed by Van Rijn (2013) to assess trench or channel siltation using simple relations, based on the mechanics discussed in Chapter 2.1. Although more sophisticated morphological models need to be used for complex situations, SedPit does provide insight in the magnitude of sedimentation to expect.

As discussed in the methodology, the goal of this chapter is to probabilistically assess trench sedimentation by means of a Monte Carlo analysis. To do so, a distinction in the input variables is made between intrinsic and epistemic uncertainty. Furthermore, this chapter focusses on the representation of the wave climate and the tidal currents. SedPit provides the opportunity to use a full set of hourly wave and current data of the period over which the sedimentation is calculated. However, for more complex models, this needs to be simplified. To do so, at first a representative year is selected, where after simplifications to a single wave and tidal current condition is made. Results obtained during this analysis can be used as base for a more detailed research with the 2DV-model.

4.2 Model input

The different (input) variables of SedPit are divided into two categories: parameters related to the intrinsic uncertainties in time and epistemic uncertainties, in accordance with Kroon *et al.* (2019). During this analysis it is assumed that between these categories no relation exist, and the parameters can therefore be considered as independent. Some parameters within one category are on the other hand dependent. Figure 4.1 provides an overview of the non-deterministic variables per category. In Appendix B, all input variables are summed up, including the underlying equations of SedPit.

4.2.1 Intrinsic uncertainties in time

For the intrinsic uncertainties in time, a distinction is made between current related variables and wave related variables. When using SedPit, it is assumed that they are independent from each other. The effect of wind cannot be taken into account directly and is therefore not considered in this analysis.
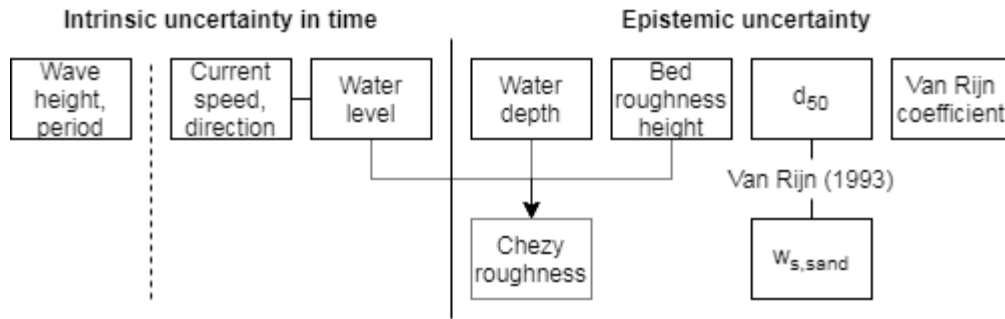
Figure 4.1: Considered variables and relations of SedPit. The forcing can be identified as intrinsic uncertainty and the epistemic uncertainties are related to the model itself. The lines indicate a dependency between the variables.

Wave climate April

As mentioned in Chapter 3.1, 20 years of wave data is available. In contrast to Chapter 3.4, not a full year is considered, but only the month April. Furthermore, the assumption is made that there is statistically no difference in wave climate between the beginning and end of the month.

From the available 20-years of wave data, in Figure 4.2 (left), the cumulative distribution of the significant wave height of the month April is shown. The best fit for a Weibull distribution through the data is plotted as well. The corresponding properties are: $\lambda = 1.09$ (scale parameter) and $k = 1.74$ (shape parameter). As expected, the wave climate in April is milder than the yearly wave climate ($\lambda = 1.09$ instead of $\lambda = 1.41$). Figure 4.2 (right) shows the corresponding distribution of the peak periods.

When analysing the years separately, it was found that the year 2003 and 2015 are the most representative years of the 20 years data set. This is based on the best Weibull fit of the wave heights for both years. Both years are also shown in Figure 4.2. However, based on the underlying model equations, discussed in previous section, not only the wave height is of influence, but the corresponding peak periods as well. Since two variables are considered, with both an own distribution, it is not possible to select the most representative year upfront. Therefore selecting a representative year to simulate the wave climate is not done based on this analysis, but the computed sedimentation, which is discussed in Chapter 4.4.
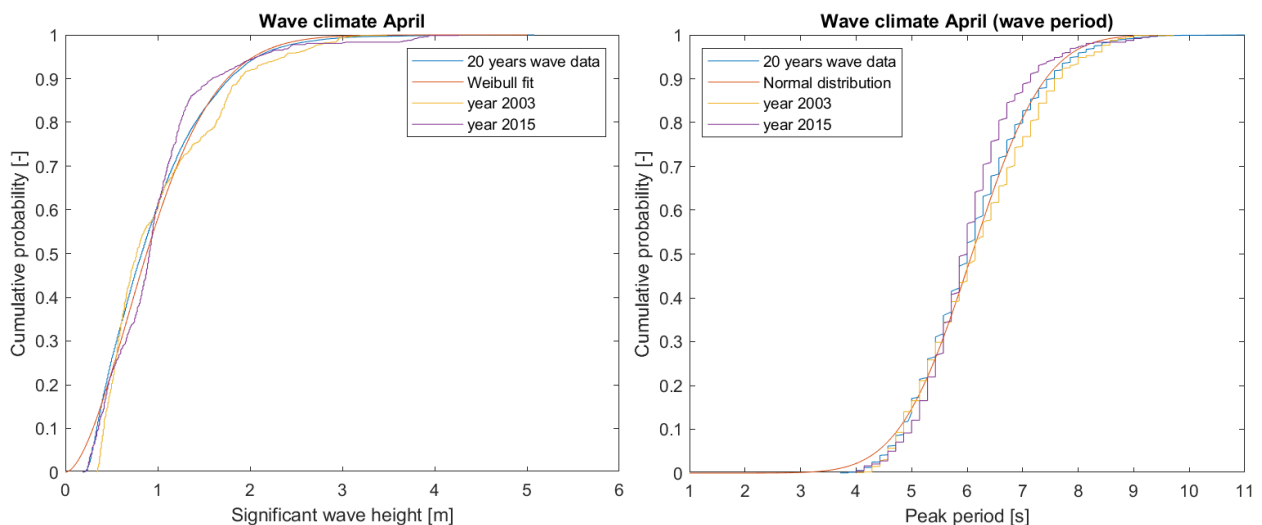

Figure 4.2: Cumulative distribution function significant wave height [m] and period [s] in April .

34

Currents and water levels

Current data is, as mentioned in Chapter 3.7, not available for the same period as the wave data. For the month april, only measements are available in 2016. Therefore, it is chosen to focus on this dataset. In the graph, a clear spring neap cycle is visible, which corresponds to the analysis of the tidal constituents in Chapter 3.6, indicating a semi-diurnal tide with large daily inequalities. The water levels are computed based on the same section.
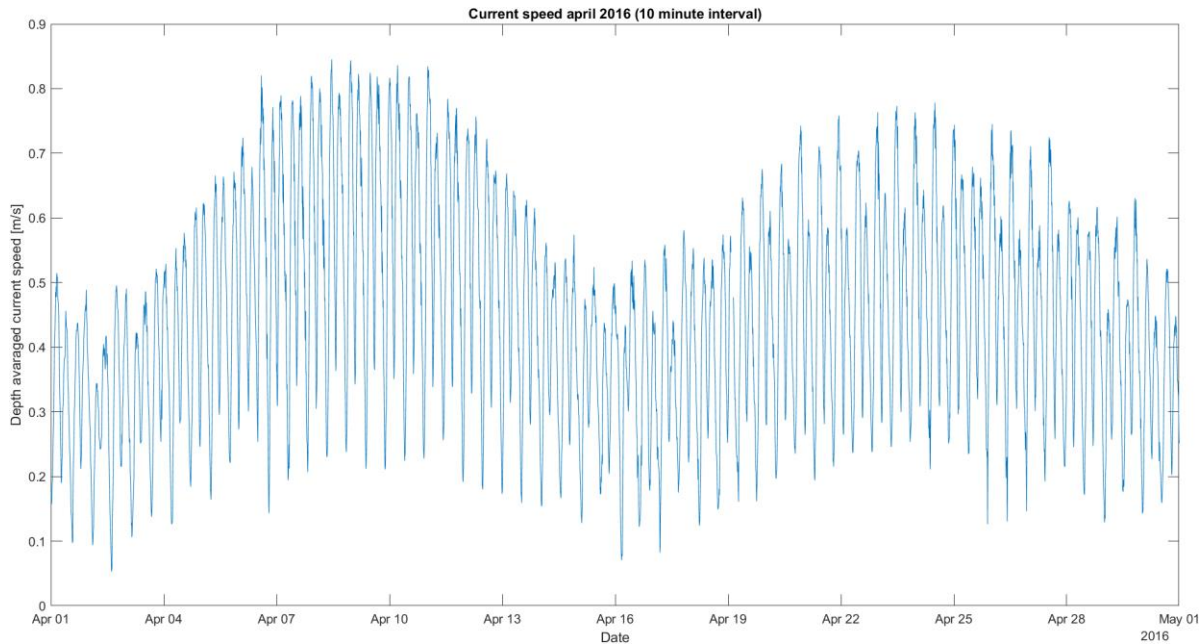

Figure 4.3: Current speeds in April 2016. Spring tide occurs around April 9. and 23., neap tide around April 2. and 16..

Similar to data analysed in Chapter 3.7, the tidal currents are mostly North East and South West directed.

4.2.2 Epistemic uncertainty

Epistemic uncertainties do not change over time and are often location dependent. As indicated in Figure 4.1, 5 different variables are considered in this category: water depth, bed roughness height, the (median) grain size, the Van Rijn coefficient and the Chezy roughness. Between these parameters some relations exist: the setting velocity is depended on the grain size, and the water depth and bed friction are related as well.

The Chezy roughness is used as measure of the bed friction. However, it is no input variable itself: it is determined by the bed roughness height, the water depth and the water level. It is assumed that the roughness height is independent and triangular distributed between 0.01 and 0.30m, with a mode of 0.10m.

According to Fugro (2015a, 2015b), sand fractions in the upper part of the sea bottom exist for more than 96% of sand fractions (from 0 to -5m). Therefore, during modelling, it is assumed that the soil consists of sand only. Based on 19 different sieve analysis, the d_{50} is estimated to be triangular distributed between 0.15mm and 0.40mm, with a mode of 0.27mm. Appendix B.2.1, shows the cumulative distribution function of the measurements and the fitted distribution.

For the relation between the grain size and the settling velocity, Van Rijn (1993) provided the following relation:

$$w_s = \frac{10\nu_w}{d}\left(\sqrt{1 + \frac{0.01(\rho_s/\rho_w - 1)gd^3}{\nu_w^2}} - 1\right)$$

In which:

- ν_w: water viscosity
- d: grain size diameter
- ρ_s: density water
- ρ_w: density soil particles

In this case, the settling velocity is determined for the median grain size diameter. The median grain size is the only non-deterministic parameter in this equation. This means, the settling velocity follows a triangular distribution as well. The mode of the distribution, corresponds to the mode of the median grain size, with a settling velocity of 0.043 m/s.

The water depth d_0 (which is the difference between MSL and the sea bottom) in the area of interest is around 31m, with variations between 17 and 40. Due to the large amount of datapoints, no estimation of a distribution is made, but the original data is used during the analysis. A cumulative distribution function of the water depth can be found in Appendix B.

Lastly, according to Van Rijn (2013), the Van Rijn coefficient varies between 0.1 and 0.4. In this case a triangular distribution between 0.1 and 0.4 is assumed with a mode of 0.4, since a high trapping efficiency is likely due to the mostly occurring cross flow conditions. All assumptions are summarized in Table 4.1.

Table 4.1: Parameter overview with corresponding minimum, maximum and base case values, with the corresponding distributions. The settling velocity is related to the median grain size, using the formulation of Van Rijn (1993). The parameters are again categorized in time varying parameters and, model settings.

Parameter			Distribution	Minimum	Base case	Maximum
Significant wave height	H_s	[m]	Weibull	0.19	1.09	5.08
Peak period	T_p	[s]	-	3.7	6.0	11.2
Current velocity	U_c	[m/s]	-	0.08	0.50	0.82
Flow angle	α	[deg N]	-	12	72	90
Water level	wl	[m]	-	-1.15	0.00	1.27
Water depth	d_0	[m]	-	17.0	31.0	40.0
Roughness height	k_s	[m]	triangular	0.01	0.10	0.30
Median grain size	d_{50}	[mm]	triangular	0.15	0.27	0.40
Van Rijn coefficient	C_{vRijn}	[-]	triangular	0.10	0.40	0.40
Settling velocity	$w_{s,sand}$	[m/s]	Van Rijn (1993)	0.037	0.043	0.050

4.2.3 Trench dimensions

The trench dimensions are formed by the trench width, depth and orientation with respect to the tidal currents. As mentioned in literature (Van Rijn, 2013), largest trench sedimentations can be expected for cross channel flow (i.e. a flow angle of 90° compared to the main axis of the trench). When looking to the trench alignment in Figure 1.2, the trench main axis is situated at the 120-300° N line, which means cross flow is mostly occurring.
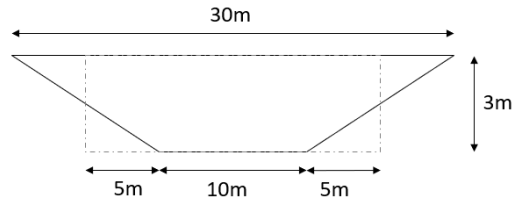
Figure 4.4: The cross-section of the trench considered in this study. The rectangular shaped trench of 20x3m is the schematization for trenches in SedPit.

Based on Boskalis (2017), the trench is in total 30m wide, including two side slopes over a horizontal distance of 10m. In the middle, the trench is 3m deep. In SedPit, the trench is schematized as a triangular cross-section of 20m wide, and 3m deep. Since the trench dimensions are deterministic, they cannot be found in Figure 4.1 and Table 4.1.

4.3 Sensitivity analysis

At first a sensitivity analysis is used to determine the sensitivity of a single parameter. This is done by means of the one-at-a-time (OAT) approach, in which parameters are varied separately. The advantage of this method is that the effect of each individual parameter on the outcome can be determined. However, a disadvantage is that the combined effect of variations of different parameters is unknown.

The sensitivity analysis itself is only performed with the epistemic uncertainties since the intrinsic variables are not constant over time. It was however found that current speeds have a large influence on the sedimentation rate, as well as the current direction. This is in accordance with literature (see Chapter 2.1), which discusses the different sedimentation processes. Especially more parallel directed flows may reduce the trench infill significantly. Besides the tidal currents, also waves affect the sedimentation: increasing the wave height or peak period leads to more sedimentation. Compared to the other time varying parameters, the influence of the water level, caused by the tidal movement is significantly less. The next section discusses modelling of all these variables.

Of the parameters related to the epistemic uncertainty, the water depth has the largest effect on the sedimentation rate. The differences can be explained by the fact that waves have a significant influence in shallow water stirring up the particles from the bed. In deep water, the wave motion does not reach the bed, which means sedimentation is to a larger extend caused by (tidal) currents.

The influence of the other parameters on the sedimentation is less. In this, the settling velocity and the grain size are related. However, their effect is opposite, which means that the effect of variations in grain size is (partly) compensated by the resulting changes in settling velocity. Changes in the Van Rijn coefficient (which is a measure of the trapping efficiency) and the roughness height do not significantly influence the sedimentation rates. All results are summed up in Figure 4.5.
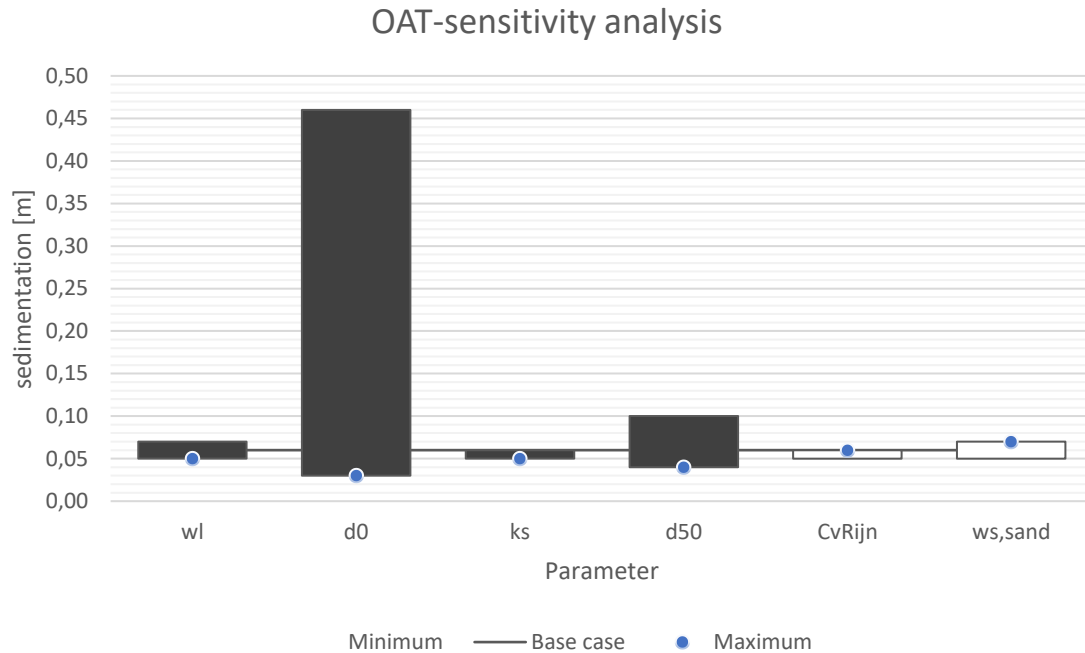
Figure 4.5: Results from the OAT-sensitivity analysis. The 30-days base case sedimentation is 0.06m. The white stocks indicate that increasing parameter values increase sedimentation rates, while black stocks represent the opposite effect. The water depth has the largest effect on the sedimentation rate.

4.4 Expected sedimentation

For the probabilistic assessment of the trench siltation, again a difference in intrinsic and epistemic uncertainties is made. To take the intrinsic uncertainties into account, 20 different Monte Carlo simulations (each with 10,000 runs) are performed. During each simulation, the wave data of one year is used. Due to the limited availability of current data, the same dataset of current speeds and directions is used in each simulation. The epistemic uncertainties are varied randomly during the Monte Carlo simulations, based on the earlier discussed distributions (see Chapter 4.2).

In this way, 20 different cumulative distribution functions, one for every year, are obtained. In Figure 4.6, these functions are shown by the 20 different gray lines. The bandwidth in sedimentation is therefore caused by the intrinsic uncertainty and the steepness of the different curves is determined by the influence of the epistemic uncertainty. Although variations in wave forcing only act over a limited period (instead of the epistemic uncertainties, which are constant during a simulation), the influence is still significant.

When combining the different sedimentation rates of every year to one cumulative distribution function, the black line is obtained. Based on the 20-years wave climate in April, this is the expected sedimentation over 30 days. With a confidence interval of 95%, a sedimentation rate between 0.04m and 0.13m is expected, with a median of 0.06m.
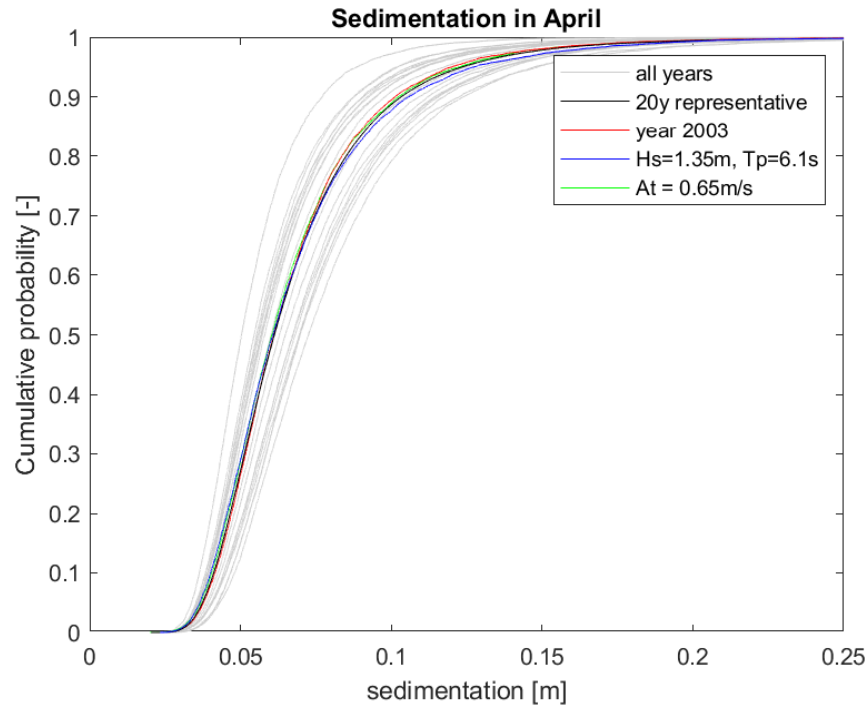
Figure 4.6: The cumulative probability of the trench-sedimentation [m] in April. The individual years are shown by the gray lines, simplifications to the representative year (black line), the individual year 2003 (red line) and simplification in forcing (waves: blue and tidal currents: green) are visible as well.

4.5 Simplifications

This section discusses simplifications in wave conditions and currents caused by the tidal forcing, since in more complex models it is not possible to include these variations to the same extend.

4.5.1 Wave climate

As discussed, the black line in Figure 4.6 is the best expected sedimentation rate based on the 20 years available wave data of the month April. In this part two simplifications are made: at first, the most representative year is selected, where after a constant wave forcing, leading to more or less the same sedimentation rates, is shown.

From the different years (gray lines), the year 2003 is closest to the cumulative distribution function of the sedimentation based on the 20-year wave data (black line). Therefore, this year is considered to be the most representative year when assessing trench sedimentation. When further simplifying this to a constant wave forcing, a significant wave height of 1.35m with a peak period of 6.1m, was found to result in comparable sedimentation rates, as indicated by the blue line in Figure 4.6. The combination of this significant wave height and peak period is based on relation between these variables discussed in Chapter 3.4.

4.5.2 Tidal forcing

In more complex models, it is not possible to implement hourly varying current data directly in the model. Usually, only one tidal constituent can be used to represent the tidal variations, including the spring-neap cycle. In Chapter 4.3, it was already shown that the effect of changes in water level on sedimentation is limited. Therefore, in this section water level changes are not considered, only the resulting current speeds.

When applying one tidal condition (the S2-constituent), with a period of 12 hours and an amplitude of 0.65 m/s, while assuming cross flow conditions, the most representative condition was found. In Figure 4.6, this is shown by the green line. In literature studies on sand waves in the North sea, (e.g. Borsje *et al.*, 2014; Leenders, 2018) often the same tidal velocity amplitude is used.

4.6 Summary

Based on the 20-year wave climate in April, the expected trench sedimentation in 30 days is between 0.04m and 0.13m, with a median of 0.06m. The year 2013 is the most representative year to assess trench infill. If simplifications have to be made, it is recommended to use a constant wave forcing with a significant wave height of 1.35m and a corresponding peak period of 6.1s. The tidal forcing can be simplified by imposing a tide velocity amplitude of 0.65m/s and a flow angle of 90° with respect to the main channel axis. Water level changes are neglected in this case due to the limited effect on trench sedimentation. A computation time of 90 minutes was needed to arrive at these results when using SedPit.

5 2DV Sand wave model

This chapter investigates the expected trench sedimentation by using a 2DV morphological model, which was earlier used to predict sand wave dynamics in Borsje *et al.* (2014) and van Gerwen *et al.* (2018). Chapter 5.2 provides insight in the model set-up and the sand wave mechanics are verified in Chapter 5.3. An overview of the trench mechanics is given in Chapter 5.4. The probabilistic assessment of the trench siltation is discussed in Chapter 5.5. Chapter 5.6 summarizes this chapter.

5.1 Introduction

The 2DV sand wave model is the second model used in this study, in which an idealised sand wave bottom perturbation can be placed. The goal of this chapter is to determine the trench sedimentation with a more complex model compared to SedPit. To do so, two different bottom configurations are considered: a flat bottom throughout the entire domain and a bottom in which sand wave bedform is imposed. The probabilistic assessment is for both situations performed by means of Latin Hypercube Sampling, since the model complexity does not allow the use of a Monte Carlo analysis.

However, before this assessment, the model set-up and the basic processes of trench siltation and sand waves are investigated. This includes an analysis of the trench – sand wave interaction for three different configurations: a trench located at the crest, trough and halfway a sand wave.

5.2 Model set-up

In order to discuss the model set-up, three different parts are distinguished: the computational domain, the bathymetry and other model settings.

Computational domain

The model used in this chapter is developed by Van Gerwen *et al.* (2018). Due to the 2DV-mode only variations in the x and z direction are considered. The computational grid extends over a horizontal distance of 50,000m with varying grid sizes. At the centre of the domain, the grid size is 5m and at the sides 1500m. Around the trench, the grid size is further decreased to 1m to able the capture potential flow separation. Between the different grid sizes, a smooth transition is made to avoid numerical errors. At the lateral boundaries, Riemann boundaries are imposed to avoid reflection of incoming waves.

The vertical consists of 60 layers. The layers are refined near the bed and most coarse at the surface (see Figure 5.1, right). In Figure 5.1 (left) the horizontal grid set-up is shown, including a detailed view on the refined grid at the center of the domain.
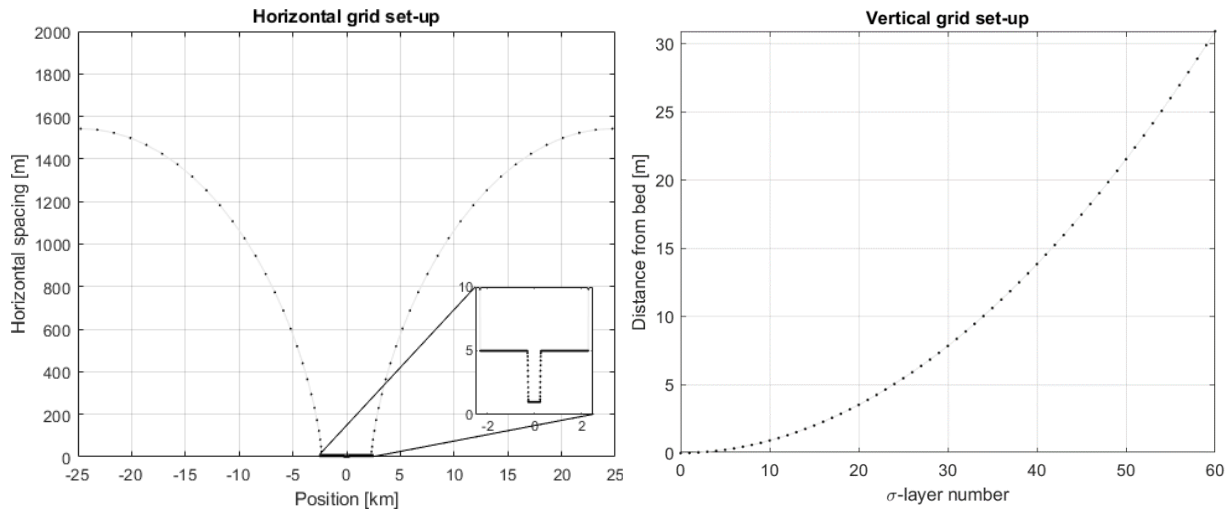
Figure 5.1: Horizontal (left) and vertical (right) grid set-up of the 2DV-model.

Bathymetry

As discussed in the introduction of this chapter, two bottom configurations are considered: a horizontal bottom and a sand wave perturbated seabed. In this last case, the sand waves are located in the central 4 km of the domain. To ensure a smooth transition between the sand waves and the surrounding flat bottom, an envelope function is used to gradually increase the initial sand wave amplitude at the center of the domain. The sand waves are only present in the center of the domain, in the region with the refined grid (1-5m). An example of the bathymetry (without trench) can be found in Figure 5.2. It has to be emphasized that the sand waves are idealized: in reality the bottom consists of a superposition of different bedforms.
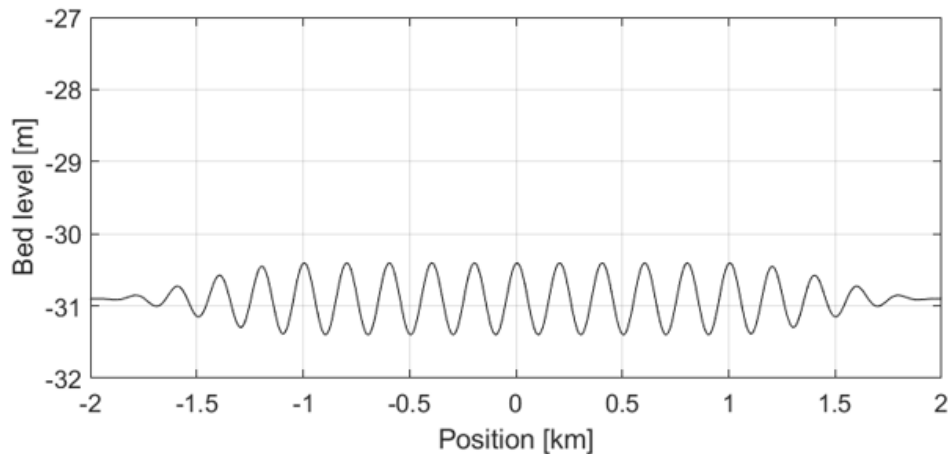
Figure 5.2: Undisturbed sand wave bed without trench at the model center.

Other settings

The hydrodynamic time step was set to 6 sec. Although the CFL condition was not met, it was found that this still provided stable solutions. The computed morphological developments with this time step is equal to the cases in which the CFL condition was met. The model is forced with the semi-diurnal tidal signal S_2 at the boundaries, with a velocity amplitude of $0.65\ m/s$ and a period of 12.00 hours. Although in the North Sea the M_2-tide is dominant, an S_2-tide is chosen for simplicity. This corresponds to the representative tide modelling obtained during the SedPit analysis in Chapter 4.5.

The model is run for two tidal cycles. The first cycle is used for spin up and during the second cycle, morphological developments are also taken into account. With a morphologic acceleration factor of 60, morphological changes over a period of 30 days are considered, similar to SedPit. The bed slope correction parameter α_{bs} is set to 3, which corresponds to an angle of repose of 19 degrees (Leenders, 2018). In contrast to SedPit, the trench is not simplified to a rectangular box, but could be modelled including the side slopes.

Table 5.1: Parameter overview of the 2DV-model (base case).

Parameter			Values
Mean water depth	$d0$	[m]	30.9
Time step	Δt	[s]	6
Tidal velocity amplitude	U_{S2}	[s]	0.65
Tidal period	T_{S2}	[hours]	12
Median grain size	D_{50}	[mm]	0.27
Bed slope correction parameter	α_{bs}	-	3
Trench slope width	W_{TS}	[m]	10
Trench depth	d_1	[m]	3
Trench width bottom	W_B	[m]	10

5.3 Sand wave dynamics

Before discussing the influence of sand wave perturbations on the trench infill, it is verified whether the sand wave dynamics known from literature, can be reproduced with the 2DV-model. In general, sand waves are considered to be fully developed in the North Sea, meaning no significant sand wave growth can be expected and morphological changes are governed by the migration of sand waves. To check whether this is also the case for the sand waves occurring around the BWFZ, a purely symmetric tide was imposed to different sand wave dimensions. For developed sand waves this would mean there are no nett morphological changes since a symmetrical tide cannot cause sand wave migration.

It was found that this is primarily the case for sand waves with a length of around 300 meters and a height of 3 to 4 meters, as indicated in Table 5.2. This is in correspondence with the sand wave dimensions measured in the field (Figure 3.3), indicating that the sand waves in this area can correctly be modelled by the sand wave model.

Table 5.2: Sand wave crest growth or decay [m] during 30 days for different sand wave lengths and heights [m].

Wave height [m]	Wavelength [m]				
	100	200	300	400	500
2	-0,030	-0,003	0,001	0,001	0,001
3	-0,052	-0,006	0,000	0,001	0,001
4	-0,086	-0,011	-0,001	0,001	0,002
5	-0,126	-0,018	-0,003	0,001	0,002

Due to the stability reached for a sand wave length of 300m and a sand wave height of 3m, this is used for a base case scenario to discuss the hydrodynamics and morphodynamic processes of sand waves.

5.3.1 Hydrodynamic processes

From the trough towards the crest, an increase in flow velocity can be observed due to the decrease in water depth. An increase in water depth from the crest towards the trough, leads to reduced flow velocities. As discussed in Chapter 2, this flow pattern results in a tide averaged recirculating cell, as provided in Figure 5.3. Near the bottom, a flow towards the crest can be observed, while a less strong flow from the crest towards the trough exists higher in the water column. Furthermore, an upward directed flow is present above the wave crest and a downward directed flow at the trough. These vertical components of the resulting flow are an order of magnitude smaller than the horizontal components. The larger the sand wave perturbations, the stronger the described process is, which corresponds to results in Leenders (2018).
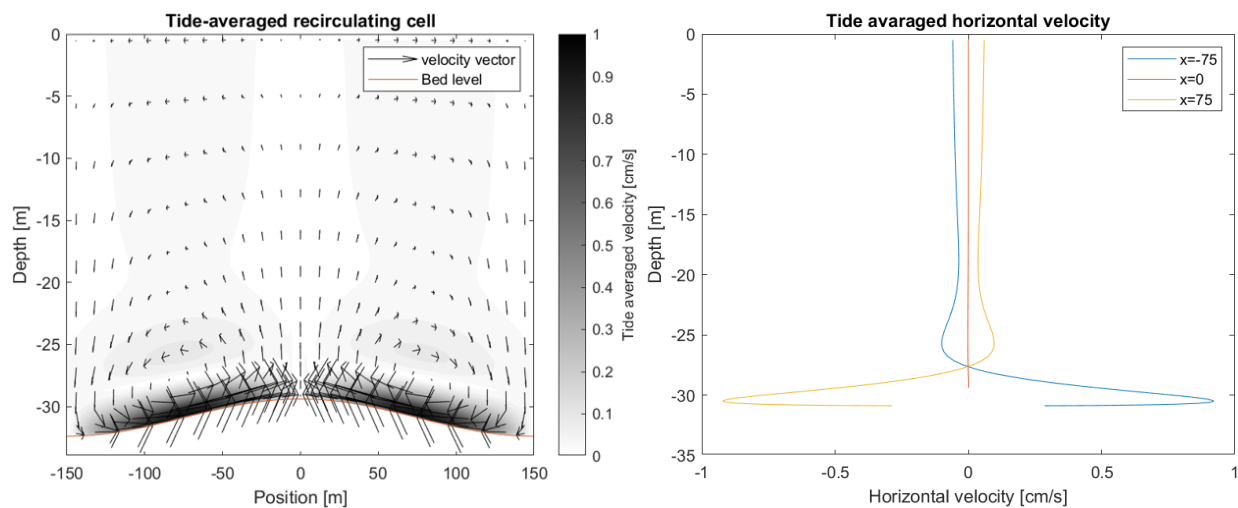

Figure 5.3: Tide averaged recirculating cells of a sand wave. In the left figure, the flow vectors are shown. In the right figure the horizontal flow velocities at the sand wave crest and halfway the sand wave can be found. The largest flow velocities are located near the seabed, higher in the water column an opposite directed weaker flow exist.

5.3.2 Morphodynamic results

The morphodynamic changes are governed by suspended load transport, bed load transport and slope-induced transport. If the bed load transport is strong enough to overcome the slope effects, the steaming near the bed (directed towards the crest) results in a growth of the sand waves. Suspended load transport is affected by the flow velocities. Due to the high flow velocities at the crest and the lower flow velocities at trough, suspended load transport is directed from the crest towards the trough, as discussed in Chapter 2.

However, as was also shown in Borsje *et al.* (2014), in case for larger grain sizes suspended load transport can also lead to the growth of sand waves (Figure 5.4). This can be explained by the fact that sediment concentrations near the bed are higher, resulting in a sort of 'bedload' transport of the suspended sediments. For smaller grains, when the sediment concentrations are higher throughout the water column, suspended sediment transport has a dampening effect on the sand waves.

Besides the sand wave growth or decay, morphological changes also concern migration, caused by tidal asymmetry or the presence of a residual current, which is not larger than 0.05 m/s in the North Sea (Besio *et al.*, 2004). It was however found that the migration of sand waves is not

significant during a period of 1 month. This is in correspondence to the measurements by Deltares (2015b, 2016), earlier discussed in Chapter 3.2. Therefore, the sand waves itself are considered to be static during in this study. On the other hand, sand waves can still have hydrodynamic or morphodynamic effects on the trench, which is shown in the next section.
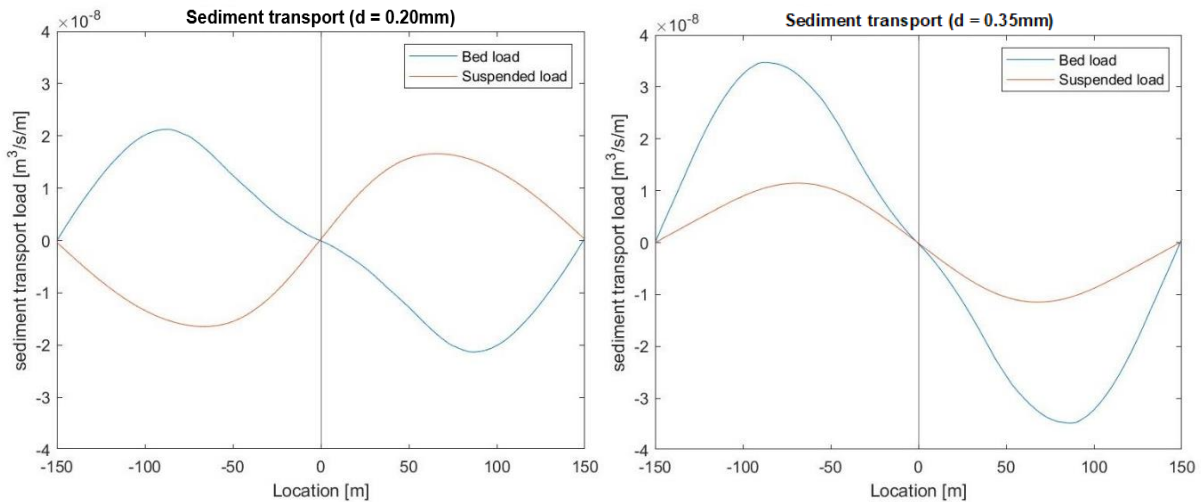
Figure 5.4: Sediment transport for d = 0.2mm (left) and d = 0.35mm (right). For d = 0.2mm, the bed load transport and suspended load transport have an opposite effect. For d = 0.35mm, both transport modes increase the sand wave height.

5.4 Trench mechanics

After discussing the sand wave hydrodynamics and morphodynamics, the interaction between the sand waves and a trench is investigated. To do so, at first the trench hydrodynamics are discussed separately before introducing the above-mentioned sand wave field. The current direction is perpendicular to the trench orientation. Combined with a current speed of 0.65m/s, this is in line with the simplifications obtained in Chapter 4.

Figure 5.5: Tide averaged flow velocities [m/s] in the trench.

5.4.1 Trench in a flat bottom

In a trench, the same mechanism can be observed as is the case for a sand wave. In the center of the trench, the tide averaged flow is downward directed, similar to a sand wave trough. Furthermore, from the trench center towards the sides, an outward directed flow over the sides slopes is present. However, the vertical component of the velocities is larger, compared to a sand wave, due to the more abrupt changes in bathymetry.
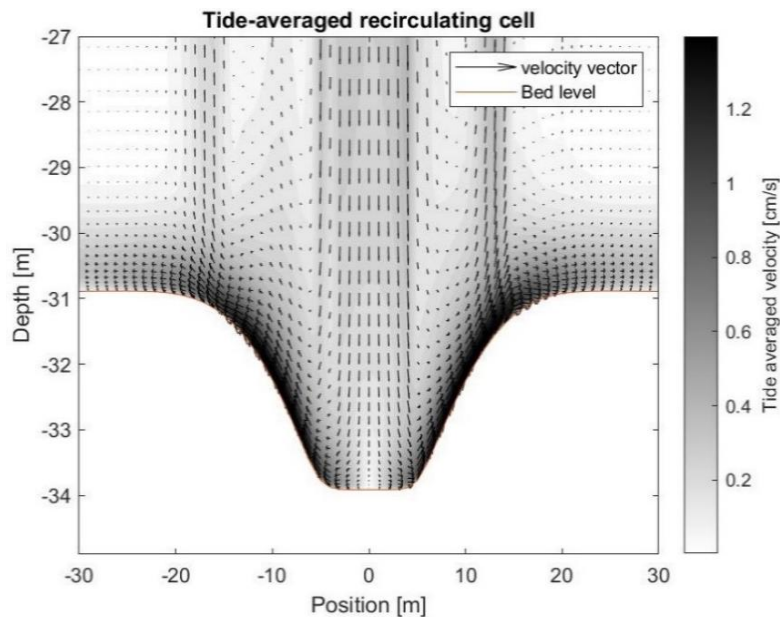
Under influence of the tide averaged flow velocities, in the trench bedload transport from the center towards the sides is expected. On the slopes however, the gravitational effects induce a bed load transport into the trench. The decrease in flow velocity leads to a decrease in suspended load transport at trench, resulting in trench sedimentation. In Figure 5.6, both types of sediment transport are plotted. Compared to the sediment transport (gradients) observed over a sand wave, the sediment transport (gradient) due to a trench is an order of magnitude larger, which can be derived by comparing Figure 5.4 and Figure 5.6. This does however not mean that the influence of sand wave bottom perturbations on trench sedimentation is neglectable.
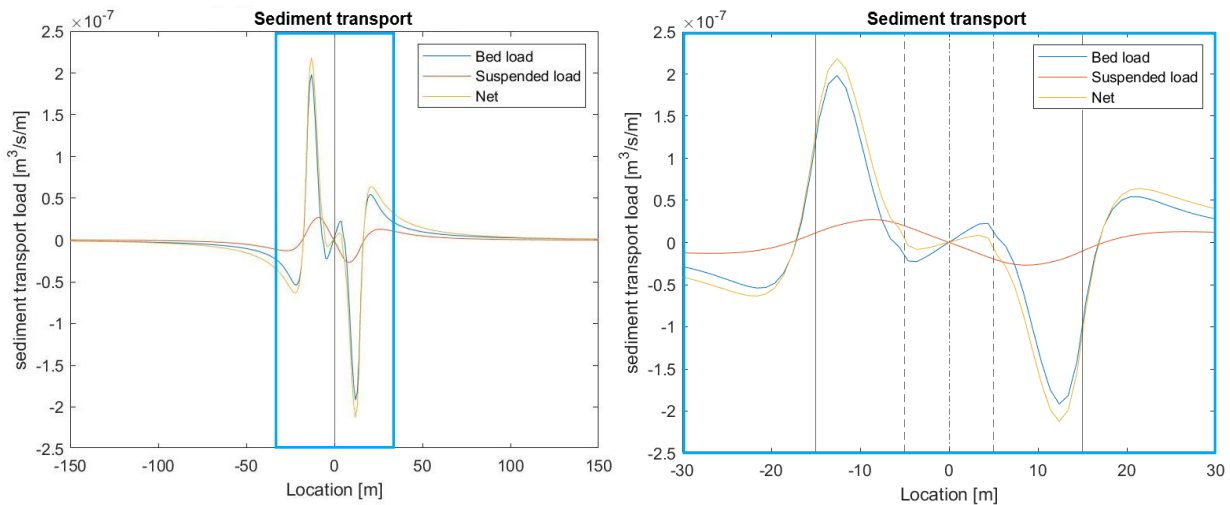
Figure 5.6: Bedload and suspended load transport over a trench. The trench is located between -15m and +15m, with the side slopes of 10m, the flat part of the trench is located between -5 and +5m.

5.4.2 Sand wave – trench interaction

To illustrate the effect of sand waves, three different configurations of the trench with respect to the sand wave locations are defined: a trench located on a sand wave crest, in the trough and in the middle. Figure 5.7 shows a schematization of the different cases. The trench is located in the center of the domain, at $x = 0$.
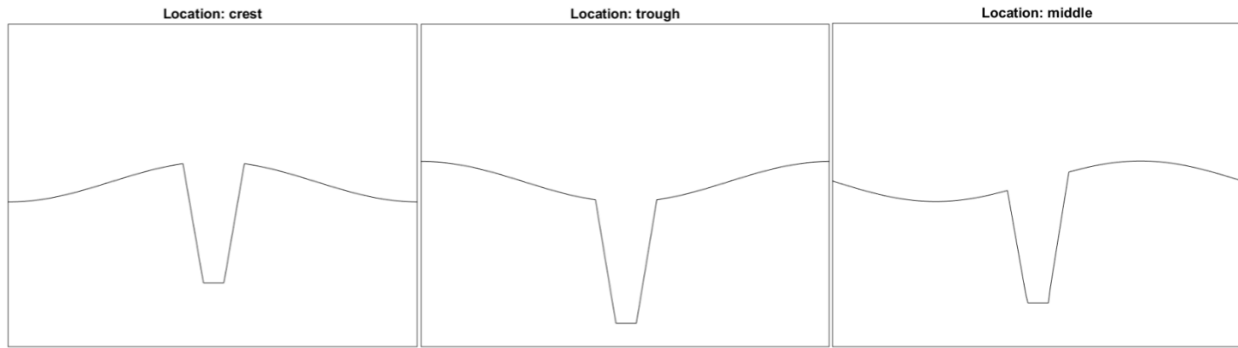
Figure 5.7: Trench configurations: a trench located on a sand wave crest (left), a trench located in a sand wave trough (center) and a trench located half way (right).

Hydrodynamics

The hydrodynamics for a trench located in a sand wave field can be described as a superposition of the hydrodynamics resulting from the trench in a flat bottom and the hydrodynamics resulting from the sand wave field separately. This is shown in Figure 5.8, for a trench located on a crest of a sand wave and halfway (compare the results to Figure 5.3 and Figure 5.5).
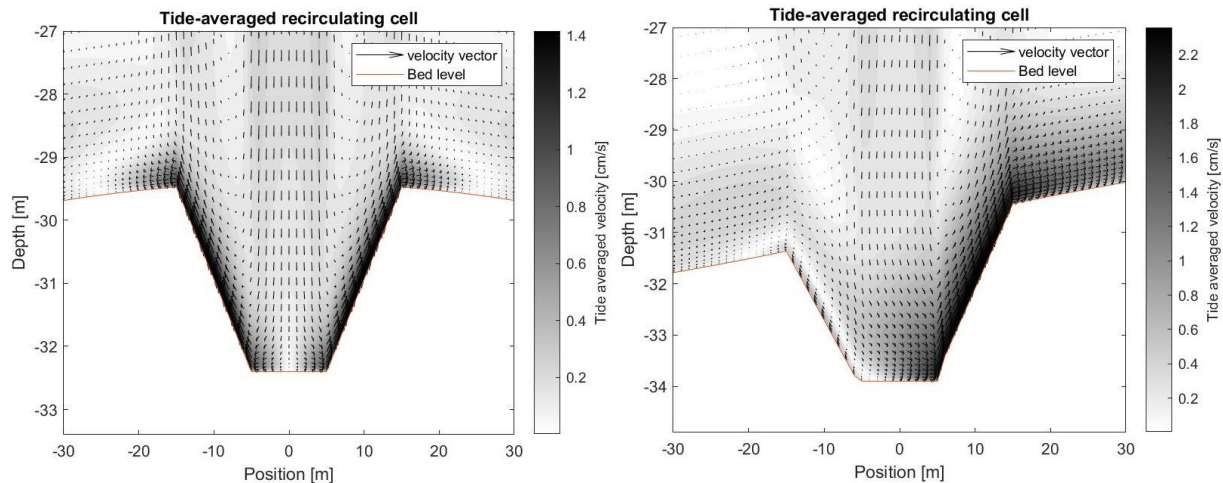
Figure 5.8: Hydrodynamics for a trench located at a crest (left) and halfway a sand wave (right).

Morphodynamics

Lastly, the influence of sand waves on the trench infill is discussed by investigating the morphodynamics. In Figure 5.9, the bed load and suspended load transport for the different trench configuration are shown. Similar to a trench located in a flat bottom, the bed load transport is dominant over the suspended load transport. The reason for this is the dominance of the slope-induced transport at the trench sides, leading to flattening of the side slopes. The bed load transport gradient is the largest in the case of a trench located on a crest and the smallest in the case of trench located in a sand wave trough. The reason for this is the less abrupt bottom changes for trenches in the trough. The opposite is true for a trench located at a sand wave crest.
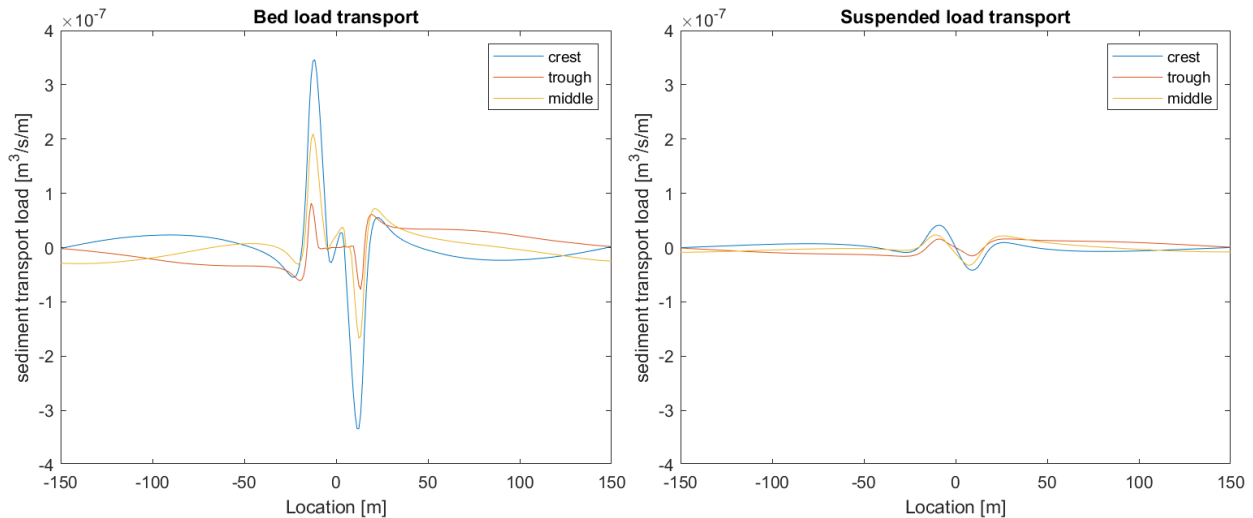
Figure 5.9: Bed load transport (left) and suspended load transport (right) for a trench located at a sand wave crest, in a trough and halfway.

These variations are less in the case of the suspended load transport. The differences are in this case caused by the different depths (and so the relative velocity change, hence sediment transport). Based on the findings discussed above, the closer the trench is located to the sand wave crest, the more sedimentation is expected.

5.5 Probabilistic assessment

Now the influence of sand waves on the trench sedimentation is known, a probabilistic assessment of the trench sedimentation is made, which is compared to the results obtained during the SedPit analysis. An overview of the variables is provided in Chapter 5.5.1. More information on the probabilistic assessment method is discussed in Chapter 5.5.2. In Chapter 5.5.3, the probabilistic infill assessment is determined for a trench surrounded by a flat bathymetry. Chapter 5.5.4 concludes this chapter by including the effects of sand wave perturbations on trench sedimentation.

5.5.1 Variables

Among variations in the location of the trench with respect to the sand wave, 6 other parameters are considered. The bed load correction factor (α_{BS}) is a function of the angle of repose of the bed material (for sand: $15 - 30$ degrees, leading to $\alpha_{BS} = 1.5 - 4.0$). Since not more information is known on the distribution, a triangular distribution is assumed with a mode of 3.0 (van den Berg *et al.*, 2012). The Chézy roughness, water depth and median grain size are the same distributed as in SedPit.

The sand wave dimensions are derived from Figure 3.3. In the area of interest, the sand wave length is between 200 and 450 m, with a wave height between 3 and 6 m. The distributions are both visually estimated to be triangular, with a mode of 300 m and 4m for the sand wave length and height respectively. The location of the trench, with the other – deterministic – parameters are kept to their values as used in earlier (sand wave) studies with this model and in correspondence to SedPit model.

An overview of all non-deterministic parameters is provided in Table 5.3.

Table 5.3: Parameter distributions for the 2DV sand wave model.

Parameter			Distribution	Minimum	Base case	Maximum
Bed slope correction factor	α_{BS}	$-$	triangular	1.5	3.0	4.0
Chézy roughness	C	$m^{\frac{1}{2}}/s^{-2}$	triangular	55	65	80
Water depth	d_0	m	-	17	31	40
Median grain size	D_{50}	mm	-	0.10	0.27	0.40
Sand wave location	Pos_{SW}	$-$	uniform	0		2π
Sand wave length	L_{sw}	m	triangular	200	300	450
Sand wave height	H_{sw}	m	triangular	3.0	4.0	6.0

5.5.2 Latin Hypercube Sampling

For the probabilistic assessment, a Monte Caro analysis was performed in the SedPit model. However, due to the longer computation times of around 2 hours, this method cannot be applied for the 2DV-model. Therefore, as discussed in Chapter 2, Latin Hypercube Sampling is used. A disadvantage is that it is not known up front how many simulations are needed for a reliable probabilistic assessment. The sample size is increased until a further increase in sample size does not change the probability distribution of the trench sedimentation.

To start with, 7 simulations are performed resulting in probability intervals of 0.16 for all variables, indicated by the red planes in Figure 5.10. Following Sallaberry, Helton and Hora (2008), the amount of samples is doubled in 2 steps to 28 samples (indicated by the green and blue planes). In this way, the number of samples is increased without losing information from the previous simulations. During the increase in sample size, the same correlation between the data has exist.

Similar to the previous analysis in SedPit, the variables are considered to be independent. Between the sand wave height and length, obviously a relation exists (see Figure 3.3). Without more information, it is assumed they are fully dependent.

In Appendix C.2.1 and overview of the non-exceedance probability of the different input variables is shown. The corresponding model input values are summarized in Appendix C.2.2. In Appendix C.2.3 the probability distribution function of the various parameters during the different LHS is shown. Kernel smoothening is used to arrive at a more realistic distribution. The resulting cumulative distribution function is shown in Appendix C.2.4.
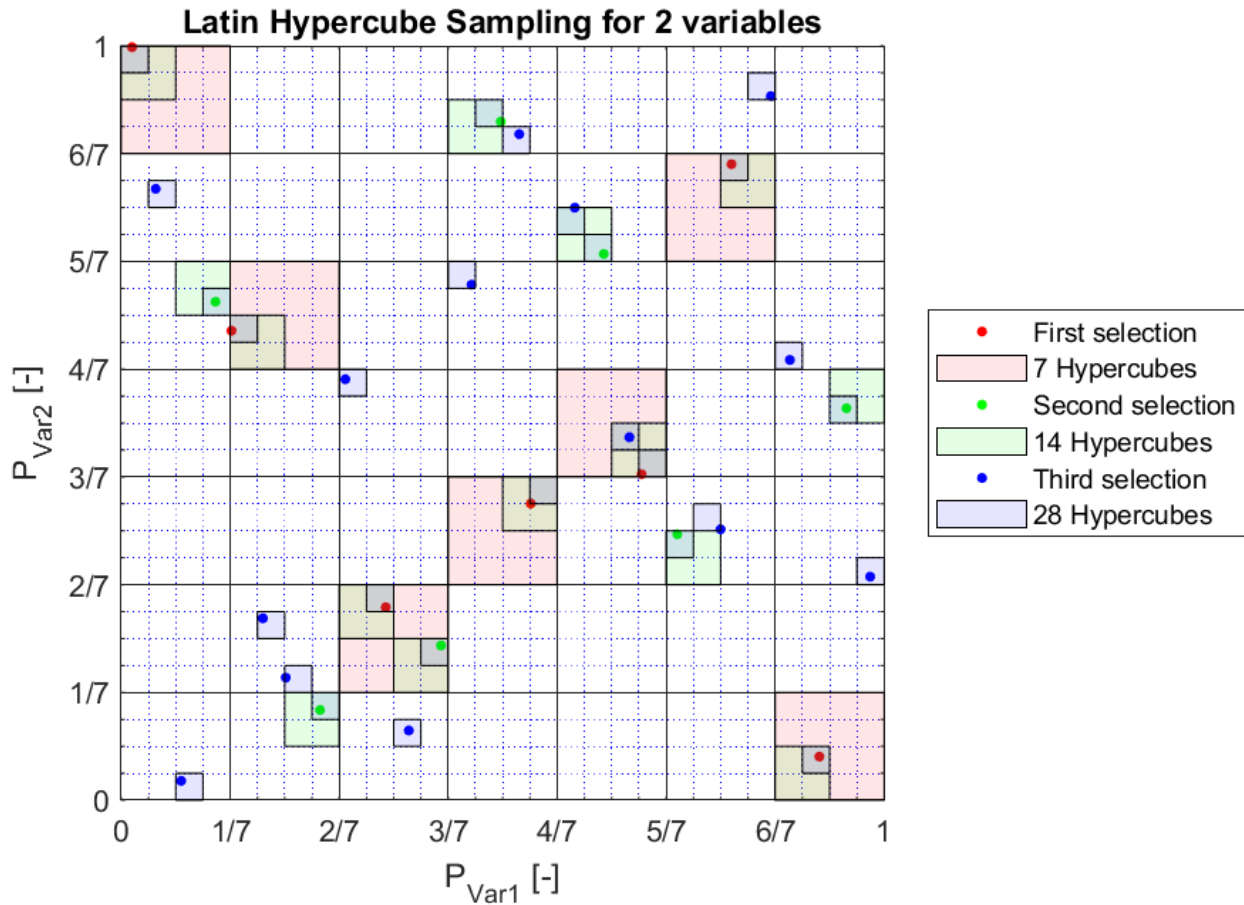
Figure 5.10: Latin Hypercube Sampling for 2 variables, with an original sample size of 7 (red). Smaller probability intervals are selected based on Sallaberry, Helton and Hora (2008) and indicated by the green and blue sub squares.

5.5.3 Flat bottom

For assessing the trench sedimentation, the same calculation is used as in SedPit, which is to divide the total sedimentation volume in the trench by the trench width, resulting in an average sedimentation over the trench. At first, the probabilistic assessment for the trench siltation surrounded by a flat bathymetry is discussed.

In Figure 5.11, the cumulative distribution function for the 2DV-model with three different sample sizes (7, 14 and 28 runs) is shown. As can be seen, the computed distribution in the case of 7 runs differs significantly from the other simulations. This difference is less between 14 and 28 runs, especially in the region with the most probable sedimentation rates (roughly between P10-P90). Closer to the tails of the distribution larger deviations between the expected sedimentation rate can be observed. Although more runs could increase the accuracy of the cumulative distribution function, 28 runs is considered to be enough.

Compared to SedPit, the sedimentation is more narrowly distributed in the 2DV-model. However, it has to be noted that due to the limited amount of runs of LHS (28) compared to the MC-simulation of 10.000 runs with SedPit, especially in the tails of the distribution differences between the models can be noted. In the more medium ranges of the distribution, the differences between the two models is small. Due to the relatively large water depths, the influence of waves on the trench sedimentation is limited.

50
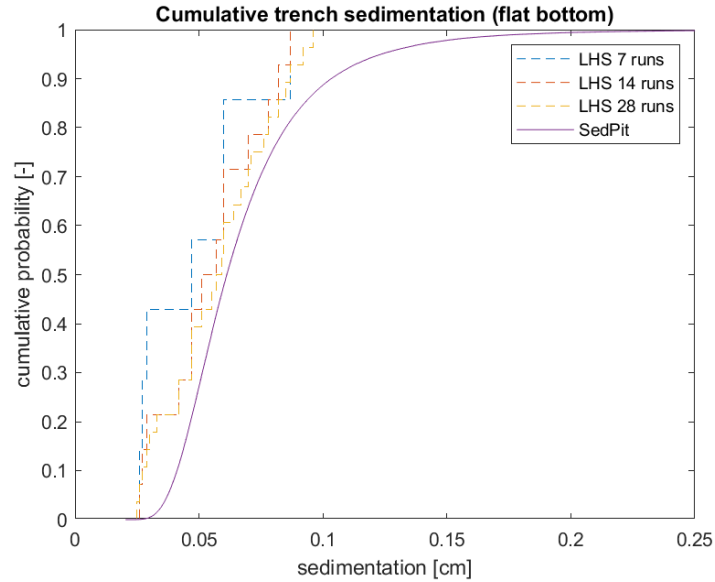
Figure 5.11: The cumulative trench sedimentation with the 2DV-model compared to SedPit for flat bottoms, for LHS with different sample sizes.

5.5.4 Sand wave bottom

As shown above, the more complex 2DV-model reduces the uncertainty in trench sedimentation in the case of a flat bottom. Moreover, the 2DV-model is able to include the effect of (idealised) sand wave perturbations. In Chapter 5.4, it was already indicated that this bedform can have a significant influence on the expected trench sedimentation. Similar to the case of a flat bottom, LHS with a maximum of 28 runs is performed. During these simulations, the same 7 variables as discussed earlier, are varied. The percentiles and corresponding values of the different variables are shown in Appendix C.2.
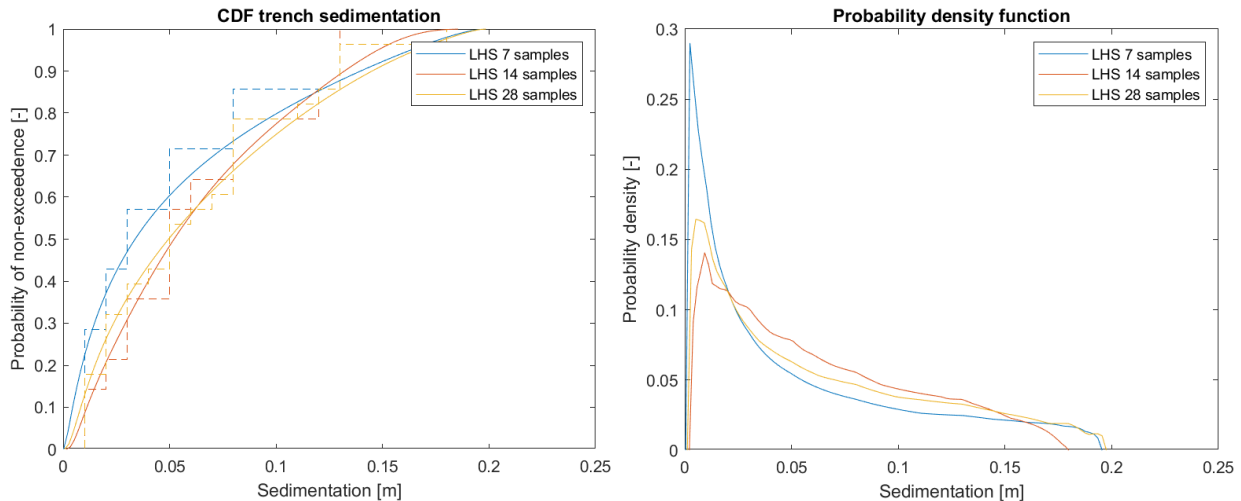
Figure 5.12: Cumulative distribution function of the infill following LHS (left) and the sedimentation as function of the trench location (right). The dashed lines show the non-smoothened empirical CDF for the different sample sizes for LHS

In Figure 5.12 (left), the cumulative distribution function of the trench sedimentation can be found, the corresponding probabilistic distribution function is shown in Figure 5.12 (right). After 28 simulations, there still is a discrepancy visible between the LHS with 14 samples and 28 samples,

although it is reduced significantly. Based on the results, a median sedimentation rate of 6 cm is expected, with the 5% and 95% confidence bounds of 1 and 13 cm.

Parameter sensitivity

Now, influence of the different parameters is investigated. Results show that the influence of the trench location with respect to the sand wave bottom is the largest. Although some variations exist, a clear decrease in trench sedimentation can be observed for trenches located further away from the sand wave crest, see Figure 5.13 (left). Furthermore, a decrease in sedimentation rates is observed for increasing water depths (Figure 5.13 (right)). However, the effect is less clear since the trench location is dominant. The effect of the water depth on the sedimentation rate was larger in the simulations in which the sand waves perturbations were not included.
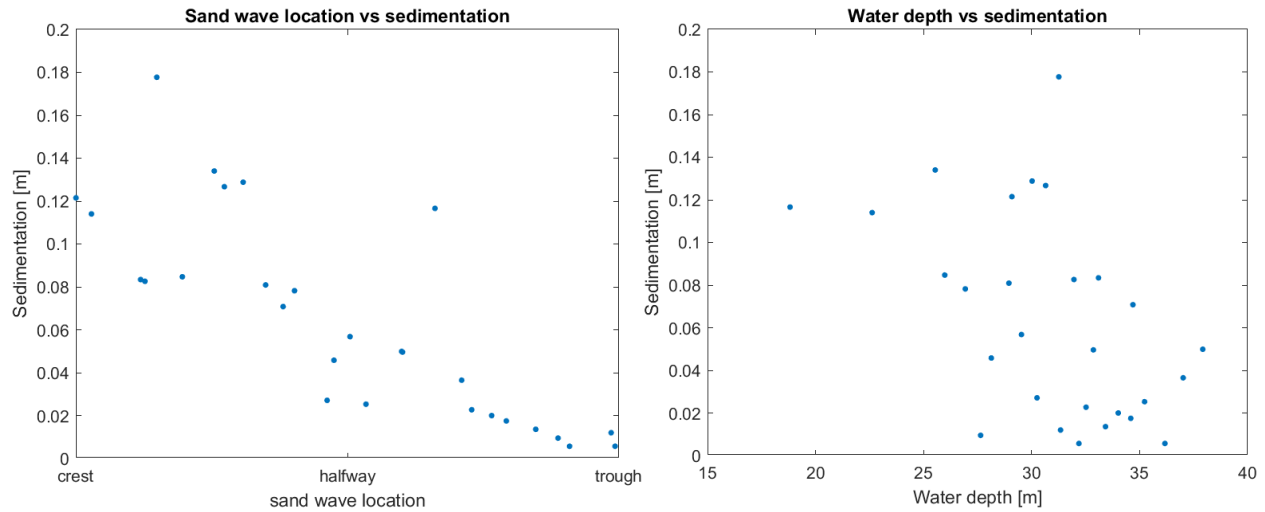
Figure 5.13: Sedimentation [m] as function of the trench location. In the right figure, the sedimentation [m] vs water depth [m] is plotted. The sand wave location has the most significant influence on the trench siltation.

Besides the visual observations described above, the influence of the different parameters on the sedimentation rates can also be expressed by means of correlation coefficients (see Table 5.4). In correspondence with the visual observations, the effect of the trench location is most important. Due to the increase in bed shear strength, the sediment transport increases for smaller water depths, resulting in a negative correlation coefficient. Since a (strong) positive correlation between the sand wave dimensions (height and length) exists, the bed slope changes are small, reducing the effect on the trench infill.

Table 5.4: Correlation between various parameters and trench sedimentation obtained by the 2DV-model. Larger (absolute) values indicate that a strong relation exists between sedimentation and this parameter.

Parameter		Correlation with trench infill
Median grain size	D_{50}	0.006
Bed slope correction factor	α_{BS}	0.2293
Chézy roughness	C	0.280
Water depth	d_0	-0.4650
Sand wave location	Pos_{SW}	-0.8634
Sand wave length	L_{sw}	-0.1814
Sand wave height	H_{sw}	-0.2042

5.6 Reflection on results

The probabilistic assessment of the trench sedimentation performed by the 2DV-model (using LHS), reduces the uncertainty resulting from SedPit (with a MC-analysis), as shown in Figure 5.11 and Table 5.5. Especially in the region around the median, the results from both models are comparable. In the tails of the distribution the difference increases, but this can also (party) be caused by the fact that LHS is not a suitable probability assessment method in this area. In line with the results found in Chapter 4, the water depth is the most sensitive parameter in both SedPit and the 2DV-model in case flat bathymetries are considered.

Table 5.5: Cumulative distribution of the trench sedimentation [m], with the different models

	SedPit	2DV-model	
Percentile	Flat bottom	Flat bottom	Sand wave bottom
5	0.04	0.03	0.01
10	0.04	0.03	0.01
30	0.05	0.05	0.03
50	0.06	0.06	0.06
70	0.08	0.07	0.08
90	0.10	0.08	0.13
95	0.13	0.09	0.13

When taking into account the presence of sand wave perturbations, the water depth is no longer the most sensitive parameter, but the location of the trench with respect to the sand wave gains importance. The sand wave dimensions are of minor importance. Although the influence of the water depth on the trench is reduced, it still is the second most important parameter to consider during the analysis.

All in all it can be concluded that the 2DV model reduces the uncertainty in the probability assessment compared to the results obtained by SedPit. However, when including the effects of sand wave perturbations, this increases the overall uncertainty of the trench infill (see Figure 5.14). In the discussion (Chapter 7) a more elaborate comparison between the different models is made.
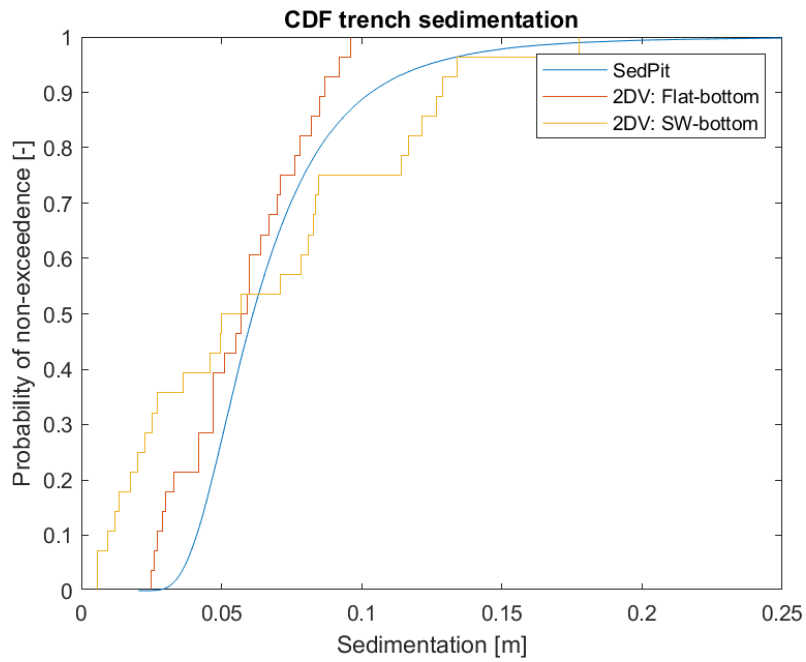
Figure 5.14: Probabilistic assessment of the trench sedimentation based on a flat bathymetry (SedPit and 2DV-model) and the presence of sand waves (2DV-model only).

6 Measurements

In the last step of the research, measurements along the cable trajectory are compared to the predicted trench sedimentation based on the model outcomes, discussed in the previous chapters. Due to a lack of detailed sedimentation surveys, this cannot solely be used as comparison. Therefore, besides the sedimentation surveys between dredging periods, also the dredging data along the trench is used as measure for sedimentation.

6.1 Data availability and cable trajectory

In order to discuss the trench sedimentation, the route is numbered with so-called 'Kilometer Points' (KP). The KP starts in the Western Scheldt estuary near Borssele where the cable is connected to the onshore grid (KP = 0) and ends at the BWFZ (KP=67,000), as indicated in Figure 6.1.
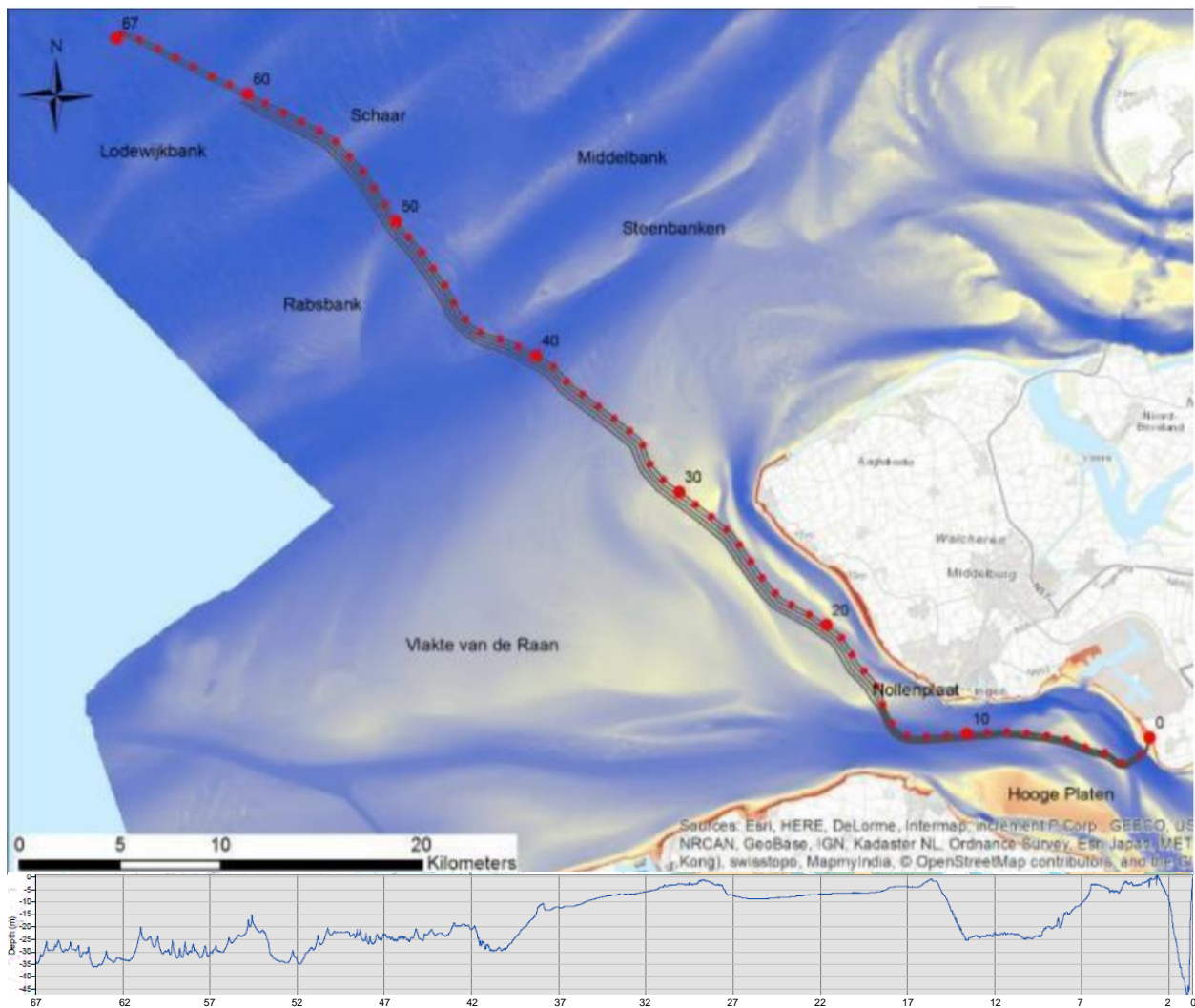
Figure 6.1: Trench trajectory and Kilometer Points (KP) (TenneT TSO, 2016).

As discussed earlier in this study, the focus of the research is at the BWFZ, which is located between KP 55,000 and KP 67,000. In the considered area, a superposition of sand banks and sand waves can be observed. The small bottom perturbations are caused by the sand waves, the larger changes are the results of sand banks with a length of around 5km (see Figure 6.1). Based on the water depth along the trajectory, sand waves only exist between KP 40,000 and 67,000. Closer to shore, the sea becomes shallower, and the sand waves can no longer be observed due to the increasing influence of waves. In the Western Scheldt estuary, large variations in water depth occur due to the presence of plates and shoals. The Honte-channel causes locally a large increase in water depth near the onshore connection at Borssele.

Two different kind of data is used to compare the model results to: a survey in which sedimentation is determined and the dredging volumes during dredging operations by Boskalis. The sedimentation surveys are limited to certain parts of the trajectories. The dredging volumes are known over a larger area but are incomplete as well. An overview of the availability of the different data is provided in Table 6.1.

Table 6.1: Data availability (sedimentation und dredging data) along the trench trajectory (Boskalis, 2018).

Area	KP start	KP end	Length (m)	Sedimentation surveys	Dredging data
Honte	750	2,050	1,300	Yes	Yes
Spijkerplaat	2,050	6,850	4,200	Yes	Yes
Rede v Vlissingen	8,000	13,800	2,400	Yes	Yes
Nollen_1	13,800	14,850	1,050	Yes	Yes
Nollen_2	14,850	16,200	1,350	Yes	Yes
Rassen	26,750	31,300	4,550	Yes	Yes
Kaloo	33,000	38,400	5,400	Yes	Yes
Beta offshore	37,000	66,800	29,800	No	Yes
Alpha offshore	38,400	59,900	21,500	No	Yes

6.2 Data interpretation

In Figure 6.2, the data from the sedimentation surveys and dredging operations is shown along the cable trajectory (Figure 6.3). Both are discussed separately in this section.

6.2.1 Sedimentation surveys

Along the cable trajectory significant differences in sedimentation rates can be observed. The largest sedimentation rates (0.95 – 1.1 m/month) are measured in the Western Scheldt estuary, which are up to an order of magnitude larger compared to other locations (0.05 m/month at Kaloo). The large sedimentation rate in the estuary can be explained by the occurrence of strong tidal currents, up to more than 1 m/s. Less sedimentation (0.05 - 0.25 m/month at Kaloo and Nollen respectively) was observed offshore. Around KP 30,000 a relatively large sedimentation rate (0.7 m/month) is observed due to the local shallow water at Rassen.

No sedimentation surveys are performed near the BWFZ. The surveys closest by are at Kaloo, located around 20km from the study area. Compared to the study area, the water depth is however significantly less. It is important to realise that the sedimentation surveys are not conducted during spring (considered in the models), but during autumn (September - October).
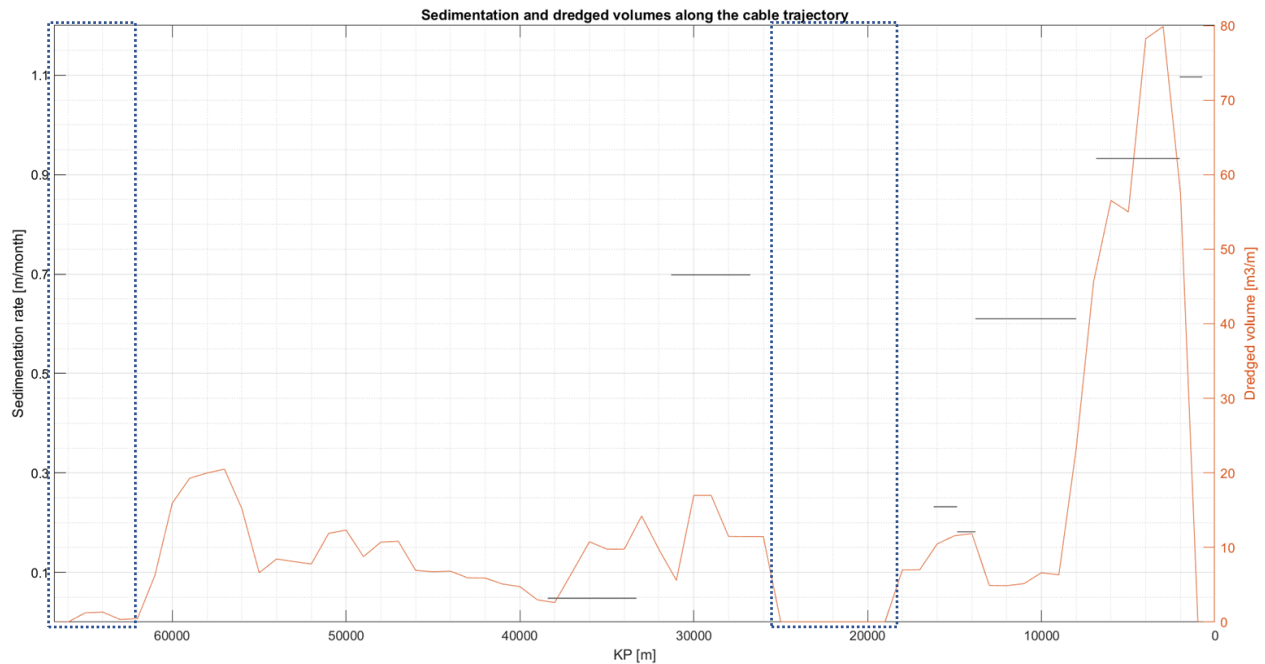
Figure 6.2: Measured sedimentation rates [m/month] (black) and dredging volumes [m³/m] (orange) along the trench trajectory. In the blue boxes no data on the dredged volumes was available.
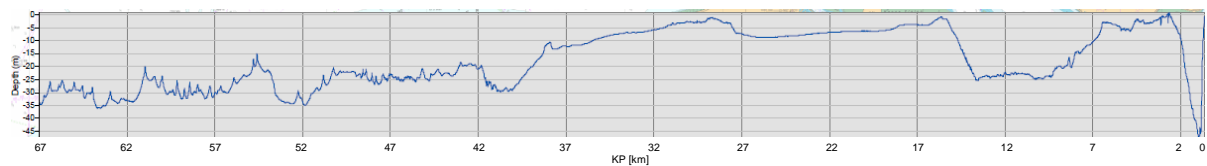
Figure 6.3: Water depth along the trench trajectory.

6.2.2 Dredging data

The dredging data is available over larger parts of the cable trench. Different dredging campaigns were needed due to the delays during the installation of the export cable. The volumes discussed in this part only include the maintenance dredging. Capital dredging (which is the dredging of the trenches itself) is not taken into account, since this is not influenced by sedimentation volumes.

As expected, the largest volumes (of around 60 m³/m) are dredged in the Western Scheldt estuary, where the largest sedimentation rates occur. At the more offshore located areas, less volume is dredged. Furthermore, similar to the sedimentation surveys, more sediment (around 15 m³/m) was dredged at the relatively shallow areas at KP 15,000 and KP 30,000. The data at the most offshore parts of the trajectory (between KP 62,000 and 67,000) is incomplete, and therefore not taken into account during the analysis. No dredging data was available between KP 18,000 and 25,000 as well.

Due to inaccurate data logging, for this research, the dredged volumes are stored per kilometre and smoothened over 5km. In this way, unrealistic peaks are averaged over a longer distance. This does however mean that a detailed comparison between dredging volumes and the underlying bedforms is not possible.

57

6.3 Comparison to model results

Both data from the sedimentation survey and the dredging operations suggest that more sedimentation occurs in shallow areas (by comparison of Figure 6.2 and Figure 6.3), similar to the model results. This relation between increasing water depths and decreasing sedimentation rates was also found in both models and in correspondence with a previous study of Boskalis (Boskalis, 2017). Furthermore, although the wave action in the Western Scheldt estuary is limited, sedimentation rates (0.95 – 1.1m/month) are large due to the high flow velocities. Closer to the BWFZ, which is the study area of this research, the dredged volumes decrease to 2 – 20 m^3/m, but are similar to the dredged volumes (10 m^3/m) at Kaloo, at which the closest sedimentation survey was performed.

Assuming a perfect match between the dredging data and sedimentation surveys, and translating these results from Kaloo to the BWFZ, the sedimentation thickness (around 0.05m) is almost the same as the median of the sedimentation volumes obtained from both models. The quality of the data does however not allow this assumption, but the conclusion that the results of both SedPit and the 2DV-model are of the same order of magnitude as the measurements from the sedimentation survey and dredging operations seems to be justified.

7 Discussion

Before drawing conclusions from the results discussed in the chapters before, some remarks have to be made. This involves a reconsideration of the assumptions made influencing the results. To do so, 5 different aspects are discussed: the model dimensions, the underlying bathymetry, the model forcing, the timescale and the probabilistic assessment.

7.1 Dimensions

Based on the results, for trenches located in sand wave fields, two main processes can be distinguished: trench siltation mechanics and the sand wave dynamics. Generally, trench siltation is process taking place in the 2DH-plane, since the currents – one of the forcing mechanisms – can be parallel, oblique or perpendicular to the trench. On the other hand, a proper modelling of sand waves requires at least an 2DV approach. Due to the perpendicular orientation of the trench axis with respect to the flow-direction, the 2DH effect for the trench infill was assumed to be limited and the 1D-SedPit and 2DV-sand wave model were used for the probabilistic assessment. This however has two consequences:

- The self-cleaning mechanism, which occurs for more parallel orientated flows, is not taken into account during this analysis. However, due to the limited occurrence of this type of flow in this specific case (see current rose in Figure 3.10), the effect is expected to be limited.

- For more parallel flows not only the results from the 2DV-model are questionable. Due to the one dimensional approach of SedPit, a correction factor on the sedimentation rates is applied for non-perpendicular flows. However Van Rijn (2013) suggests that this may lead to an overestimation of the trench siltation. Therefore, at least an 2DH-model is required for flow angles of less than 60 degrees. When taking into account the effect of sand waves, this would mean that only a 3D-model can lead to reliable assessments.

7.2 Bathymetry

In this study, two types of bathymetries are used in the models: a flat bottom (SedPit and the 2DV-model) and an bottom solely covered by idealised sand waves (2DV-model). As mentioned in Chapter 5 however, the sand wave location is an important parameter to take into account. It was therefore investigated whether the calibration parameter for sand transport could be adjusted such that the results from SedPit match results from the 2DV-model. Of all input parameters from SedPit (see Appendix B for an overview), the calibration parameter is best suited to change due the fact that the location of the sand wave in particular influence the sediment transport.

As expected, in the case of a trench located near the sand wave crest, more sedimentation occurs, hence a higher calibration parameter for sand transport (about 1.5) is needed in SedPit. The opposite is true for trenches found around sand wave troughs (calibration factor around 0.3). For trenches halfway a sand wave, a calibration parameter around 0.9 provides the best fit. These results are plotted in Figure 7.1. Furthermore, a higher calibration parameter leads to a larger uncertainty in the predicted sedimentation.

Since the variations in the calibration parameter are limited between 0.5 and 1.0 according to Van Rijn (2013), it has to be concluded that the bottom perturbations of sand waves cannot be accurately predicted with SedPit, especially for trenches located at the trough and crest.
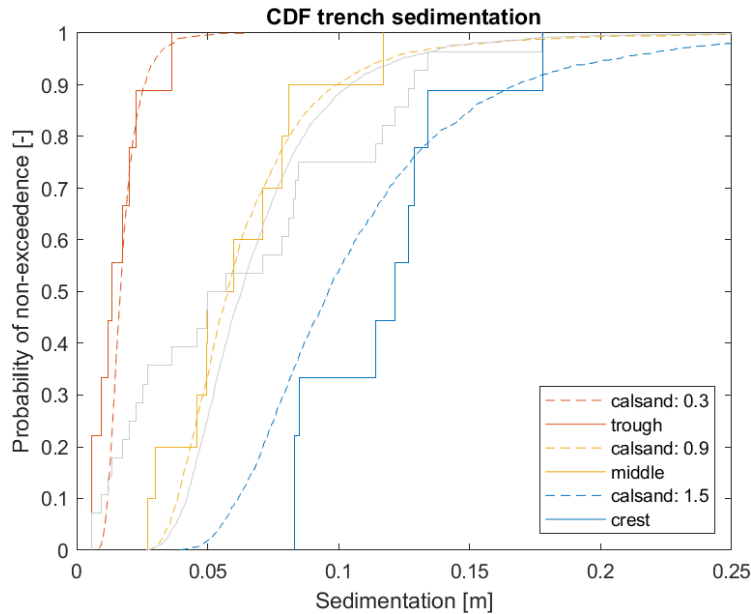

Figure 7.1: Calibration parameter for sand transport, which is varied to match the 2DV-results for trenches located around the crest, trough and halfway a sand wave.

Besides the flat bottom in SedPit it has to be realised that the bathymetry of the 2DV-model is also idealised, since in reality the seabed consists of the superposition of different bedforms. More complicated flow patterns and resulting morphological processes, are therefore not included in the results. This may influence the probabilistic assessment of the trench sedimentation.

7.3 Forcing

Tidal currents are an important forcing parameter of both sand waves and trench sedimentation. As was shown in Chapter 3.6, the tide is composed of different tidal constituents of which the 11 most important were summed up. Two well-known characteristics of the tide at the Borssele Wind Farm Zone are the semi-diurnal tide and the spring-neap cycle. For modelling purposes however, some simplifications were made.

In SedPit, due to a lack of more data, the hourly data of April 2016 was used. In this way, the effect of different tidal constituents was included in the study. Since a less detailed modelling of the forcing has to be imposed at the 2DV-model, it was researched which simplifications lead to similar sedimentation rates. In this analysis it was found that a S2 – constituent with an amplitude of 0.65m/s does so. The effect of tidal asymmetry and the resulting migration of sand waves is not included in this way. However due to the short timescale this process could be neglected. To illustrate the possible influence of other tidal modelling ways, some typical scenarios are discussed:

- Addition of a residual current (S2: 0.65 m/s, U0 = 0.05m/s): When a residual current is imposed, the magnitude of the highest ebb and flood velocities change to 0.60 and 0.70 m/s. Due to the strongly non-linear relation between the flow velocity and sedimentation, the trench siltation increases with 30%

- Asymmetrical tide (S2: 0.65m/s, S4 = 0.05 m/s): The influence of tidal asymmetry is, similar to Leenders (2018), schematised by adding an S4-overtide with an amplitude of 0.05m/s. The same result as with the addition of a residual current could be seen: Due to the higher maximum flow velocities, the sedimentation increases, but less compared to the previous case: 20%. In contrast, the averaged flow velocity is equal to the base case.

Both scenarios underline the sensitivity of the sedimentation resulting from changes in flow velocity. A proper estimation of the tidal forcing is therefore important. Due to the inclusion of current data of April 2016 only, the uncertainty related to current forcing, may be underestimated.

7.4 Duration and period

In the beginning of this study, two important assumptions were made. First of all, the sedimentation was considered over a period of one month. Secondly, the dredging works were executed during spring, specifically during the month April. The effect of both choices is discussed in this section.

Duration

In this research, only monthly sedimentation rates are investigated. However, in reality due to delays in the execution phase, the period between the dredging works and the installation of the export cables can be extended. This was also experienced by Boskalis in 2018, during the installation of the cables for the Borssele windfarms. Due to the extreme draught, material could only be limited transported by vessels on the rivers, leading to delays. Meanwhile, more sedimentation can be expected in this extended period.

The migration of sand waves is for delays in the order of months still limited. This was verified for a period of 3 months by the model runs and confirmed by literature (Deltares, 2015b), in which it was stated that the migration rates usually do not exceed 1m per year. The uncertainties during the extended period however, can significantly influence the probabilistic assessment. This is discussed for the epistemic and intrinsic uncertainty separately.

- The input values for the parameters categorized as *epistemic uncertainty*, related to the models itself, do not change. This can be explained by the fact that the same model is used, and hence the same inaccuracies are taken into account. Their effect can however be larger due to the longer duration on which they act, increasing the overall uncertainty from this group of parameters.

- The *intrinsic uncertainty*, related to the model forcing however, changes. Due to the fact a longer period is considered, the probability of a storm during this period increases. Since the effect of such extreme events is not investigated in this study, the effect can only be qualitatively estimated. Due to the strong non-linear relation between current speeds and the sedimentation rate, it is expected to have a significant influence. Since in SedPit hourly forcing is applied, it is more easy to implement such events compared to the 2DV-model in which a representative forcing needs to be selected. Moreover, similar to the remarks on the *epistemic uncertainty*, inaccuracies in forcing can have a larger effect due to the increased duration.

Period

As mentioned in the introduction, this study focuses on the sedimentation during the month April. Due to smaller variations in wave climate compared to autumn and winter months, this limits the in intrinsic uncertainty. On the other hand, summer months (as June and July) are more stable.

Similar to the discussion on the duration of the considered period, a possible extreme event might influence the results significantly, increasing the intrinsic uncertainty.

7.5 Probabilistic assessment

Probabilistic assessment method

Two different methods are used for the probabilistic assessment of the trench sedimentation: Latin Hypercube sampling is combined with the 2DV-model and a Monte Carlo analysis was applied with SedPit. Due to the fact that LHS is a variance reduction method, the accuracy of the assessment is less compared to the Monte Carlo-analysis. Especially in the tails of the distribution, the applicability of LHS is limited. This means the more extreme situations are not properly assessed by this method. On the other hand, for contractors like Boskalis, this is for most situations an acceptable risk.

Furthermore, due to the nature of LHS, it is hard to predict the number of samples needed for a proper assessment. Especially when more non-deterministic parameters are included more simulations might be required. Therefore, in the cases in which the sand wave patterns are imposed, it cannot with certainly be concluded that the number of samples (28) is enough for an accurate prediction of the cumulative distribution function for the trench sedimentation.

Selection of the non-deterministic variables

The selection of the non-deterministic variables is done based on various literature studies (Borsje *et al.*, 2014; Boskalis, 2017; Leenders, 2018). However, the exclusion of certain parameters can significantly influence the results. Due to the limited amount of input parameters in SedPit and the short computation times, the most important parameters can easily be assessed by means of a sensitivity-analysis. For the 2DV-model this approach was not feasible due to the increase in computation time and a more extensive literature study was needed. The exclusion of important parameters is therefore more likely in the last case.

8 Conclusion

The goal of this research is to investigate to what extend trench sedimentation of trenches located in sand wave fields can be assessed with a reduced complexity model in combination with an extensive uncertainty analysis, or when a computationally more demanding model with a limited probabilistic assessment is required. To do so, two different models were used: a 1D-SedPit model, and a 2DV- sand wave model. This leads to the following research question:

> **How to probabilistically assess trench sedimentation for trenches located in sand wave fields, such as at the Borssele Wind Farm Zone?**

Before answering the research question, the conclusions of the 5 sub questions are discussed.

1. *What are the morphological processes leading to trench siltation?*

In Van Rijn (2013), three mechanisms causing trench sedimentation are distinguished: the reduction of the flow velocity at the trench, sliding of sand particles of the side slopes and shifting of shoals and banks. The reduction in flow velocity at the trench is the largest for currents perpendicular directed to the channel axis, a smaller flow angle reduces this effect. In the case of nearly parallel flows, the bottom friction is reduced at the trench, which results in higher flow velocities, such that even erosion is possible. Due to the short timescale considered in this research, shifting of shoals or banks is not affecting trench sedimentation. Lastly, the effect of waves, stirring up the sediment from the surrounding bottom, increases the sedimentation rates. This effect is significant in shallow seas or in the case of large waves.

2. *What is the influence of sand wave bottom perturbations on the trench infill?*

The influence of a sand wave bedform on trench sedimentation is dependent on the location of the sand wave with respect to the trench. For this conclusion roughly three locations are distinguished: trenches located near the crest, halfway and near the trough of a sand wave. In the base case, which covers the trench siltation over 30 days, the sand waves were found to be more or less stable. This means there is no effect of sand wave migration on the infill of trenches in this case. However, it was found that sand waves perturbations still influence the hydrodynamic and morphodynamic processes.

The hydrodynamic processes of trenches in sand wave fields can be interpretated as a superposition of the hydrodynamics originating from the sand waves and trenches separately. Similar to trenches located in flat bathymetries, bed load transport is dominant for the trench sedimentation. Due to the abrupt changes in bed level, larger changes in bed load transport is expected for trenches located near sand wave crests, leading to more sedimentation. The opposite was found around the sand wave trough: due to the relatively gradual change in bathymetry, the trench sedimentation is limited in this case.

3. *What are the most important parameters when assessing trench sedimentation and how are they related?*

During the analysis with SedPit, at first a sensitivity analysis was performed to investigate the influence of a single parameter on the outcome (sedimentation rate). It was found that the water depth is by far the most important parameter to consider, which can be explained by the fact that

the shear stress increases, and the influence of wave motion is more significant. Furthermore, changing the grain size diameter is of influence, but around an order of magnitude less than the water depth. At the Borssele Wind Farm Zone variations in water depth between 17 and 40m led to sedimentation rate between 3 and 46 cm, while the effect of variations in grain size (between 0.1 and 0.4mm) was limited to a infill rate of 4 and 10cm.

In accordance with the theory explained in sub question 1, the current direction is important to consider as well, since this determines to what extend the flow velocity at the trench is reduced, resulting in sedimentation. Furthermore, the larger the current speed, the more sedimentation can be expected.

When taking into account sand wave perturbations, the location of the trench with respect to the sand wave is the most important variable to consider, as discussed in sub question 2. Due to the fact that the sand wave height and the sand wave length are related (larger sand wave heights are found for longer sand waves), their combined effect is limited.

4. *What is the difference in probabilistic sedimentation rate in the trenches computed by the different models?*

The median trench sedimentation during the month April is in both SedPit and the 2DV-model 0.06m. Due to the increased complexity of the 2DV-model, the cumulative distribution function obtained from this model is narrower than SedPit. The P05/P95 values are 0.04/0.13m and 0.03/0.09m respectively. Including (idealised) sand wave perturbations in the 2DV-model, increases the range of the P05-P95 values for in trench sedimentation to 0.01 and 0.13m.

When a distinction is made between trenches located at sand wave crests, troughs and halfway, the accuracy of the SedPit results can be better compared. SedPit overestimates the siltation for trenches located in sand wave troughs compared to the 2DV-model. Even adjusting the sediment transport calibration parameter to its minimum of 0.5 does not lead to similar results. The opposite is true for trenches located at sand wave crests: keeping the calibration parameter at the maximum of 1, leads to an underestimation of the trench siltation compared to the results obtained with the 2DV-model.

5. *What is the quality of the predictions from the various models compared to measurements of back fill?*

The quality of the sedimentation surveys is not good enough to compare the model results to. When taking into account data obtained during dredging operations as well, it can be observed that similar to the model results, decreasing water depths and an increase in current velocity enhance sedimentation. Due to the insufficient quality of both measurements, it can only be concluded that the sedimentation thickness obtained during the model study is of the same order of magnitude as the data from the survey and dredging campaigns. The data is not accurate enough to distinguish differences in sedimentation along the sand wave perturbations.

How to probabilistically assess trench sedimentation for trenches located in sand wave fields, such as at the Borssele Wind Farm Zone?

Based on the results, it can be concluded that SedPit can be used as first assessment tool for the trench sedimentation, since it covers the range obtained with the more complex 2DV-model. The main advantage is the limited computation time of around 1.5 hours, compared to of around 48 hours with the sand wave model. On the other hand, the 2DV-model is able to produce more accurate results.

For trenches located near sand wave crests and troughs it is furthermore advised to use at least the 2DV-model. If for some reason, this is not possible, it is recommended to adjust the calibration parameter of sand transport in SedPit such that more realistic sedimentation rates are obtained. This means a higher value (1.0), has to be applied for trenches at sand wave crests, a low value (0.5) can be used at sand wave troughs. Although this still leads to an overestimation of the trench siltation in the case of a trench located near the crest, and an underestimation near sand wave troughs compared to the results of the 2DV-model, the differences are reduced. It is not advised to adjust the calibration parameter outside the range of 0.5-1.0, provided by Van Rijn (2013).

Moreover, the 2DV-model can only be used in the case of perpendicular flow with respect to the trench-axis. Although SedPit is theoretically able to include the effect of non-perpendicular flows, the overestimation of trench sedimentation (Van Rijn, 2013) underlines the importance of 2DH-modelling in this case, and hence 3D-modelling for trenches located in sand wave fields.

Furthermore, due to the that the probabilistic assessment of the 2DV-model is done by means of Latin Hypercube Sampling, extreme conditions cannot be taken into account. If the influence of extreme events is of interest, SedPit in combination with a Monte Carlo analysis is more suitable. With the addition of a single run with the 2DV-model, these results can be verified, increasing the quality of the prediction.

9 Recommendations

Based on the discussion in chapter 7 and the conclusions drawn in chapter 8, recommendations are made regarding possibilities for further research on the assessment of trench siltation in sand wave fields. This includes the introduction of a non-idealised bathymetry, the addition of other case study areas, the consideration of extreme events and the usage of more detailed measurement campaigns.

Realistic bathymetry

In this research idealised bathymetries were used: for SedPit a flat bottom is the base in which a trench is located and the 2DV-model was able to include the influence of sand wave perturbations, however only in an idealized situation. In reality the seabed consists of the superposition of different bedforms, such as sand banks and (mega) ripples.

Although sand banks are stable on the timescale in which sedimentation take place, the presence of the sand banks itself might influence the trench sedimentation, similar to sand waves. However, the effect is expected to be limited due to the gradual changes in bed level. On the other hand, according to Leenders (2018), large sand banks could increase sand wave migration almost by a factor 10. In this way sand wave migration can significantly affect trench sedimentation. Moreover, imposing a realistic bathymetry would also provide more insight in the potential risks of migration of the smaller, but more dynamic ripples. Due to the effect of the e.g. the Coriolis force on sand banks, this would require an 3D modelling approach.

Other locations

The conclusions drawn are based on the case study at the Borssele Wind Farm Zone. Although this provides an insight on the effects of sand waves on the probabilistic assessment of trench sedimentation, other locations might be interesting to consider as well in which for example the tide is composed of other tidal constituents.

It is furthermore interesting to investigate the trench siltation for trenches with a different orientation compared to the sand wave field. More oblique or even parallel flows will significantly reduce the sedimentation. This can affect the model selection upfront as well, since the accuracy of the results obtained by SedPit is reduced for non-perpendicular flows (Van Rijn, 2013). Furthermore, the present 2DV-model will not be suitable as well, as mentioned in the discussion (chapter 7). The required selection of new (3D) models, gives a better insight in the probabilistic assessment for multiple trench – sand wave configurations.

Extreme conditions

The occurrence of extreme events is not been accounted for in this study, since this is usually not of interest for contractors as Boskalis. Although this might be of minor importance for contractors, the ability for a proper estimation of e.g., severe weather conditions can be important to other parties. Since this study does not include such events, it cannot be concluded whether both models arrive at comparable results. Furthermore, by selecting Latin Hypercube Sampling as probabilistic assessment method, the tails of the cumulative distribution function of the sedimentation computed by both models cannot be compared. In future research, extreme conditions with a low probability of occurrence can included to be able to compare the overall model performance of both models. This requires another probabilistic assessment method for the 2DV-model.

Detailed measurement campaigns

The quality of the measurements used in the present study does not provide the opportunity for a detailed comparison between sedimentation surveys and the computed trench siltation by the different models. The therefore included dredging data is not accurate enough as well. If the sedimentation surveys or dredging volumes are more detailed, the effect of different bedforms on the sedimentation can be distinguished. In this way a better validation of the model results can be performed, and a link between measurements and literature studies can be established.

References

Bayes server (2019) *Bayesian networks - an introduction*. Available at: https://www.bayesserver.com/docs/introduction/bayesian-networks/ (Accessed: 3 October 2019).

Berends, K. D. *et al.* (2019) 'Towards efficient uncertainty quantification with high-resolution morphodynamic models: A multifidelity approach applied to channel sedimentation', *Coastal Engineering*, 152(October 2018). doi: 10.1016/j.coastaleng.2019.103520.

van den Berg, J. *et al.* (2012) 'Non-linear process based modelling of offshore sand waves', *Continental Shelf Research*, 37, pp. 26–35. doi: 10.1016/j.csr.2012.01.012.

Besio, G. *et al.* (2003) 'Migrating sand waves', *Ocean Dynamics*, 53(3), pp. 232–238.

Besio, G. *et al.* (2004) 'On the modeling of sand wave migration', *Journal of Geophysical Research*, 109.

Borsje, B. W. *et al.* (2011) 'Modeling sandwave formation in a numerical shallow water model', in *7th IAHR symposium on river coastal and estuarine morphodynamics, Beijing, China*.

Borsje, B. W. *et al.* (2013) 'Modeling tidal sand wave formation in a numerical shallow water model : The role of turbulence formulation', *Continental Shelf Research*, 60, pp. 17–27. doi: 10.1016/j.csr.2013.04.023.

Borsje, B. W. *et al.* (2014) 'The role of suspended load transport in the occurrence of tidal sand waves', *Journal of Geophysical Research: Earth Surface*, 119(4), pp. 701–716.

Bosboom, J. and Stive, M. J. F. (2015) *Coastal Dynamics*. Version 0. Delft: Delft University of Technology.

Boskalis (2017) *Borssele export cables: assessment of the infill in the dredged trenches before cable installation*.

Boskalis (2018) *Sedimentation surveys and dredging data from the export cables of Borssele*. Papendrecht.

Dagalaki, V. (2018) *Quantifying coastline change uncertainty using a multi-model aggregation approach*. Delft University of Technology, Deltares.

Deltares (2015a) 'Metocean study for the Borssele Wind Farm Zone Site I'.

Deltares (2015b) 'Morphodynamics of Borssele Wind Farm Zone WFS-I and WFS-II Final Report', p. 71.

Deltares (2016) 'Morphodynamics of Borssele Wind Farm Zone WFS-III, WFS-IV and WFS-V Update version January 25th, 2016', (1210520-000-HYE-0012).

Deltares (2020) 'Delft Dashboard, tidal stations'.

Enschedé, M. O. (2019) *Stochastic beach width prediction at a recently nourished beach*. Delft University of Technology and Boskalis.

Fugro (2015a) *Geotechnical Report, Borssele Wind Farm Site I*. Nootdorp.

Fugro (2015b) *Geotechnical Report, Borssele Wind Farm Site II*. Nootdorp.

van Gerwen, W. *et al.* (2018) 'Modelling the effect of suspended load transport and tidal asymmetry on the equilibrium tidal sand wave height', *Coastal Engineering*, 136(January), pp. 56–64. doi: 10.1016/j.coastaleng.2018.01.006.

Hendriks, A. (2019) 'Uncertainty effects: personal conversation'.

Holthuijsen, L. H. (2017) *Waves in oceanic and coastal waters*. New York: Cambridge University Press.

Hossain, F., Anagnostou, E. N. and Bagtzoglou, A. C. (2006) 'On Latin Hypercube sampling for efficient uncertainty estimation of satellite rainfall observations in flood prediction', *Computers & Geosciences*, 32(6), pp. 776–792. doi: https://doi.org/10.1016/j.cageo.2005.10.006.

Hulscher, S. J. M. H. (1996a) 'Tidal-induced large-scale regular bed form patterns in a three-dimensional shallow water model', *Journal of geophysical research: Oceans*, 101(C9), pp. 20727–20744.

Hulscher, S. J. M. H. (1996b) 'Tidal-induced large-scale regular bed form patterns in a three dimensional shallow water model', *Journal of Geophysical Research*, 101, pp. 20,727-20,744.

Hurtado, J. E. and Barbat, A. H. (1998) 'Monte Carlo techniques in computational stochastic mechanics', *Archives of Computational Methods in Engineering*, 5(1), p. 3. doi: 10.1007/BF02736747.

Iman, R. L. and Conover, W. J. (1982) 'A distribution-free approach to inducing rank correlation among input variables', *Communications in Statistics - Simulation and Computation*, 11(3), pp. 311–334. doi: 10.1080/03610918208812265.

Jensen, J. H., Madsen, E. O. and Fredsoe, J. (1999a) 'Oblique Flow over Dredged Channels. I: flow description', *Journal of Hydraulic Engineering*, 125(November), pp. 1181–1189.

Jensen, J. H., Madsen, E. O. and Fredsoe, J. (1999b) 'Oblique Flow over Dredged Channels. II: Sediment Transport and Morphology', *Journal of Hydraulic Engineering- ASCE.*, 125(4), pp. 369–375. doi: 10.1061/(ASCE)0733-9429(1999)125.

Jonkman, S. N. *et al.* (2017) *Probablistic design: risk and reliability analysis in civil engineering*. 4th edn. Delft University of Technology.

De Koning, M. F. (2007) *The stochastic characteristics of geometric properties of sand waves in the North Sea*. University of Twente.

Krabbendam, J. (2018) *Modelling the long term evolution of observed tidal sand waves in the North Sea*. University Utrecht, WaterProof B.V.

Kroon, A. *et al.* (2017) 'Uncertainty Assessment in Coastal Morphology Prediction With a Bayesian Network', *Coastal Dynamics*, (254).

Kroon, A. *et al.* (2019) 'Incorporating model uncertainty in building with nature designs', *preprint submitted to Coastal Engineering*.

Leenders, S. (2018) *Numerical modelling of the migration direction of offshore sand waves using Delft3D*. Delft University of Technology.

Leser, G., van Kester, J. and Roelvink, J. A. (2000) *On-line Sediment Transport within Delft3D-flow*. Delft.

Li, F. *et al.* (2013) 'Probabilistic modeling of wave climate and predicting dune erosion', *Journal of Coastal Research*, 65(February 2014), pp. 760–765. doi: 10.2112/si65-129.1.

Luijendijk, A. P. *et al.* (2017) 'The initial morphological response of the Sand Engine: A process-based modelling study', *Coastal Engineering*, 119(September 2016), pp. 1–14. doi: 10.1016/j.coastaleng.2016.09.005.

Van Maren, D.J.; Cronin, K. (2016) 'Uncertainty in complex three-dimensional sediment transport models: equifinality in a model application of the Ems Estuary, the Netherlands', *Ocean Dynamics*, 66(12), pp. 1665–1679. doi: 10.1007/s10236-016-1000-9.

McCave, I. N. (1971) 'Sand waves in the North Sea off the coast of Holland', *Marine geology*, 10(3), pp. 199–225.

Menninga, J. (2012) *Analysis of variations in characteristics of sand waves observed in the Dutch coastal zone: a field and model study*. Utrecht University.

Németh, A. A., Hulscher, S. J. M. H. and de Vriend, H. J. (2002) 'Modelling sand wave migration in shallow shelf seas', *Continental Shelf Research*, 22(18–19), pp. 2795–2806.

Nemeth, A., Hulscher, S. J. M. H. and de Vriend, H. J. (2003) 'Offshore sand wave dynamics, engineering problems and future solutions', *Pipeline and gas journal*, 230, pp. 67–69.

Noordzeeloket (2019) *Cables and pipelines*. Available at: https://www.noordzeeloket.nl/en/functions-and-use/kabels-leidingen/ (Accessed: 10 October 2019).

Olsson, A., Sandberg, G. and Dahlblom, O. (2003) 'On Latin hypercube sampling for structural reliability analysis', *Structural safety*, 25(1), pp. 47–68.

Owen, K. and Basu, B. A. (2018) 'Quasi-Monte Carlo for an Integrand with a Singularity Along a Diagonal in the Square', in Dick, J., Kuo, F. Y., and Woźniakowski, H. (eds) *Contemporary Computational Mathematics - A Celebration of the 80th Birthday of Ian Sloan*. Cham: Springer International Publishing, pp. 119–130. doi: 10.1007/978-3-319-72456-0_6.

Packham, N. and Schmidt, W. M. (2008) 'Latin hypercube sampling with dependence and applications in finance', *CPQF Working Paper Series*, 15. Available at: http://hdl.handle.net/10419/40177.

Provinciale Zeeuwse Courant (2019) *Bouw windpark Borssele 1 en 2 begint in december*, *Vlissingen*. Available at: https://www.pzc.nl/zeeuws-nieuws/bouw-windpark-borssele-1-en-2-begint-in-december~a418d034/ (Accessed: 25 October 2019).

Rijksoverheid (2018) 'Windenergie op zee'. Available at: https://www.rijksoverheid.nl/onderwerpen/duurzame-energie/windenergie-op-zee.

Van Rijn, L. (1993) *Principles of Sediment Transport in Rivers, Estuaries and Coastal Seas*. Amsterdam: Aqua Publications.

Van Rijn, L. (2013) *Basics of Channel deposition/siltation*. Available at: https://www.leovanrijn-sediment.com/papers/Channelsedimentation2013.pdf (Accessed: 20 January 2020).

Van Rijn, L., Walstra, D. and Van Ormondt, M. (2004) *Description of TRANSPOR2004 and Implementation in Delft3D-online*. Delft.

Rip, J. (2015) *Probabilistic downtime analysis for complex marine projects*. Delft University of Technology, Boskalis.

Sallaberry, C. J., Helton, J. C. and Hora, S. C. (2008) 'Extension of Latin hypercube samples with correlated variables', *Reliability Engineering and System Safety*, 93(7), pp. 1047–1059. doi: 10.1016/j.ress.2007.04.005.

Sociaal-economische raad (2013) 'Energieakkoord voor duurzame groei', *Rapport energieakkoord*.

Svasek Hydraulics (2016) 'Metoceandata export cables Borssele Methodology and model validation', p. 23.

TenneT TSO (2016) *Aanvulling milieueffectrapport net op zee Borssele*. Arnhem.

Uusitalo, L. *et al.* (2015) 'An overview of methods to evaluate uncertainty of deterministic models in decision support', *Environmental Modelling and Software*, 63, pp. 24–31. doi: 10.1016/j.envsoft.2014.09.017.

Whipple, K. (2004) 'Surface Processes and Landshape evolution', *MIT, earth, atmosphere and planetary sciences*.

Yan, K. *et al.* (2017) 'Managing information uncertainty in wave height modeling for the offshore structural analysis through random set', *Complexity*, 2017. doi: 10.1155/2017/9546272.

Appendix A. Data

In Appendix A.1 an overview of the available data is given. Besides the data discussed in Chapter 3 and 4, the soil characteristics are provided in Appendix A.2, additional information on the sand wave dimensions are given in Appendix A.3.

A.1 Summary of all available data

Data is available from different sources. A distinction is made between raw data and processed data, mainly available from previous research.

A.1.1 Raw data

An overview of the raw data is presented below, categorized by type. Furthermore the covered time range is given as well.

Wave data (Euro Platform)

- Wave direction (20 years, hourly)
- Significant wave height (20 years, hourly)
- Wave period (20 years, hourly)

Wind data (Euro Platform)

- Wind speed (20 years, hourly)
- Wind direction (20 years, hourly)

Tide information

- Tidal constituents (phase + amplitude), retrieved from Delft dashboard and Bosboom and Stive (2015)

Current information

- Current speed, 4 - 30m depth (Borssele, 1.5 years, 10 minutes)
- Current direction, 4 - 30m depth (Borssele, 1.5 years, 10 minutes)

Bathymetry and soil characteristics

- Bathymetry: EMODnet
- Soil characteristics (Hulscher, 1996a; Fugro, 2015a, 2015b), limited measurements

A.1.2 Processed data

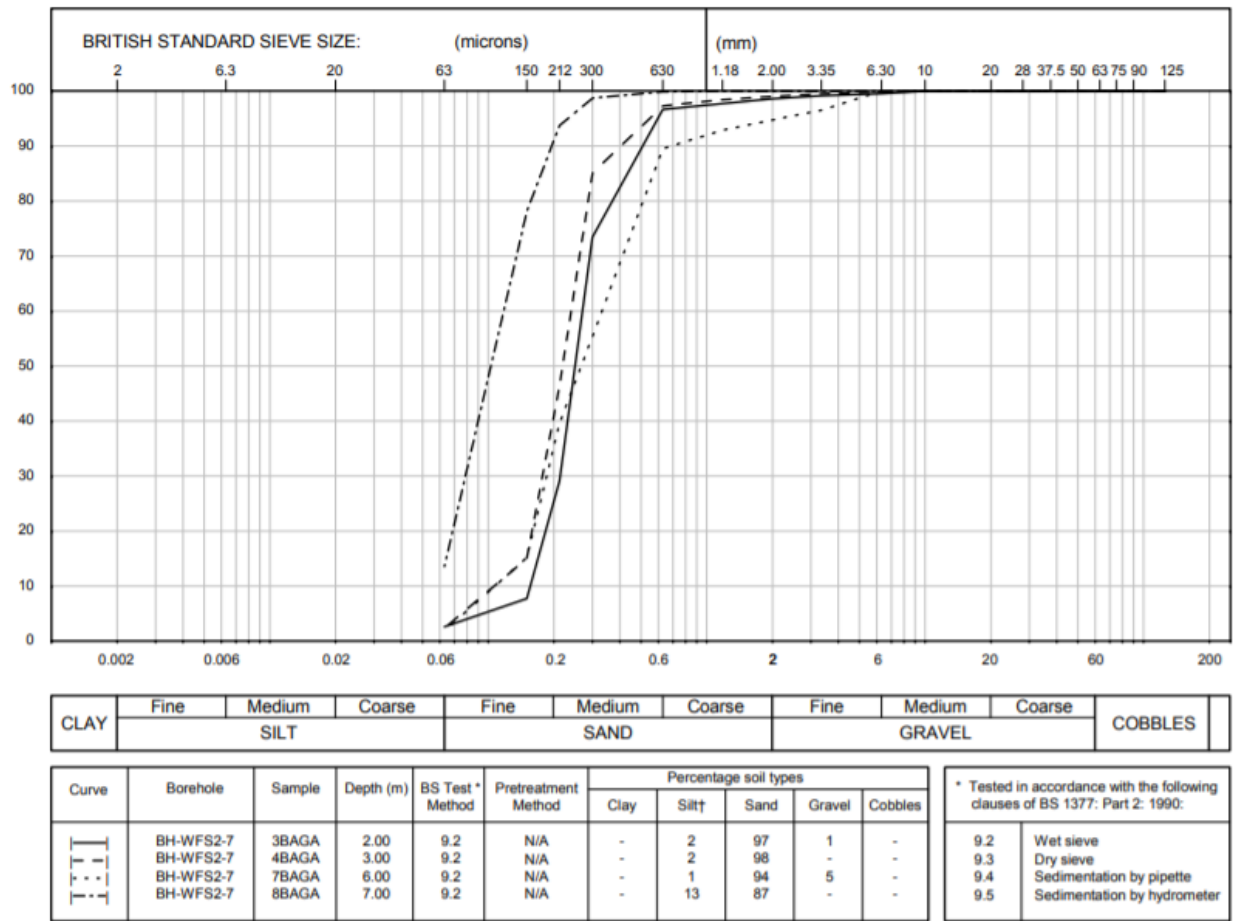Furthermore, from two different sources, processed data is available:

- Model output of a study of Svasek Hydraulics (2016), at six locations along the trench. At these locations, wave and wave data, tidal information, and current speeds and directions are computed with FINEL2D.
- Deltares (2015) also used numerical models to determine the sea state at different locations in the Wind Farm Zone.

A.2 Soil characteristics

An example of a borehole analysis can be found in Figure A.1.

Curve	Borehole	Sample	Depth (m)	BS Test * Method	Pretreatment Method	Clay	Silt†	Sand	Gravel	Cobbles
	BH-WFS2-7	3BAGA	2.00	9.2	N/A	-	2	97	1	-
	BH-WFS2-7	4BAGA	3.00	9.2	N/A	-	2	98	-	-
	BH-WFS2-7	7BAGA	6.00	9.2	N/A	-	1	94	5	-
	BH-WFS2-7	8BAGA	7.00	9.2	N/A	-	13	87	-	-

Percentage soil types

* Tested in accordance with the following clauses of BS 1377: Part 2: 1990:
9.2 Wet sieve
9.3 Dry sieve
9.4 Sedimentation by pipette
9.5 Sedimentation by hydrometer

† Note: Where a sedimentation test was not carried out, this figure represents total fines, i.e., particles of diameter less than 63 microns

Figure A.1: An example of the soil-analysis obtained from a bore-hole in the Borssele Wind Farm Zone. The grain size diamter is taken into account at depths between 0 and 5m.

A.3 Sand wave characteristics

The sand wave characteristics are known from the different sites at the Borssele Wind Farm Zone. In Figure A.1, a map of the different sites is shown. Deltares (2015b, 2016) provides information on the sand wave length (Figure A.2), sand wave height (Figure A.4) and the sand wave migration speed (Figure A.5).
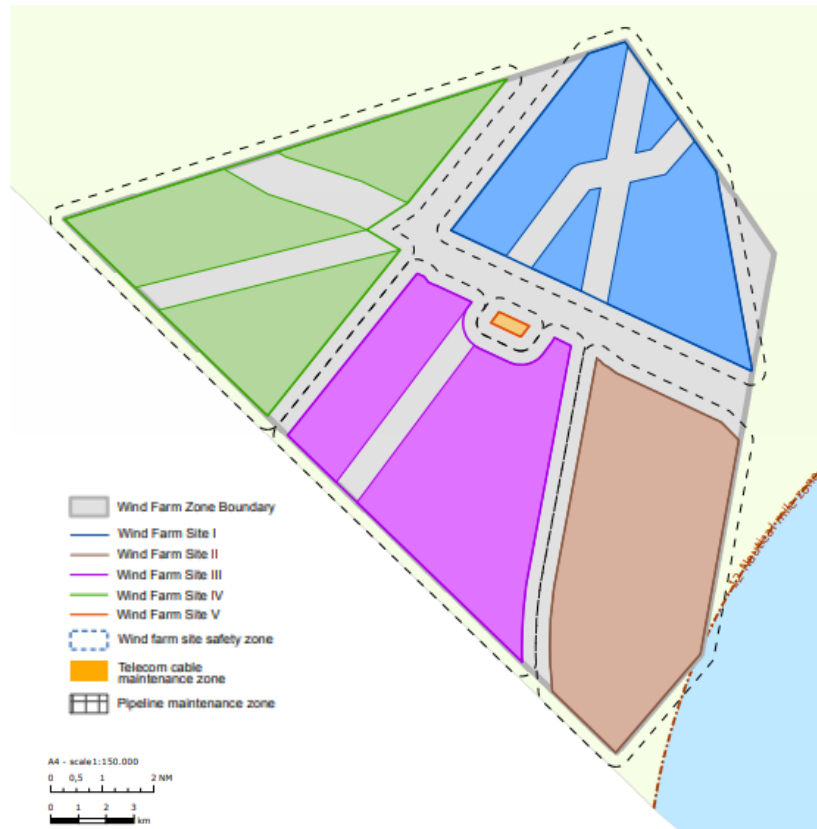

Figure A.2: A map of the different sites of the Borssele Wind Farm Zone (Deltares, 2015b)
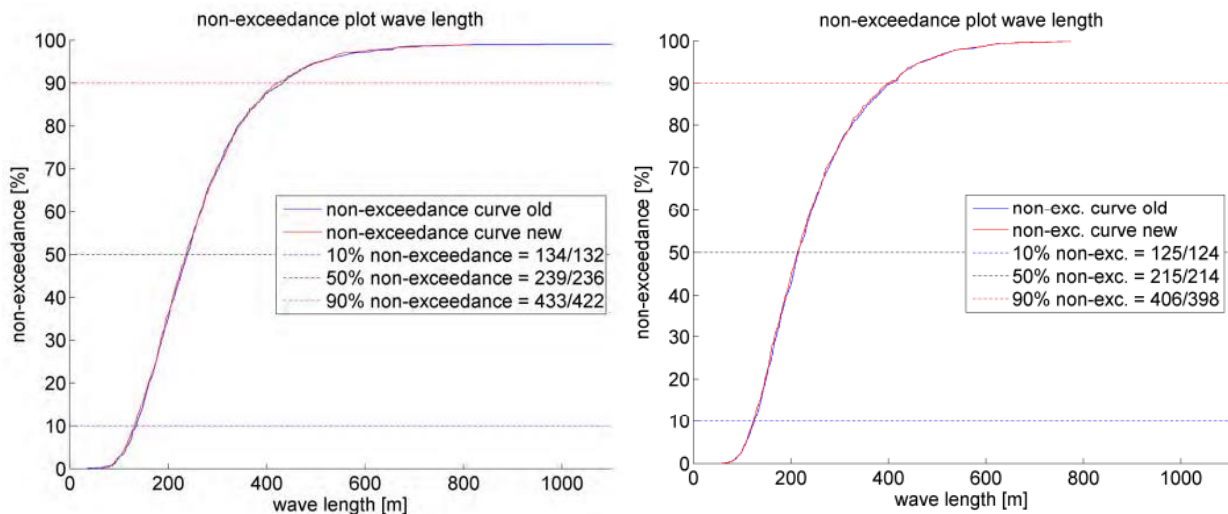

Figure A.3: The sand wave length of Borssele site I & II (left) and Borssele site III, IV and V (right) (Deltares, 2015b, 2016)
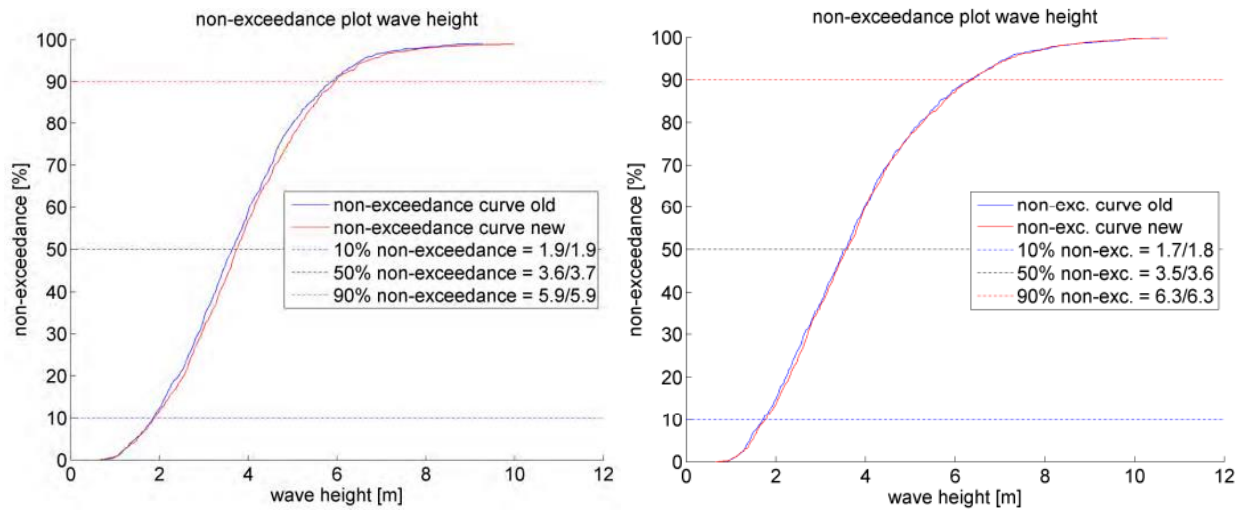
Figure A.4: The sand wave height of Borssele site I & II (left) and Borssele site III, IV and V (right) (Deltares, 2015b, 2016).
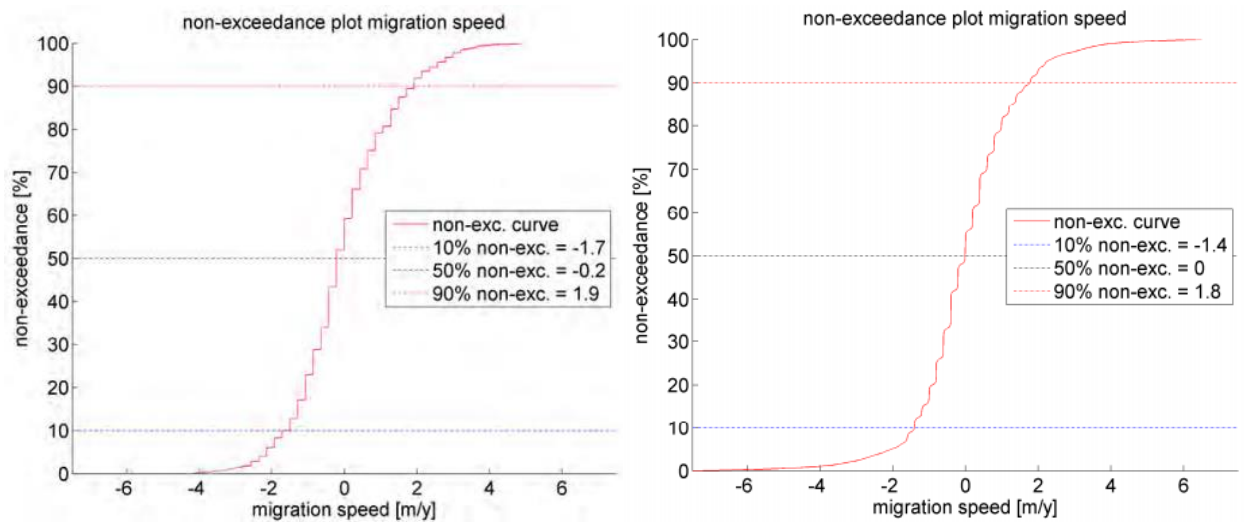

Figure A.5: The sand wave migration speed [m/year] of Borssele site I & II (left) and Borssele site III, IV and V (right) (Deltares, 2015b, 2016).

Appendix B. SedPit

In this appendix additional information on the SedPit model is provided. First, in Appendix B.1, the model formulations are discussed. An overview of all parameters is given in Appendix B.2. A more detailed overview of the mathematical expressions of SedPit are shown in Appendix B.3.

B.1 Underlying mathematics

The three-dimensional sediment transport is calculated by solving a three-dimensional advection-diffusion equation (Leser *et al.*, 2000):

$$\frac{\delta c}{\delta t} + \frac{\delta}{\delta x}(uc) + \frac{\delta}{\delta y}(vc) + \frac{\delta}{\delta z}[(w - w_s)c] - \frac{\delta}{\delta x}\left[\epsilon_{s,x}\frac{\delta c}{\delta x}\right] - \frac{\delta}{\delta y}\left[\epsilon_{s,y}\frac{\delta c}{\delta y}\right] - \frac{\delta}{\delta z}\left[\epsilon_{s,z}\frac{\delta c}{\delta z}\right] = 0$$

in which:

- u, v, w: Flow velocities in x, y, z direction
- $\epsilon_{s,...}$: Turbulent sediment mixing in x, y, z direction
- w_s: (Hindered) settling velocity of particles

Furthermore, the depth-integrated suspended transport rates in x and y directions are:

$$q_{s,x} = \int \left(uc - \epsilon_{s,x}\frac{\delta c}{\delta x}\right) dz \ \text{and} \ q_{s,y} = \int \left(vc - \epsilon_{s,y}\frac{\delta c}{\delta y}\right) dz$$

The bed level change follows from (Van Rijn, 2013):

$$[(1-p)\rho_s]\frac{\delta z_b}{\delta t} + \left[\frac{\delta}{\delta x}(q_{t,x}) + \frac{\delta}{\delta y}(q_{t,y})\right] = 0$$

With:

- p: Porosity of the bed material
- ρ_s: Sediment density
- z_b: Bed level to horizontal reference plane
- $q_{t,...}$: Depth integrated sediment transport (bed load plus suspended load) in *x* - and *y*- direction

These equations can be solved for given flow velocities, sediment mixing coefficients, settling velocity, sediment concentrations at all boundaries and at initial time (t=0). In this way, the bed level change (sedimentation or erosion) in for instance trenches can be calculated.

Due to schematized conditions, in SedPit a simple engineering method, based on trapping efficiency, can be used to calculate trench sedimentation. To start with, in Figure B.1 a definition sketch is shown. The trench is simplified to a rectangular cross-section with a width *B1* and depth *d* (see second sketch in the figure), making intersections halfway the side slopes. The flow which carries suspended sediment, flows from left to right, crosses the trench in this schematization under an angle α_0.

The sedimentation rate per unit of length is determined by the reduction of suspended sediment transport and bed load transport over the trench:

$$\Delta S_{sand} = \left(\frac{b_0}{b_1}(q_{s,0,sand} - q_{s,1,sand})\right) e_{s,sand} \, sin(\alpha_0) \, \Delta t$$

$$+ \left(\frac{b_0}{b_1}(q_{b,0,sand} - q_{b,1,sand})\right) e_{s,sand} \, sin(\alpha_0) \, \Delta t$$

In which:

- b_0:   Ambient stream width
- b_1:   Stream width in the trench
- $q_{s,0,sand}$:   Equilibrium suspended sediment transport at upstream boundary
- $q_{s,1,sand}$:   Equilibrium suspended sand transport in the trench
- $q_{b,0,sand}$:   Equilibrium bed load sediment transport at upstream boundary
- $q_{b,1,sand}$:   Equilibrium bed load sand transport in the trench
- $e_{s,sand}$:   Van Rijn - trapping efficiency of the trench
- α_0:   Angle of incidence of flow with respect to trench alignment

Furthermore the bulk density of the deposited material is:

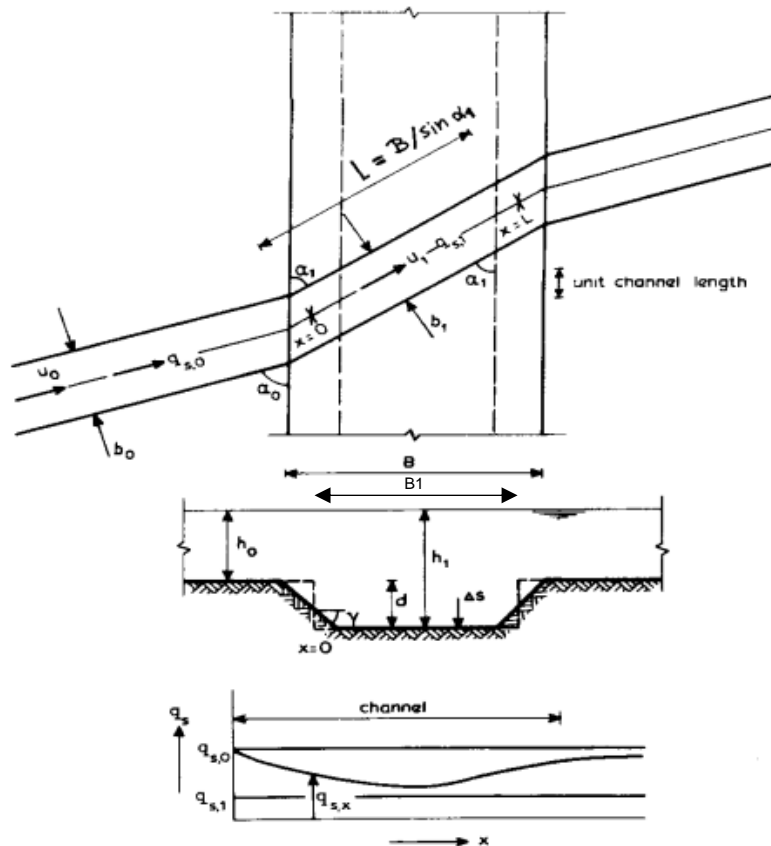- $$\rho_{bulk} = \Delta S_{sand} * 1.55$$

Figure B.1:definition sketch of the SedPit-model

Which leads to a sedimentation thickness per unit length in the trench:

$$\Delta H_{tot} = \frac{\dfrac{\Delta S_{sand}}{\rho_{bulk}}}{B_1}$$

In these formulations, the sediment transport capacity (suspended and bed load transport) is depended of the effective flow velocity u_e, consisting of flow generated by the currents (u_e) and flow generated under the influence of waves U_w:

$$u_e = u + 0.4U_w$$

Under the assumption of linear wave theory, the current velocity amplitude of waves is:

$$U_w = \frac{\pi H_s}{T_P \sinh(kh_0)}$$

In this analysis it is assumed that for both bed load transport and suspended load transport, the effective flow velocity has to exceed a certain critical velocity, before particles start to move. A complete overview of all equations used in SedPit can be found in Appendix B.3.

B.2 Input parameters

Table B.1: Input parameters for SedPit for sediment consisting of sand only

Parameter	Symbol	Dimension	Base case
Water level	ζ	[m]	Varying
Significant wave height	H_s	[m]	Varying
Peak wave period	T_p	[s]	Varying
Ambient current velocity	u_0	[m/s]	Varying
Number of time steps	n_{t_step}	[-]	720
Number of tides with a period of 12 hours	n_{tides}	[-]	1
Angle of incidence of flow with respect to trench alignment	α_0	[rad]	Varying
Length of trench	L_1	[m]	100
Ambient stream width	B_0	[m]	1
Width of trench	B_1	[m]	17
Ambient depth	d_0	[m]	Varying
Depth of trench with respect to the ambient depth	d_1	[m]	3
Median grain size diameter	d_{50}	[m]	Varying
90th percentile grain size diameter	d_{90}	[m]	0.001
Soil particle density	ρ_s	[kg/m^3]	1650
Water density	ρ_w	[kg/m^3]	1020
Viscosity	ν	[m^2/s]	0.000001
Fall velocity of sand fraction	$w_{s,sand}$	[m/s]	Varying
Ambient bed roughness	r_0	[m]	Varying
Bed roughness of trench	r_1	[m]	Varying
Calibration factor for sand transport	c_{sand}	[-]	1
Van Rijn coefficient	c_{vRijn}	[-]	Varying

B.2.1 Grain size distribution

In total 19 different sieve analysis were performed to determine the grain size distribution (Fugro, 2015a, 2015b). Due to the limited measurements, a triangular distribution of median the grain size is assumed. The cumulative distribution function of the measurements and the estimated triangular distribution are shown in Figure B.2.
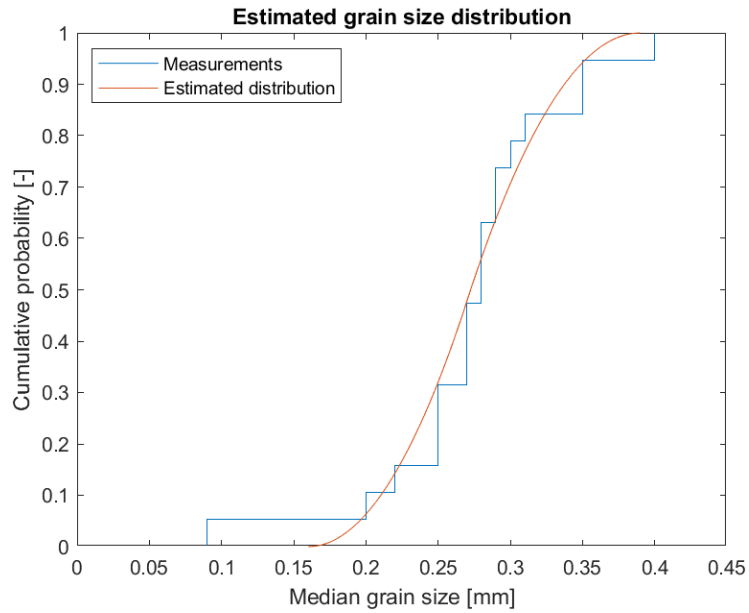
Figure B.2: Measurements and fitted distribution (triangular 0.16, 0.39, 0.27mm) of the median grain size diameter.

B.2.2   Water depth

The bathymetry measurements are obtained from EMODnet, for the area of interest and converted to water depth, relative to MSL. A Normal distribution (30.9, 4.1) provided the best fit. Figure B.3 shows the measurements and the assumed distribution.
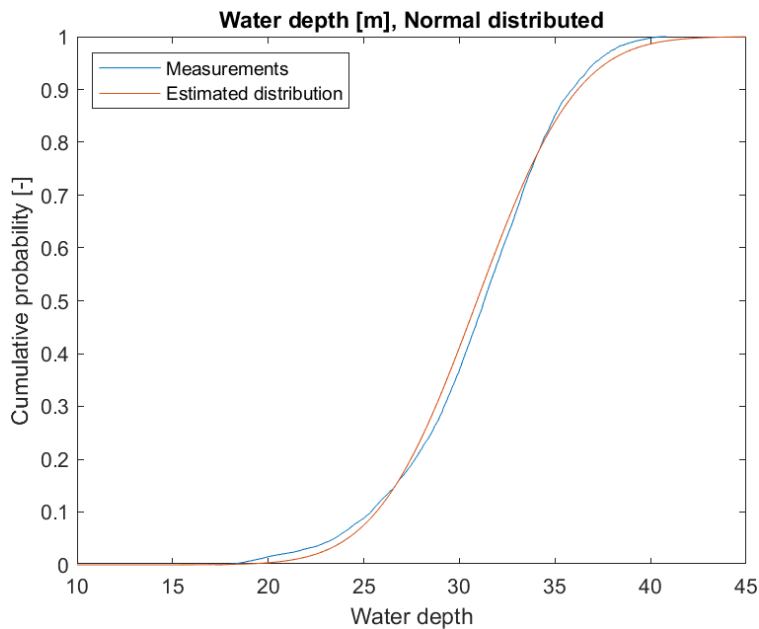

Figure B.3: Water depth (in m MSL) of the considered area, with an estimated distribution of N(30.9, 4.1).

B.3 SedPit relations

Time:

$$T = \frac{n_{tides} n_{tstep}}{365 \cdot 24}$$

Ambient water depth and trench depth:

$$h_0 = d_0 + \zeta, \qquad h_1 = d_1 + h_0$$

Chézy roughness:

$$C_{0,1} = 18 \log\left(\frac{12 h_{0,1}}{r_{0,1}}\right),$$

Critical velocity for currents:

$$u_{cr,c} = 0.19 d_{50}{}^{0.1} \log\left(\frac{12 h_0}{3 d_{90}}\right), \qquad for\ 0.0001 < \ d_{50} < 0.0005\ m$$

$$u_{cr,c} = 8.5 d_{50}{}^{0.6} \log\left(\frac{12 h_0}{3 d_{90}}\right), \qquad for\ 0.0005 < \ d_{50} < 0.002\ m$$

Critical velocity for waves:

$$u_{cr,w} = 0.24[(\Delta - 1)g]^{0.66} d_{50}{}^{0.33} T_p{}^{0.33}, \qquad for\ 0.0001 < \ d_{50} < 0.0005\ m$$

$$u_{cr,w} = 0.95[(\Delta - 1)g]^{0.57} d_{50}{}^{0.43} T_p{}^{0.14}, \qquad for\ 0.0005 < \ d_{50} < 0.002 m$$

Current velocity amplitude of waves (according to linear wave theory):

$$U_w = \frac{\pi H_s}{T_P \sinh(k h_0)}$$

in which:

$$k H_0 = \left(\frac{4.02 h_0}{T_p{}^2}\right)^{0.5} \left[1 + 0.166\left(\frac{4.02 h_0}{T_p{}^2}\right) + 0.031\left(\frac{4.02 h_0}{T_p{}^2}\right)^2\right]$$

Effective velocity:

$$u_e = u + 0.4 U_w$$

Critical velocity:

$$u_{cr} = \left(\frac{u}{u + U_w}\right) u_{cr,c} + \left(1 - \frac{u}{u + U_w}\right) u_{cr,w}$$

Mobility parameter:

$$M_e = \frac{u_e - u_{cr}}{\sqrt{(\Delta - 1)g d_{50}}}$$

in which the relative density is:

$$\Delta = \frac{\rho_s}{\rho_w}$$

Ambient bed transport:

$$q_{b,0,sand} = 0.015\gamma_s\rho_s(1-p_{mud})u_0h_0M_e^{1.5}\left(\frac{d_{50}}{h_0}\right)^{1.2}, \qquad if \; u_e > u_{cr}$$

Ambient suspended transport:

$$q_{s,0,sand} = 0.008\gamma_s\rho_s(1-p_{mud})u_0h_0M_e^{2.4}\left(\frac{d_{50}}{h_0}\right)^{1.2}D_*^{-0.6}, \qquad if \; u_e > u_{cr}$$

in which the dimensionless particle size is:

$$D_* = d_{50}\left[\frac{(s-1)g}{v^2}\right]$$

Deflection angle of the flow:

$$\alpha_1 = atan\left(\left[\frac{h_0}{h_1}\right]tan(\alpha_0)\right)$$

Current velocity in trench:

$$u_1 = u_0\left[\left(\frac{h_0}{h_1}\right)\left(\frac{\sin(\alpha_0)}{\sin(a_1)}\right)\right]$$

Bed transport in trench:

$$q_{b,1,sand} = \left(\frac{u_1}{u_0}\right)^3 q_{b,0,sand}$$

Suspended particulate matter transport in trench:

$$q_{s,1,sand} = \left(\frac{u_1}{u_0}\right)^3 q_{s,0,sand}$$

Trapping efficiency of trench:

$$e_{s,sand} = 1 - \exp\left(-c_{vRijn}\left(\frac{w_{s,sand}}{u_{*,1}}\right)\left(1+2\left(\frac{w_{s,clay}}{u_{*,1}}\right)\right)\frac{L_{eff}h_0}{h_1^2}\right)$$

in which:

- o the effective length is:

$$L_{eff} = \left(\frac{B_0}{sin(\alpha_1)}\right)$$

- o the friction velocity is:

$$u_{*,1} = \frac{\sqrt{g}}{C_1u_1}$$

- o wave enhancement factor is:

$$\varepsilon = 1 + \frac{H_s}{h_1}$$

Sedimentation rate in trench:

$$\Delta S_{sand} = e_{s,sand}\left(\frac{B_0}{L_{eff}}q_{s,0,sand} - q_{s,1,sand}\right)L_1 sin(\alpha_0)\left(\frac{n_{tides}\cdot 3600}{1000}\right)$$

$$+e_{s,sand}\left(\frac{B_0}{L_{eff}}q_{b,0,sand} - q_{b,1,sand}\right)L_1 sin(\alpha_0)\left(\frac{n_{tides}\cdot 3600}{1000}\right)$$

Bulk density of deposited material in trench:

$$\rho_{bulk} = \Delta S_{sand} * 1.55$$

in which the consolidation factor is:

$$\gamma = \left(\frac{T}{T-1}\right)\log(T) - 1$$

Total sedimentation volume in trench:

$$\Delta S_{tot,volume} = \frac{\Delta S_{tot}}{\rho_{bulk}}$$

Total sedimentation thickness in trench:

$$\Delta h_{tot} = \frac{\Delta S_{tot,volume}}{L_1 B_1}$$
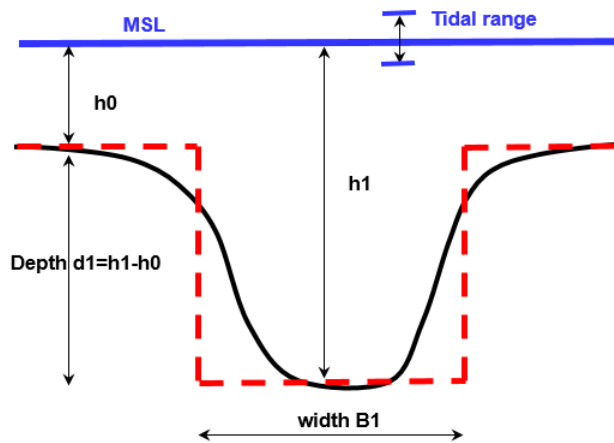

Figure B.4: A cross section of the channel schematization in SedPit.

Appendix C. 2DV – model

In this appendix, more information on the analysis of the 2DV-sand wave model is provided. To do so, the model equations are discussed in Appendix C.1. More information on probabilistic assessment method (Latin Hypercube sampling) is provided in Appendix C.2.

C.1 Model equations

The system of equations consists of (horizontal) momentum equations, a continuity equation, a turbulence closure model, a sediment transport equation and a sediment continuity equation. The presented overview is based on Borsje *et al.*, (2013, 2014).

C.1.1 Hydrodynamics

In the model, the equations are solved by sigma-layering of the vertical z- dimension. An 2DV-model means that flow and other variations are considered in x- and z- direction only, while in y-direction uniformity is assumed. This furthermore means that the Coriolis-force is neglected, which can be done in accordance to literature (see chapter 2.2) for sand waves. Since the vertical accelerations are assumed to be small compared to the gravitational accelerations, the vertical momentum equation is reduced to the hydrostatic pressure relation. The hydrostatic shallow water equations therefore are:

$$\frac{\delta u}{\delta t} + u\left(\frac{\delta u}{\delta x}\right) + \frac{\omega}{H + \zeta}\left(\frac{\delta u}{\delta \sigma}\right) = -\frac{1}{\rho_w}P_u + F_u + \frac{1}{(H + \zeta)^2}\frac{\delta}{\delta \sigma}\left(v\frac{\delta u}{\delta \sigma}\right)$$

$$\frac{\delta \omega}{\delta \sigma} = -\frac{\delta \zeta}{\delta t} - \frac{[(H + \zeta)u]}{\delta x}$$

In which:

- u:　　　　　　　　horizontal velocity (in x-direction)
- ω:　　　　　　　vertical velocity relative to the vertical σ-plane
- H:　　　　　　　　water depth below reference datum
- ζ:　　　　　　　free surface elevation
- P_u:　　　　　　　hydrostatic pressure gradient
- F_u:　　　　　　　horizontal exchange of momentum due to turbulent fluctuations
- v:　　　　　　　　vertical eddy viscosity

The vertical eddy viscosity (variable in both time and space) is determined by the k-ϵ turbulence model.

At the bed ($\sigma = 0$), a no-stress condition is applied and the vertical velocity (ω) = 0. The bed shear stress (τ_b), based on the assumption of a logarithmic velocity profile, is defined as:

$$\tau_b \equiv \rho_w \frac{v}{(H + \zeta)}\frac{\delta u}{\delta \sigma} = \rho_w u_* |u_*|, \qquad \omega = 0$$

In which:

- u_*:　　　　　　　shear velocity

At the free surface ($\sigma = 0$), a no-stress condition is applied and the vertical velocity (ω) = 0:

$$\rho_w \frac{v}{H + \zeta}\left(\frac{\delta u}{\delta \sigma}\right) = 0, \qquad \omega = 0$$

C.1.2 Sediment transport

The sediment transport can be divided into two categories:

- Bed load transport
- Suspended load transport

The bed load transport q_b is calculated by Van Rijn, *et al.* (2004):

$$q_b = 0.006\alpha_s \rho_s w_s d M^{0.5} M_e^{0.7}$$

In which:

- α_s: the bed slope correction parameter
- ρ_s: specific density of the sediment
- w_s: settling velocity of the sediment
- d: sediment grain size
- M: sediment mobility number
- M_e: excess sediment mobility number

Furthermore the sediment mobility number (M) and the excess sediment transport mobility number (M_e) are defined as:

$$M = \frac{u_r^2}{(\rho_s/\rho_w - 1)gd}$$

$$M_e = \frac{(u_r - u_{cr})^2}{(\rho_s/\rho_w - 1)gd}$$

In which:

- u_r: depth-averaged velocity (assuming a logarithmic velocity profile)
- u_{cr}:   critical depth-averaged velocity, based on the Shields curve.

In this model, only sediment is transported if the flow velocity exceeds the critical flow velocity.

Lastly, the bed slope correction parameter can be calculated by the inverse of the tangent of the angle of repose of sand (φ_s) (Van den Berg, *et al.*, 2012):

$$\alpha_s = \frac{1}{\tan \varphi_s}$$

The bed load transport is limited to the sediment transport below the reference height a, which is defined as: $a = 0.01H$. The sediment transport above this level is considered to be suspended load transport.

The suspended sediment concentration is calculated by solving the advection–diffusion equation:

$$\frac{\delta c}{\delta t} + \frac{\delta}{\delta x}(uc) + \frac{\delta}{\delta z}[(w - w_s)c] - \frac{\delta}{\delta x}\left[\epsilon_{s,x}\frac{\delta c}{\delta x}\right] - \frac{\delta}{\delta z}\left[\epsilon_{s,z}\frac{\delta c}{\delta z}\right] = 0$$

In which:

- c: mass concentration of sediment
- $\epsilon_{s,\ldots}$:   sediment diffusivity coefficients in x- and z- direction.

The reference concentration c_a, at height a is given by:

$$c_a = 0.015\rho_s \left(\frac{dT_a^{1.5}}{aD_*^{0.3}}\right)$$

T_a is the nondimensional bed shear stress:

$$T_a = \frac{\mu\tau_b - \tau_{cr}}{\tau_{cr}}$$

In which:

- μ: efficiency factor
- τ_b: critical bed shear stress
- D_*:   nondimensional particle diameter

The suspended load transport in x-direction is finally defined as:

$$q_{s,x} = \int_a^{H+\zeta} \left(uc - \epsilon_{s,x}\frac{\delta c}{\delta x}\right)dz$$

At the end, the bed level changes are determined by the Exner equation, which states that a change in bed level is the result of a change in sediment transport:

$$\left(1 - \epsilon_p\right)\frac{\delta z_b}{\delta t} + \frac{\delta(q_b + q_s)}{\delta x} = 0$$

In which:

- ϵ_p: the bed porosity
- $q_{b,x}$:   bed load sediment transport in x-direction
- $q_{s,x}$:   suspended load sediment transport in x-direction

C.2 Latin Hypercube Samples

As discussed in Chapter 5, Latin Hypercube Sampling was applied for the probabilistic assessment.

C.2.1 Probabilities during samples

The cases considered during Latin Hypercube Sampling are summed up in Table C.1

Table C.1: Probabilistic input values for the 7 non-deterministic input parameters for Latin Hypercube Sampling

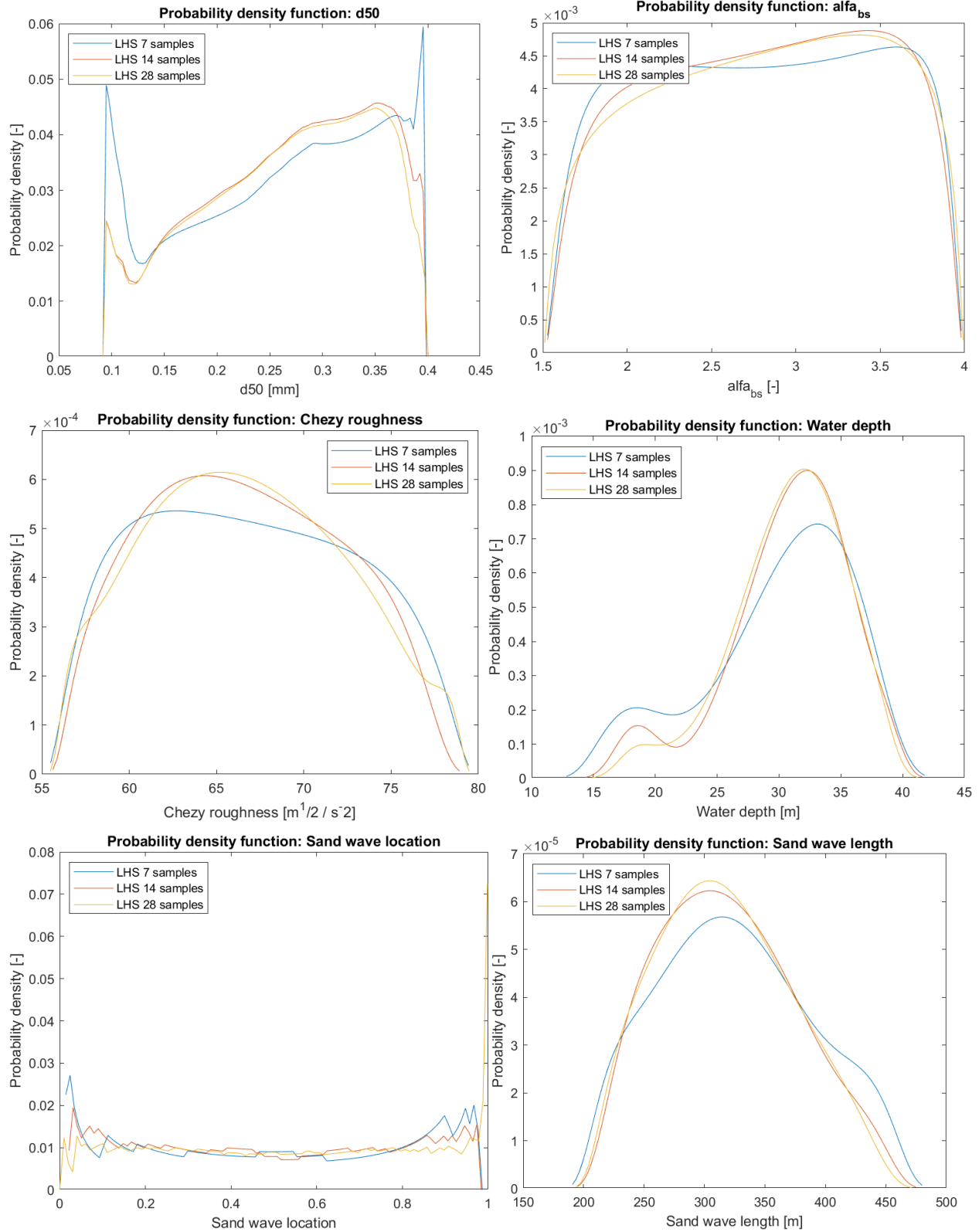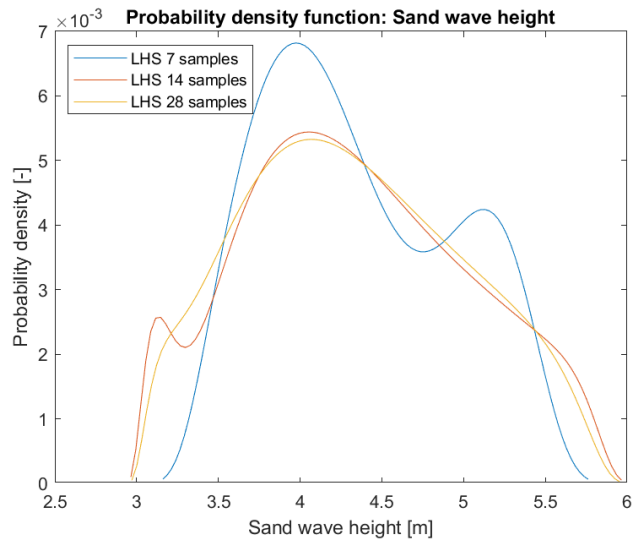|	P(D50)	P(α_{bs})	P(C)	P(d0)	P(loc)	P(L_{SW})	P(H_{SW})
Sample 1	0.9564	0.0588	0.6385	0.8669	0.7329	0.0543	0.1405
Sample 2	0.7217	0.6098	0.1354	0.3274	0.2524	0.2829	0.2784
Sample 3	0.4972	0.9476	0.5159	0.4965	0.0745	0.4202	0.375
Sample 4	0.2502	0.3138	0.373	0.1979	0.5561	0.5559	0.4399
Sample 5	0.3506	0.1484	0.1799	0.8184	0.6037	0.6933	0.6112
Sample 6	0.0036	0.4319	0.8881	0.6809	0.9404	0.8036	0.8512
Sample 7	0.7099	0.8142	0.8233	0.0056	0.3306	0.9829	0.8858
Sample 8	0.1785	0.404	0.3406	0.2784	0.1747	0.1339	0.0099
Sample 9	0.3715	0.9114	0.7432	0.3714	0.846	0.1516	0.1951
Sample 10	0.5816	0.0795	0.2341	0.5695	0.0636	0.3186	0.3553
Sample 11	0.8832	0.7462	0.6715	0.1071	0.8726	0.4827	0.5577
Sample 12	0.795	0.6439	0.458	0.973	0.7001	0.5922	0.645
Sample 13	0.0951	0.2183	0.0412	0.7723	0.3828	0.7668	0.7385
Sample 14	0.56	0.5551	0.929	0.5921	0.4545	0.8842	0.9696
Sample 15	0.3121	0.9885	0.0913	0.5055	0.5072	0.0279	0.3173
Sample 16	0.4075	0.0112	0.5497	0.3945	0.2313	0.0781	0.0388
Sample 17	0.9121	0.3774	0.2568	0.2269	0.7624	0.2058	0.0795
Sample 18	0.8474	0.778	0.7566	0.4337	0.1367	0.22	0.1648
Sample 19	0.036	0.829	0.9862	0.1247	0.902	0.3298	0.2419
Sample 20	0.1346	0.693	0.7127	0.6561	0.3007	0.3813	0.4103
Sample 21	0.2147	0.2519	0.9019	0.2886	0.9999	0.4564	0.4911
Sample 22	0.1969	0.3278	0.7924	0.6239	0.6356	0.5224	0.5099
Sample 23	0.6169	0.6044	0.0175	0.7167	0.4234	0.6106	0.5898
Sample 24	0.5295	0.1828	0.4199	0.8259	0.8092	0.6483	0.7114
Sample 25	0.9816	0.5236	0.3107	0.1637	0.2013	0.7187	0.764
Sample 26	0.6633	0.8688	0.1598	0.9483	0.6448	0.8285	0.7877
Sample 27	0.7517	0.4949	0.599	0.9128	0.4964	0.9123	0.8945
Sample 28	0.4559	0.1243	0.4791	0.0368	0.0143	0.948	0.9429

C.2.2 Corresponding parameter values

The cases considered during Latin Hypercube Sampling are summed up in Table C.2.

Table C.2: Corresponding values to the previous probabilistic input values for all non-deterministic input variables.
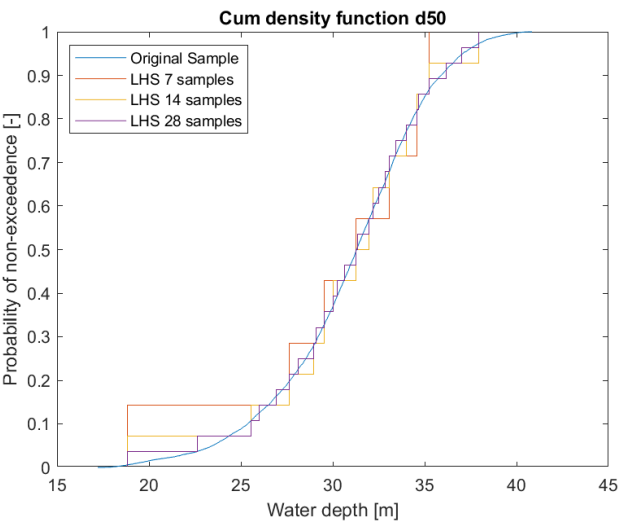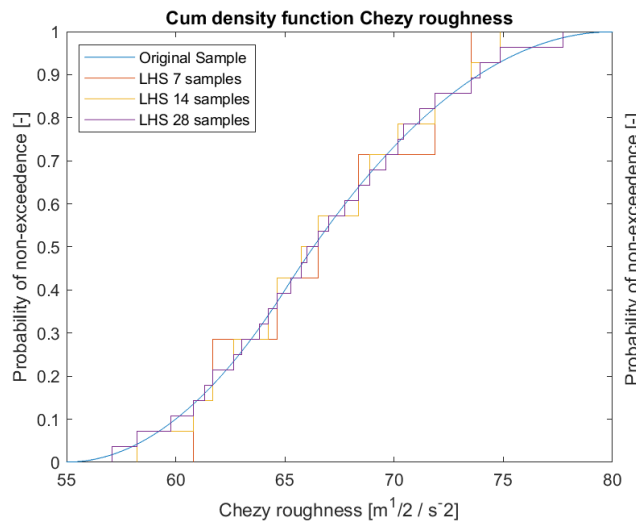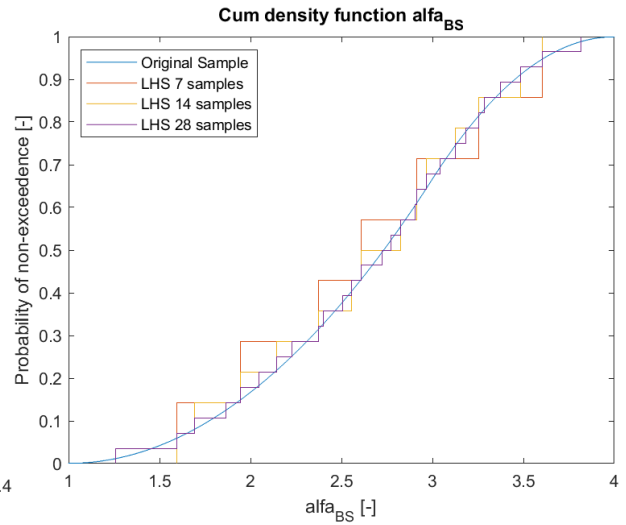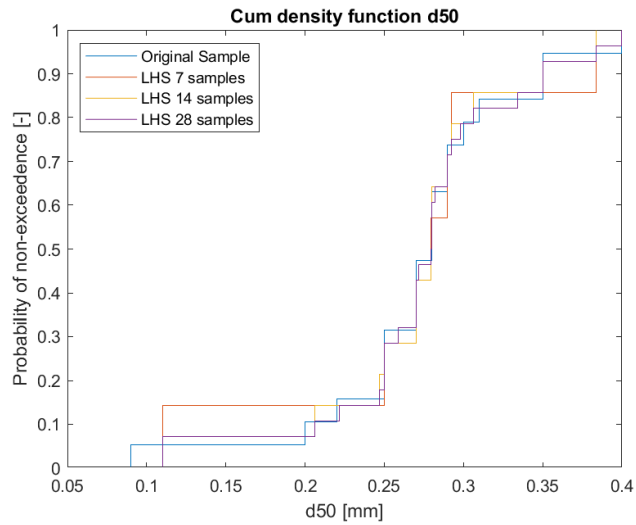
	D50	α_{bs}	C	d0	loc	L_{SW}	H_{SW}
Sample 1	0.10	1.6	68.4	35.2	0.73	236.84	3.65
Sample 2	0.29	2.9	60.8	29.5	0.25	284.10	3.91
Sample 3	0.28	3.6	66.5	31.3	0.07	302.55	4.06
Sample 4	0.25	2.4	64.7	27.6	0.56	320.95	4.17
Sample 5	0.27	1.9	61.7	34.6	0.60	342.76	4.47
Sample 6	0.09	2.6	73.5	33.1	0.94	364.18	5.06
Sample 7	0.29	3.3	71.9	18.8	0.33	424.68	5.17
Sample 8	0.25	2.6	64.2	29.0	0.17	257.86	3.17
Sample 9	0.27	3.5	70.2	30.0	0.85	261.56	3.77
Sample 10	0.28	1.7	62.7	32.0	0.06	289.25	4.03
Sample 11	0.35	3.1	68.9	25.5	0.87	310.72	4.37
Sample 12	0.31	3.0	65.7	37.9	0.70	326.34	4.54
Sample 13	0.21	2.1	58.2	34.0	0.38	356.49	4.75
Sample 14	0.28	2.8	74.8	32.2	0.45	384.10	5.57
Sample 15	0.26	3.8	59.8	31.3	0.51	226.41	3.98
Sample 16	0.27	1.3	67.0	30.3	0.23	244.19	3.34
Sample 17	0.35	2.5	63.0	28.1	0.76	271.73	3.49
Sample 18	0.33	3.2	70.4	30.7	0.14	274.16	3.70
Sample 19	0.11	3.3	77.7	26.0	0.90	290.80	3.85
Sample 20	0.22	3.0	69.6	32.9	0.30	297.63	4.12
Sample 21	0.25	2.2	73.9	29.1	1.00	307.22	4.25
Sample 22	0.25	2.4	71.2	32.5	0.64	316.17	4.29
Sample 23	0.28	2.9	57.1	33.4	0.42	329.16	4.43
Sample 24	0.28	2.0	65.3	34.7	0.81	335.16	4.68
Sample 25	0.40	2.8	63.8	26.9	0.20	347.29	4.81
Sample 26	0.29	3.4	61.3	37.0	0.64	369.80	4.87
Sample 27	0.30	2.7	67.7	36.2	0.50	392.65	5.20
Sample 28	0.27	1.9	66.0	22.6	0.01	405.84	5.41

C.2.3 Estimated probability density functions

Probability density function: Sand wave height

C.2.4 Cumulative probability density functions

Cum density function d50

Cum density function alfa$_{BS}$

Cum density function Chezy roughness

Cum density function d50

Cum density sand wave position

Cum density sand wave length

Cum density sand wave height
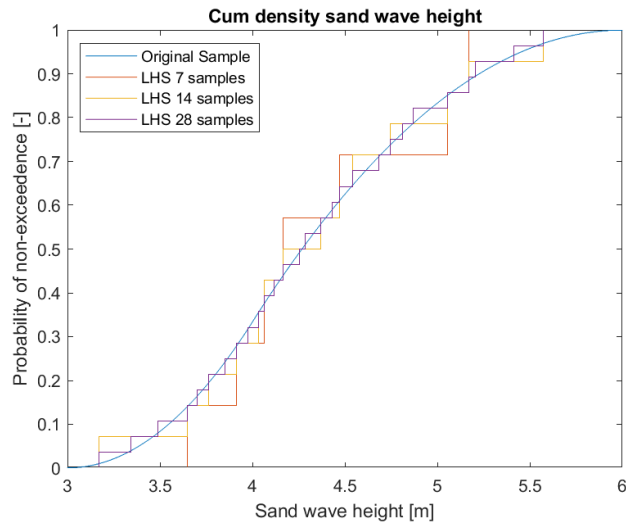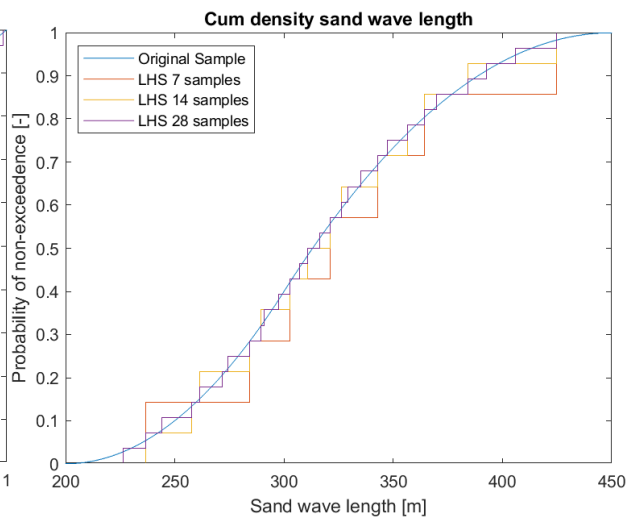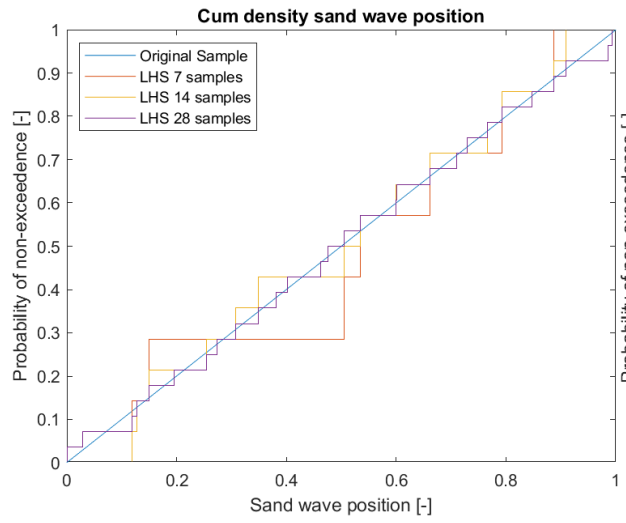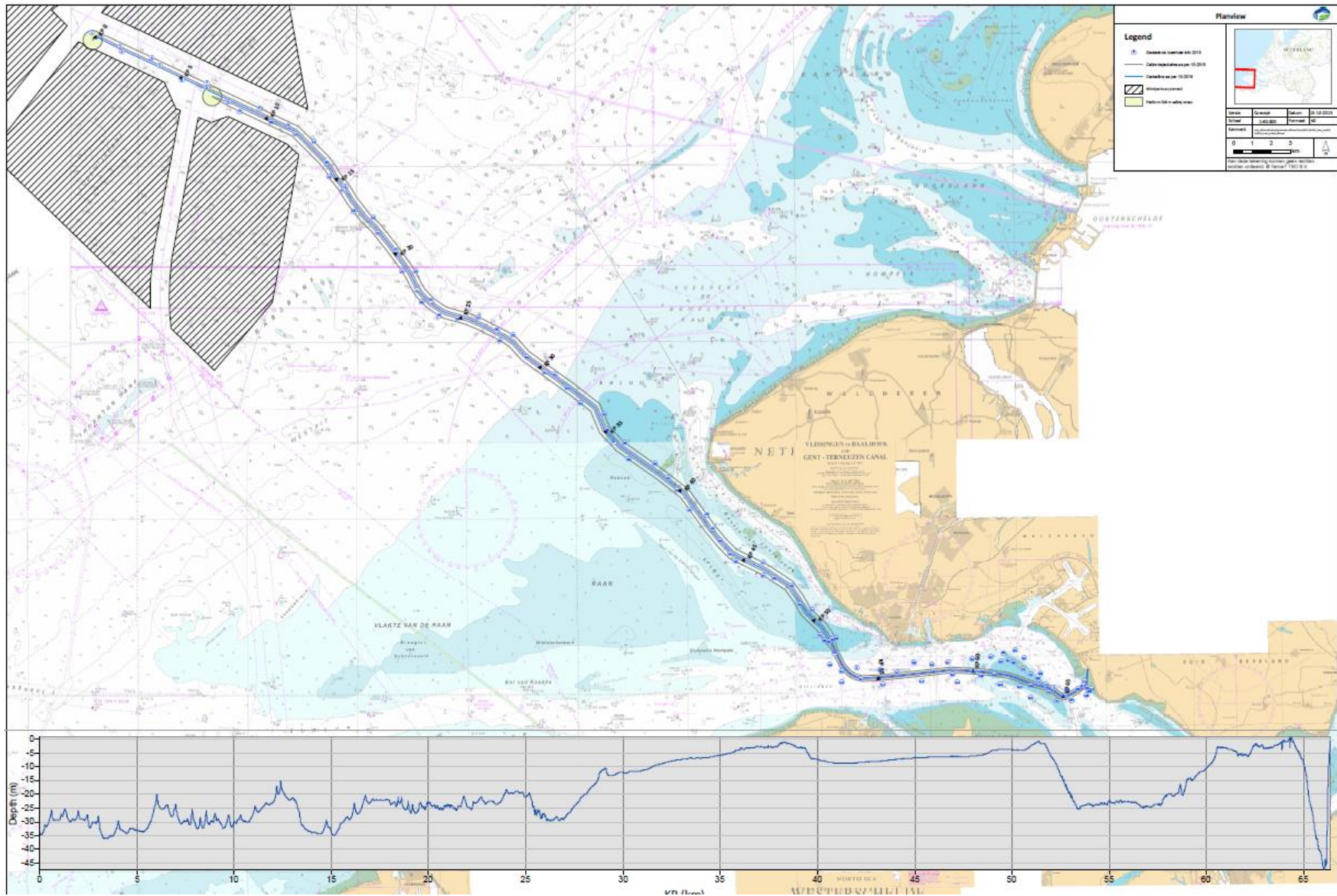
Appendix D. Detailed map of the cable trajectory

Figure D.1: The water depth along the cable trajectory from the onshore grid connection (KP: 67.300) to the Borssele Wind Farm Zone itself (KP: 0).